



Hard tissue anatomy of the cranial joints in *Sphenodon* (Rhynchocephalia): sutures, kinesis, and skull mechanics

Marc E.H. Jones, Neil Curtis, Michael J. Fagan,
Paul O'Higgins, and Susan E. Evans

ABSTRACT

The anatomy of the extant lepidosaur *Sphenodon* (New Zealand tuatara) has been extensively examined by palaeontologists and comparative anatomists because of its phylogenetic status as the only living member of the Rhynchocephalia. It is also of interest because of its sophisticated feeding apparatus and a prooral (anteriorly directed) mode of shearing used to rip food apart. However, despite several detailed descriptions of the skull, the three-dimensional relationship between individual bones of the skull has generally been ignored. Here we provide the first joint by joint description of the hard tissue anatomy for almost every cranial suture in the skull of *Sphenodon*. This survey shows that most joints involve either abutments (e.g., along the midline) or extensive overlaps (e.g., more peripheral areas) but there are others that are heavily interlocked (e.g., postorbital-postfrontal) or involve a notable amount of soft tissue (e.g., vomer-premaxilla). There is variation in facet surface texture (e.g., smooth, ridged, pitted) but extensive interdigitation is uncommon and generally restricted to one plane. The joints do not appear suited to promote the marked intracranial movement reported in lizards such as geckos. However, it is possible that the base of the premaxillae would have been able to pivot slightly when loaded or impacted by the lower jaw during shearing. The extensive overlapping joints probably serve to maximise the surface area available for soft tissues that can dissipate and redistribute stress while maintaining the rigidity of the skull. These joints are larger in adults which bite more forcefully and may feed on harder prey.

Marc E.H. Jones. Research Department of Cell and Developmental Biology, Anatomy Building, Gower Street, UCL, University College London, London, WC1E 6BT, United Kingdom. marc.jones@ucl.ac.uk

Neil Curtis. Department of Engineering, University of Hull, Cottingham Road, Hull, HU6 7RX, United Kingdom. n.curtis@hull.ac.uk

Paul O'Higgins. Centre for Anatomical and Human Sciences, The Hull York Medical School, University of York, York, YO10 5DD, United Kingdom. paul.ohiggins@hyms.ac.uk

Michael J. Fagan. Department of Engineering, University of Hull, Cottingham Road, Hull, HU6 7RX, United Kingdom. m.j.fagan@hull.ac.uk

Susan E. Evans. Research Department of Cell and Developmental Biology, Anatomy Building, Gower Street, UCL, University College London, London, WC1E 6BT, United Kingdom. ucgasue@ucl.ac.uk

PE Article Number: 14.2.17A

Copyright: Palaeontological Association July 2011

Submission: 2 August 2010. Acceptance: 20 March 2011

KEY WORDS: cranium; feeding; joints; kinesis; ontogeny; sutures; tuatara

INTRODUCTION

The tuatara, or *Sphenodon* Gray, 1831 (Günther 1867), is a reptile of about 300 mm snout to vent length (SVL) found on islands off the coast of New Zealand (Daugherty et al. 1990; Cree et al. 1995; Gaze 2001; Parkinson 2002; MacAvoy et al. 2007). For a long time many aspects of its anatomy were thought to represent the ancestral diapsid or even amniote condition (e.g., Cope 1896; Byerly 1925; von Wettstein 1931; Romer 1956; Sharell 1966), and it was therefore of great interest to comparative anatomists. This perception of *Sphenodon* led to many anatomical studies including those on the skeleton, muscles, major organs and vascular system (reviews include von Wettstein 1931, 1932, 1937; Robb 1977; Dawbin 1982). More recent research has shown that many features previously considered to be “primitive” or plesiomorphic, such as the complete lower temporal bar, absence of an external ear, and reduced copulatory organ, are more parsimoniously interpreted as derived or secondary (Gans 1983; Whiteside 1986; Thompson and Daugherty 1992; Evans 2003; Böhme and Ziegler 2008; Jones et al. 2009). Nevertheless, the phylogenetic position of *Sphenodon* as the only living member of Rhynchocephalia (Jones 2008), and therefore the only living sister taxon to Squamata (Rest et al. 2003; Evans 2003; Evans and Jones 2010), has meant that interest in *Sphenodon* anatomy remains high (e.g., Schwenk 1986, 2000; Rieppel 1992; Schmid et al. 1992; Witmer 1995; Reynoso 1996, 2003; Herrel et al. 1998, 2007; Reynoso and Clark 1998; Reiner and Northcutt 2000; Evans et al. 2001, 2002; Alibardi and Maderison 2003; Seligmann et al. 2003, 2008; Meyer-Rochow et al. 2005; Alibardi and Gill 2007; Holliday and Witmer 2007, 2008; Jones 2008, 2009; Evans 2008; Jones et al. 2009; Kieser et al. 2009; Johnston 2010). However, despite several descriptions of the skull (e.g., Günther 1867; Siebenrock 1893, 1894; Romer 1956; Rieppel 1992; Evans 2008; Jones et al. 2009), the cranial joints have been largely overlooked.

Cranial Joint Structure

The skull is made up of bones that are united by fibrocellular joints at sutures (Pritchard 1956; Kokich 1976; Persson et al. 1978; Cohen 2000; Herring 2008). The term “suture” itself may be used

to refer solely to the soft tissue component of a joint (e.g., Pritchard 1956; Moss and Young 1960; Bolt 1974; Mao 2002) or more generally to the joint as a whole including the edges of bone that are involved (e.g., Jaslow 1990; Cohen 2000). The exact histological structure of cranial joints may vary with age and location (Kokich 1976; Wage-mans et al. 1988; Cohen 2000) but, in mammals at least, they are generally considered to comprise either three or five different tissue layers (Pritchard 1956; Hinton 1988; Cohen 2000; Rafferty and Herring 1999; Herring and Teng 2000). Each facial bone is surrounded by a layer of periosteum (an inner cambial layer and an outer capsular layer), and between the bones is a central vascular “middle space” spanned by collagen fibres (Figure 1; for abbreviations in figures see Appendix 1) (Pritchard 1956). For cranial vault bones however the capsular layer and middle space are essentially absent. Instead the periosteum and dura converge into a central “ectomeninx” (Rafferty and Herring 1999). The fibrocellular nature of cranial joints has prompted comparisons to the periodontal ligament that surrounds the tooth roots in mammals (e.g., Nanda and Hickory 1984; Herring 2000).

Here, ‘facet’ refers to the articulating surfaces of individual bones (following e.g., Evans 1980),

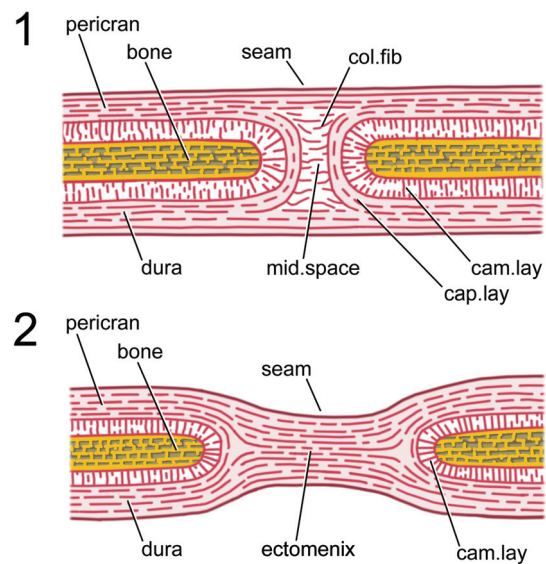


FIGURE 1. Suture histology. 1. facial suture. 2. cranial suture. Redrawn from Pritchard (1956) and Cohen (2000).

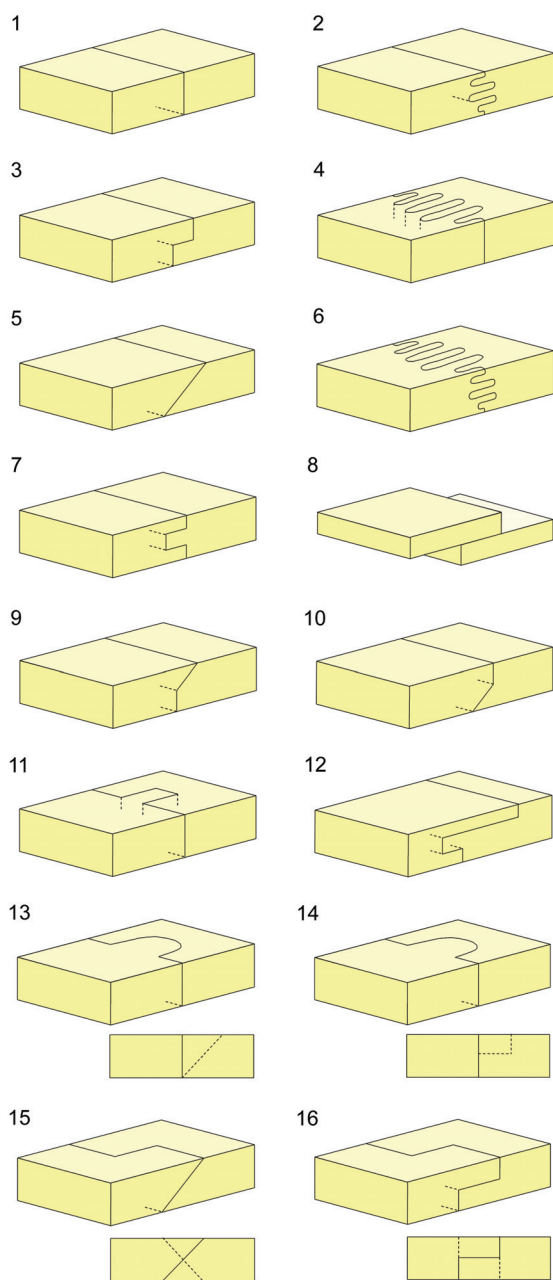


FIGURE 2. Types of planar joints. 1. butt joint. 2. joint with Type-A interdigitations. 3. stepped joint. 4. joint with Type-B interdigitations. 5. scarf joint. 6. joint with Type-C interdigitations. 7. horizontal or transverse slot joint. 8. lap joint (Weishampel 1984). 9. raised scarf joint. 10. recessed scarf joint ('basal shelf' of Kathe 1995). 11. vertical slot joint. 12. asymmetrical horizontal slot joint with a tab and pocket. 13. scarfed tongue in groove. 14. stepped tongue in groove joint. 15. bird's mouth joint. 16. bear's mouth joint. Unbroken line represents external seam whereas dashed line represents portions of internal interface.

'seam' refers to the boundary between the bones in articulation (following Kathe 1995, 1999), and 'interface' is used to refer to the articulation in cross-section.

Cranial joints can exhibit a variety of different constructions, and three main categories are recognised: butt joints, scarf joints and interdigitated joints. Butt joints (Figure 2.1), where bones meet at a flat wall perpendicular, or near perpendicular, to the outer surface of the bones (Moss 1957; Bolt and Wassersug 1975; Weishampel 1984; Busbey 1995) are also sometimes termed vertical wall in Kathe (1995), flat in Bolt and Wassersug (1975), end-to-end in Moss (1957) and Wagemans et al. (1988). Scarf joints (Figure 2.5) involve a partial overlap between two bones (Weishampel 1984; Busbey 1995) and may also be referred to as bevelled (Moss 1957; Kathe 1995, 1999), overlapping (Moss 1957), shelved (Kathe 1995, 1999) or squamous (Moss 1957; Bolt and Wassersug 1975). Interdigitated joints (Figures 2.2, 2.4 and 2.6) occur where processes from neighbouring bones interfinger and the externally visible seam may be complex and meandering (serrate in Weishampel 1984).

These three categories are relatively easy to define, but difficult to apply without grouping together very differently shaped joints (Kathe 1995, p. 257; Clack 2002). This problem is particularly true of overlapping and interdigitated joints. Variation in the degree and type of facet texture (e.g., gutters and striations or more conspicuous ridges, grooves and fluting) blur the boundaries between these three different joint categories. Moreover, bones do not always overlap in a simple slope-like fashion (Figure 2.5), the interface may be a stepped joint (Figure 2.10) or the overlapping bone may extend a tongue into an evenly recessed groove on the other bone (Figure 2.13-14). Kathe (1995) recognised the problem of using only three categories and expanded their number, for example dividing scarf joints into 'shelf', 'basal shelf' and 'steep bevel' joints. He referred to the sloping facets of scarf joints as 'shelves', but the term 'shelf' is here considered more useful for describing rectangular planar projections of bone. Therefore, 'recessed scarf' is used here instead (Figure 2.10, 'butt-lap' of Daza et al. 2008). A further overlapping joint type, referred to as a 'lap joint' by Weishampel (1984), occurs where the facets are not inset (Figure 2.8).

Interdigitated joints also show a variety of forms depending on the number and shape of interdigitations, their depth from the cranial surface

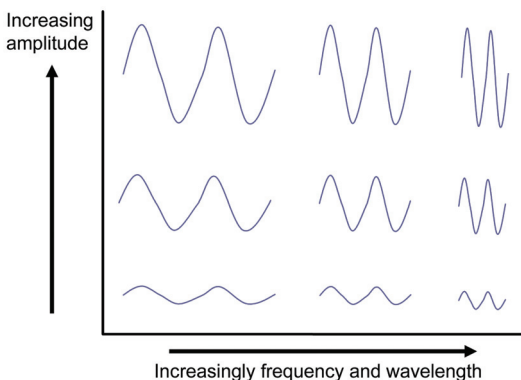


FIGURE 3. Graph depicting waveforms of different amplitudes and frequency.

and their orientation. Problematically, the latter characteristic is not always clearly described. Here interdigitated joints are divided into three main categories:

- Type-A (Figure 2.2): several horizontal slots and shelves with facet surfaces generally parallel to the outer surface of the bone.
- Type-B (Figure 2.4): several vertical slots and projections with facets generally perpendicular to the outer surface of the bone.
- Type-C (Figure 2.6): spine-like projections overlapping in three planes, essentially a combination of Type A and Type B.

Type-A may be thought of as an exaggerated form of a slot contact (Figure 2.7). Similarly, Type-C interdigitations were described as “hypertrophied plug contacts” by Clack (2002). Some joints may contain radially distributed shelves of bone, for example the interfrontal or interparietal joint of some turtles (e.g., Kesteven 1910; MEHJ, pers. obs.), and involve a transition from Type-A to Type-B interdigitation within the same joint. Only Type-B and Type-C necessarily exhibit interdigitated external seams, and descriptions can be made more specific by reference to wavelength and amplitude (e.g., Figure 3; Henderson 1998; Clack 2002; Rayfield 2005a). Herring (1972, p. 224) used four ordinal categories to differentiate between seams of different complexity.

Previous Work on Cranial Joints

Joint morphology has been examined to assess the growth and functional morphology of the skull in a range of tetrapod taxa. To varying degrees this includes fish (e.g., Markey et al. 2005, 2006; Markey and Marshall 2007a), ‘lizards’ (e.g.,

Frazzetta 1968; Impey 1973; Bell et al. 2003; Evans 2008; Daza et al. 2008; Moazen et al. 2009; Payne et al. 2011), amphisbaenians (e.g., Gans 1960, 1974), snakes (e.g., Rieppel 1978), turtles (e.g., Kesteven 1910; Wegner 1959; Gaffney 1979), crocodiles (e.g., Lordansky 1973; Busbey 1995; Cong et al. 1998; Montero and Lessa 2000), birds (e.g., Bock 1964; Cracraft 1968), cats (e.g., Buckland-Wright 1972; Segura and Flores 2009), pigs and peccaries (e.g., Herring 1972, 1974; Herring and Mucci 1991; Rafferty and Herring 1999; Herring and Teng 2000; Herring et al. 2001; Rafferty et al. 2003; Sun et al. 2004), goats (e.g., Jaslow 1989, 1990; Jaslow and Biewner 1995; Farke 2008), deer (Nicolay and Vaders 2006; Slater et al. 2009; Sánchez-Villagra 2010), rabbits (e.g., Persson et al. 1978, 1979; Oudhof and Markens 1982; Nash and Kokich 1985; Bramble 1989; Burrows et al. 1997; Mao 2002; Mao et al. 2003; Radhakrishnan and Mao 2004; Sarnat 2008), rodents (e.g., Moss 1954, 1957, 1961; Miyawaki and Forbes 1987; Gardner and Anderson 2001; McLaughlin et al. 2000; Byron et al. 2004, 2008; Shibazaki et al. 2007; Wilson and Sánchez-Villagra 2009), non-human primates (e.g., Beherents et al. 1978; Nanda and Hickory 1984; Wang et al. 2006) and humans (e.g., Kokich 1976; Persson and Thilander 1977; Persson et al. 1978; Anton et al. 1992; White 1996; Margulies and Thibault 2000; Sherick et al. 2000; Morriss-Kay and Wilkie 2005; Mann et al. 2009). Joints have also been considered in a growing number of fossil taxa, particularly Palaeozoic tetrapods (e.g., Bolt 1974; Bolt and Wassersug 1975; Klembara 1994; Kathe 1995, 1999; Thompson 1995; Clack 2002; Klembara et al. 2002; Markey and Marshall 2007b) but also ornithopod dinosaurs (e.g., Weishampel 1984; Norman and Weishampel 1985; Rybczynski et al. 2008), theropod dinosaurs (e.g., Henderson 1998; Currie et al. 2003; Hurum and Sabath 2003; Rayfield 2004, 2005b), mosasaurs (e.g., Baur 1892; Callison 1967), plesiosaurs (e.g., Taylor 1992; Taylor and Cruickshank 1993), choristoderes (Evans and Klembara 2005) and non-mammalian synsids (e.g., Kemp 1972; Jenkins et al. 2002; Jasinowski et al. 2010a, 2010b).

Complete surveys of all the cranial joints in the skull are rare but examples include those carried out on modern pigs (Herring 1972), crocodiles (Lordansky 1973), ornithopod dinosaurs (Weishampel 1984) and a range of early tetrapods (e.g., Bolt and Wassersug 1975; Kathe 1999; Klembara 1994; Clack 2002). Otherwise examinations tend to be more localised focused on one region of the

skull in one taxon, such as the roofing bones (e.g., Sun et al. 2004; Markey and Marshall 2007a), nasal-frontal (e.g., Rieppel 1978), frontal-zygomatic (jugal) (e.g., Kokich 1976) or zygomatic(jugal)-maxilla (e.g., Nanda and Hickory 1984). For recent reviews of cranial joints see Herring (2000, 2008), Cohen (2000), Alaqeel et al. (2006) and Depew et al. (2008)

Cranial Joint Function

Cranial joints are sites of bone growth (e.g., Oudhof 1982; Koskinen et al. 1975; Persson 1995; Cohen 2000; Opperman 2000; Morriss-Kay 2001; Mao 2002; Sun et al. 2004; Sarnat 2008). They are particularly important in humans that demonstrate a dramatic postnatal increase in brain volume, and premature closure of cranial joints can lead to abnormal growth and conditions such as craniosynostosis (e.g., Cohen and Kreiborg 1998; Morriss-Kay and Wilkie 2005; Adamo and Pollack 2009; David et al. 2009). Nevertheless, growth of skull bones also occurs through internal and external surface remodelling (Brash 1934; Enlow 1990) and surgical removal of cranial sutures in rabbits does not universally lead to an absence or even reduction of skull growth (Persson et al. 1979; Sarnat 2008).

As well as being fundamental to growth, increasing evidence suggests that cranial joints also play an important role in skull mechanics (e.g., Gans 1960; Buckland-Wright 1972; Herring 1972; Jaslow 1990; Herring and Mucci 1991; Rafferty et al. 2003; Byron et al. 2004, 2008; Markey et al. 2006; Moazen et al. 2009), a hypothesis supported by several observations:

1. In many taxa a number of cranial joints remain open after adult size is attained (e.g., Moss 1961; Herring 1972).
2. The fibrocellular nature of cranial joints means that they have very different material properties to those of the surrounding bone (e.g., Buckland-Wright 1972; Jaslow 1990; Herring 2000; Margulies and Thibault 2000; Radhakrishnan and Mao 2004; Kupczik et al. 2007; Moazen et al. 2009; Jasinowski et al. 2010b). Correspondingly, they can respond very differently to stress, experiencing much higher levels of strain (e.g., Beherents et al. 1978; Jaslow and Biewener 1995; Rafferty and Herring 1999; Herring and Teng 2000; Thomason et al. 2001; Markey et al. 2006). This observation has led to sutures being described as “shock absorbers” (Buckland-Wright 1972) and “strain sinks” (Rafferty et al., 2003) because the small movements they allow between bones may help to dissipate stress from the bones themselves. This role would be analogous to the expansion joints inserted between the concrete sections of buildings (McCormack 2006).
3. As discussed above, cranial joints can vary dramatically in shape both within a single taxon and between the skulls of different taxa with no obvious link to different growth regimes (e.g., Kathe 1995). The size and shape of cranial joints determines the amount of surface area available for soft tissue attachment (e.g., Gans 1960; Herring 1972; Jenkins et al. 2002). Therefore, more complex joints should be able to deal with greater stress (Buckland-Wright 1972). Scarf joints provide more surface area than butt joints but not as much as interdigitated joints (Herring 1972; Jaslow 1990). More complex joints also offer the potential for greater variation in orientation of the collagen fibres (Gans 1960; Herring 1972; Kemp 1972; Jaslow 1990). Hence, interdigitated joints allow fibres to be arranged obliquely so as to resist compression (Herring 1972).
4. Highly complex sutures are often found in locations where high stress might be expected, for example, in the rostra of squamates and mammals that use their head as a digging tool (e.g., Gans 1960, 1974; Herring 1972; Montero and Gans, 1999; Kearney et al. 2005; Daza et al. 2008), and around the horn cones of mammals that clash their heads during the rut (e.g., Jaslow 1989, 1990; Jaslow and Biewener 1995; Nicolay and Vaders 2006). Similarly, locations of high stress found in Finite Element Models of dinosaur skulls correspond to the position of complex or sliding joints (Rayfield 2004, 2005a).
5. Experiments on rats have shown that one month after surgery, neonates with both temporal muscles removed possess sagittal joints of relatively low complexity compared to control rats of similar age (Moss 1961). Also, myostatin-deficient mice that have hypertrophied temporal muscles and enhanced bite force compared to wild type mice also possess a sagittal joint seam of greater complexity and/or demonstrate greater squamosal-parietal overlap (Byron et al. 2004, 2008).
6. In vivo work on miniature pigs (Herring and Mucci 1991; Rafferty and Herring 1999; Her-

ring and Teng 2000; Rafferty et al. 2003) and fish (Markey and Marshall 2007ab) suggests that interdigitation is found at joints subject to compression, whereas simpler abutting scarf joints are associated with locations of tensile or torsional forces. Note that this differs somewhat from suggestions by other researchers (e.g., Gans 1960; Bolt and Wasserug 1975; Thomson 1995; Busbey 1995: 190) who considered butt contacts to be for compressive forces, overlapping joints for torsion and shear and interdigitated joints for tensile forces. Perhaps correspondingly, Massler and Schour (1951) found that interdigitation may be the result of growth under tension. Alternatively, Taylor (1992) suggested that butt joints, scarf joints and interdigitated joints represented a continuum of increased ability to withstand torsional forces. It is logical that an interdigitated joint can resist forces in a greater number of directions because of an increase in potential fibre orientations.

7. Histological examination shows that soft-tissue arrangements do appear to correspond with both overall cranial joint shape and local mechanical conditions (Buckland-Wright 1972; Rafferty and Herring 1999; Herring and Teng, 2000; Sun et al. 2004). Therefore, butt-like joints incorporate connective tissues aligned to resist tension and interdigitated joints include soft tissues oriented obliquely to resist compression. Thus, the soft tissue component of cranial joints does not compensate for gross differences in skeletal anatomy.
8. The composition and stiffness of the soft tissue component is also subject to variation (e.g., Radhakrishnam and Mao 2004) and, at least in some cases, this appears related to mechanical environment. Studies on rodents demonstrated that a decrease in mechanical loading led to a reduced secondary cartilage content of sutures (Hinton 1988). Connective tissue was also found to be more compliant in interparietal sutures experiencing higher tensile stress (Byron et al. 2004) and in vitro studies of rabbit cranial joints held in tension demonstrated increased synthesis of Type III collagen compared to control tissues (Meikle et al. 1984).
9. Finite element analysis of 3-D computer skull models with a representation of cranial joints suggests that these joints do alter local stress regimes and dissipate stress in the skull (Moazen et al. 2009).

Regardless of whether cranial joints play a mechanical role in skull function there is considerable evidence that the morphological appearance of cranial joints reflects their mechanical environment. For example, when sections of two different cranial joints (from mammals, e.g., rodents, rabbits) are swapped surgically (reciprocal translocation) in live animals each alters in time to resemble the original local joint morphology (e.g., Massler and Schour 1951; Moss 1954, 1957; Watanabe et al. 1957; Markens and Oudhof 1980; Oudhof 1982; Oudhof and Markens 1982; Nash and Kokich 1985). Similarly, sutures have been shown to alter or fuse in experimental animals and in explanted tissue specimens when stress is artificially increased or decreased (e.g., Moss 1961; Meikle et al. 1979; Nanda and Hickory, 1984; Miyawaki and Forbes 1987; Mao 2002, Mao et al. 2003; Heller et al. 2007). This adaptability of cranial joints parallels the plastic response to mechanical stimuli widely observed in bone itself (e.g., Moore 1965; Hinrichsen and Storey 1968; Schumacher 1973; Jones et al. 1977; Lanyon 1980; Corruccini and Beecher 1982; Biewener and Bertram 1994; Judex et al. 1997; Lieberman 1997; Hunt 1998; Burr et al. 2002; Boyde 2003; Frost 2003).

Cranial joints probably also contain mechanoreceptors that provide feedback important for modulating muscle activity (Paphangkorakit and Osborn 1989), reducing the risk of damage to the feeding apparatus that may occur when excessive biting force is applied to hard food items. This potential function may be particularly important in *Sphenodon* which, unlike most mammals, does not have teeth held within sockets by periodontal ligament (Kieser et al. 2009; Curtis et al. 2010a).

Cranial Joints and Kinesis in *Sphenodon*

In a seminal work of feeding in lepidosaurs Schwenk (2000, p. 199) referred to cranial kinesis as “any intracranial mobility of the skull.” However, as relative movements will occur between all cranial bones, albeit sometimes being very small (e.g., Behrents et al. 1978; Buckland-Wright 1978; Jaslow 1990; Rafferty and Herring 1999; Herring and Teng 2000), a qualitative distinction between the presence or absence of cranial kinesis under this definition is arbitrary. Rayfield (2005a) used the terms “active” and “passive” kinesis to distinguish between movements that occur during jaw loading and those generally larger movements associated with jaw opening and muscle contraction (such as those found in geckos, Herrel [1999]). Over the past hundred years different forms of

TABLE 1. Types of kinesis defined in lepidosaurs. Based mainly on Schwenk (2000), Metzger (2002) and Evans (2008).

Type of kinesis	Action	Relevant joints potentially involved or modified
Metakinesis	Movement of the viscerocranium and dermatocranium relative to the braincase.	pterygoid-basisphenoid, parietal-supraoccipital, squamosal-opisthotic, epipterygoid-prootic, epipterygoid-parietal
Streptostyly	Anteroposterior movements of the quadrate relative to the rest of the skull.	quadrate-squamosal, quadrate-pterygoid, quadrate-supratemporal, quadrate(quadratejugal)-jugal quadrate-quadratejugal
Pleurokinesis	Mediolateral movements of the quadrate relative to the rest of the skull.	quadrate-squamosal, quadrate-pterygoid, quadrate-supratemporal, quadrate(quadratejugal)-jugal quadrate-quadratejugal
Mesokinesis	Dorsoventral flexion of the skull roof (probably not possible without hypokinesis).	frontal-parietal, frontal-postfrontal, postfrontal-postorbital, frontal-postorbital, and also other joints of the dermatocranium such as the ectopterygoid-pterygoid
Hypokinesis	Dorsoventral flexion of the palate (probably not possibly without mesokinesis).	palatine-pterygoid suture, ectopterygoid suture,
Amphikinesis	Mesokinesis and metakinesis.	As listed above for mesokinesis and metakinesis

“active” kinesis present in lepidosaurs (or at least squamates) have become defined (Table 1; Evans 2008). The role of these various movements remains unclear but a number of possible advantages have been discussed including more effective prey acquisition, prey handling, prey transport, muscle leverage, tongue protrusion, tooth alignment, shearing, skull flattening, tooth disengagement and shock absorption (e.g., Frazzetta 1962; Impey 1967; Arnold 1998; Herrel 1999; Schwenk 2000; Metzger 2002; Evans 2003, 2008; Moazen et al. 2009).

The skull of *Sphenodon* is generally considered incapable of “active kinesis” (e.g., Günther 1867; Versluys 1912; Haas 1973; Bellairs and Kamal 1981; Gorniak et al. 1982; Schwenk 2000; Metzger 2002; Evans 2008). This inference is largely based on the appearance of external suture seams or manipulation of articulated material (e.g., Ostrom 1962; Arnold 1998). Gorniak et al. (1982) did not observe any obvious skull kinesis during cineradiography of live animals feeding but admitted that the resolution was limited and none of the footage has been published. It has been suggested

that limited metakinesis may be present in hatching or juvenile *Sphenodon* (e.g., Howes and Swinerton 1901; Edgeworth 1935; Ostrom 1962; Arnold 1998). This hypothesis is based largely on the presence of constrictor dorsalis muscles, which run between the braincase and palate and are associated with metakinesis in squamates (e.g., Ostrom 1962; Johnston 2010). Similarly, the presence of the protractor pterygoidei (part of the constrictor dorsalis) prompted Lakjer (1926) and Anderson (1936) to suggest that flexion between the front and back of the skull (akin to mesokinesis) might be possible. An alternative explanation for the presence of the constrictor dorsalis muscles is that they fulfill a proprioceptive role (to provide sensory feedback) and/or to support the skull during torsional strain (Evans 2008; Johnston 2010). Gardiner (1983, p. 50) referred to *Sphenodon* as possessing a “kinetic palate” but provided no clarification as to whether he considered this kinesis equivalent to hypokinesis or metakinesis.

Despite the widespread interest in lepidosaur cranial kinesis descriptions of internal joint structure in *Sphenodon* are few in number, are generally

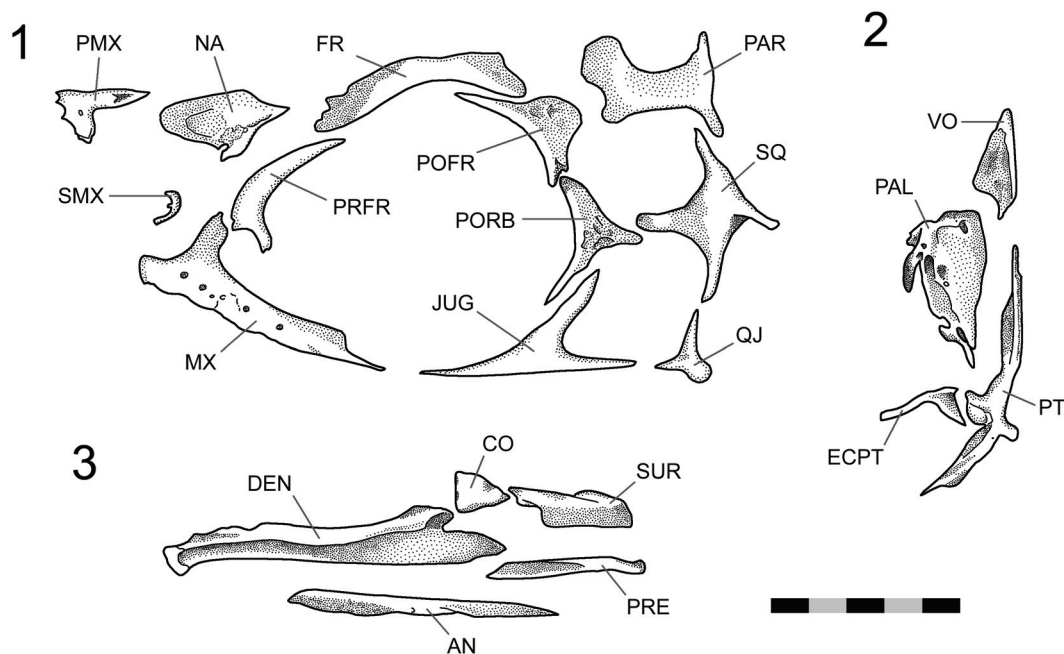


FIGURE 4. Disarticulated hatchling *Sphenodon* skull at stage S. 1. bones of the cranium (left side) in dorsal or lateral view. 2. palatal bones (left side) shown in dorsal view. 3. left lower jaw bones shown mainly in lingual view although the surangular may be shown in ventral view. Redrawn from Howes and Swinnerton (1901), surangular re-labelled as the angular and articular re-labelled as the prearticular. Scale bar equals 5 mm.

brief and often concentrate on the basiptyergoid articulation (e.g., Howes and Swinnerton 1901; Bolt 1974; Arnold 1998; Holliday and Witmer 2008; Johnston 2010). Images are also limited, mainly comprising isolated figures of facets or joint overlaps that are not discussed in the text, for example, a disarticulated parietal and vomer in Siebenrock (1894), a squamosal in Schauinsland (1903), a dotted line representing the overlap between the pterygoid and epiptyergoid in Lakjer (1926), dentaries in Robb (1977, p. 14) and a photo of the exposed ventral surfaces of the palatines in Sharrel (1966, p. 29). Information regarding the overlaps in hatchling *Sphenodon* are provided by the “exploded” skull (Figure 4) and cross-sections figured by Howes and Swinnerton (1901, plate 6.1, 6.3) as well as the cleared-and-stained specimen described by Rieppel (1992). Only recently have Holliday and Witmer (2008) and Johnston (2010) re-examined the basiptyergoid articulation in any detail using computed tomography (CT).

Objectives

Here we present the first systematic survey of the cranial joints in *Sphenodon* with regard to the osteological component (Jones 2006, 2007). It will be used to assess the potential for skull kinesis

and, in conjunction with observations of general skull structure, to generate hypotheses relating to skull mechanics (e.g., Herring 1972; Buckland-Wright 1978; Taylor 1992). This study will facilitate comparisons with fossil relatives of *Sphenodon* that are often known only from isolated skeletal material (e.g., Evans 1980; Fraser 1982; Whiteside 1986; Säilä 2005; Jones 2006) as well as providing the basis for future computer modelling work (e.g., Moazen et al. 2009; Curtis et al. 2010 a, 2010b, 2010c).

MATERIAL AND METHOD

Skeletal material of *Sphenodon* from a number of collections was examined:

Angela Milner Personal Collection, NHM, UK (AMPC); Auckland Museum, New Zealand (AIM); University of Auckland, New Zealand (AUP); Booth Museum of Natural History, Brighton, UK (BMB); Grant Museum of Zoology, UCL, London, UK (LDUCZ); Kings College London, Life Sciences, London, UK (KCL); The Manchester Museum, University of Manchester, Manchester, UK (MANCH); Natural History Museum, London, UK (BMNH); Oxford Museum of Natural History, Oxford, UK (OUMNH); David Gower Personal Collection, NHM, UK (DGPC); University Museum of Zoology,

TABLE 2. *Sphenodon* material primarily used.

Reference number	Skull Length (mm)	Notes
AIM LH617	?	Disarticulated skull bones, Lady Alice Island, collected 1983.
AIM LH833	?	Disarticulated skull bones, Middle Island, Mercury Group, collected 1983.
BNMH.K	?	Partially disarticulated skull. Frontals, parietal and left postfrontal remain articulated. Premaxillae, vomers, right maxilla and right nasal bones also remain articulated. Some teeth removed from maxilla.
CM 30660	11.9	CT scan slices of a wet specimen head. With permission from L.K. Murray and C.J. Bell.
DGPC1	~62	Left half of a parasagittally sectioned skull now disarticulated. Partial midline bones (premaxilla, nasal, frontal, vomer, palatine and parietal). On loan from Dr David Gower (personal collection) given to him by Alick Walker with DGP2, Gower pers. comm. 2002. Was photographed by Pamela L Robinson at some point.
DGPC2	~63	Skull with posterior parts of both postorbitals and parietals have been sectioned away. Posterior end of left jugal also absent. Right and left squamosals absent. Previously figured in Gower and Weber, 1998. Also on loan from Dr David Gower.
LDUCZ x036	67.7	Whole skull. Slight damage to left epipterygoid and pterygoid. Partial atlas and 1 st intercentrum attached to the basioccipital.
LDUCZ x146	58.1	Skull with premaxillae held to vomers by wire. Dorsomedial part of both the left and right squamosal and anterior process of right squamosal damaged. Coronal break in left pterygoid and left epipterygoid fractured.
LDUCZ x723	57.7	Whole skull but left upper temporal bar broken.
LDUCZ x343	55.8	Whole skull. Right squamosal damaged anteriorly and medially, ectopterygoids absent. Left squamosal and quadrate loose. Dorsal tips of premaxillae displaced anteriorly and posterior of maxillae displaced ventrally.
LDUCZ x1176	43.8	Whole skull, partially disarticulated. Previously referred to as "LDUCZ x804" in Evans et al. 2001; Evans 2008; Jones 2008 and "UCL X.809" in Evans et al. 2002.
YPM 11420	~55	Photos and some limited first hand examination (was 'YPM 939').
YPM 11419	~60	Photos and some limited first hand examination (was 'YPM 5436').
YPM 9194	48.75	CT scan slices of a wet specimen head. With permission from L.K. Murray and C.J. Bell.

Cambridge, UK (UMZC); The Field Museum, Chicago, USA (FMNH); Museum of New Zealand Te Papa Tongarewa, Wellington, New Zealand (NMNZ); Yale Peabody Museum of Natural History, New Haven, USA (YPM). The main specimens used are listed in Table 2. Unfortunately, much of this material lacks locality or sex data. Most specimens probably represent *Sphenodon punctatus* Gray, 1831, rather than the rarer second species *S. guntheri* Buller, 1877, but this is not always certain. Moreover, the status of *S. guntheri* as a valid species has once again been recently questioned by Hay et al. (2010).

A *Sphenodon* skull, DGPC1, was kindly provided by David Gower (NHM) from his personal collection, with permission for it to be disarticulated. Prior to disarticulation this skull was drawn in several views to illustrate the external appearance of the cranial joints (e.g., Figures 5, 6). The skull

was cleaned in a solution of 5% tergezime heated to 50 °C, and individual joints were additionally cleaned using acetone. Disarticulation was achieved using 48 h submersion in pectinase (pig gut enzyme) with the assistance of Wendy Birch (UCL). The individual bones were rinsed thoroughly in running water for a week and left to dry in air. The DGPC1 skull had already been sagittally sectioned and therefore information on the midline articulations was obtained from other specimens.

All drawings were made using a Wild stereomicroscope with *camera lucida*. Sand was used to control and maintain orientation. In general, lighting was directed on to the specimens from the top left hand corner, although for some facets low angled lighting was used to examine and draw particularly subtle texture. As stated in some figure captions, drawings were occasionally made in a view per-

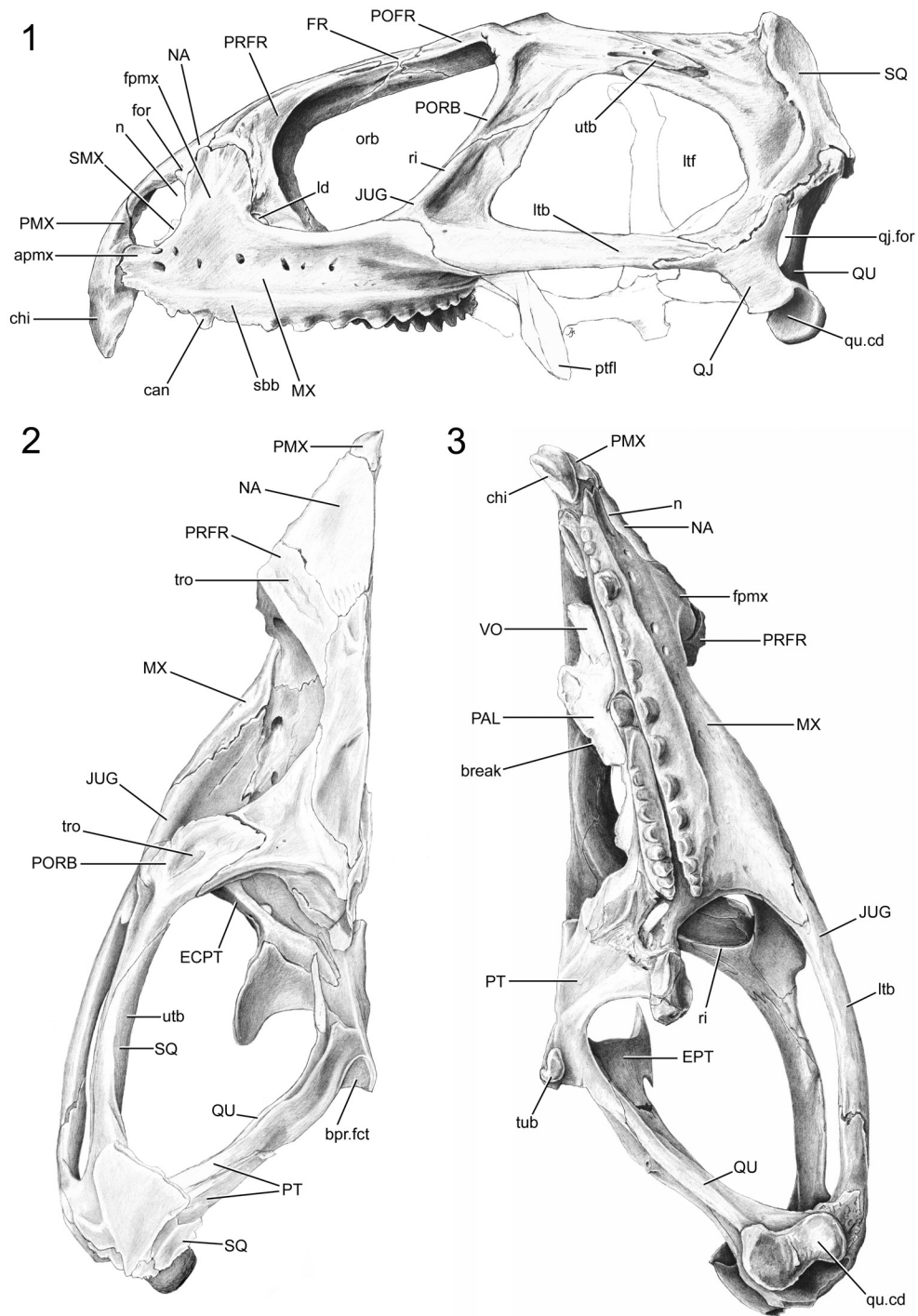


FIGURE 5. *Sphenodon* skull DGPC1 prior to disarticulation. 1. lateral, 2. dorsal, 3. ventral views. Skull length approximately 61 mm.

pendicular to the surface of a facet rather than of the bone as a whole.

The sutures of adult *Sphenodon* were also manually segmented in two specimens using data from microCT. The first specimen, YPM 9194, was

segmented using VG Studio MAX (Volume Graphics GmbH, Heidelberg, Germany) under the supervision of Dr Jessie Maisano at the High-Resolution X-ray Computed Tomography Facility, University of Texas, Austin, USA. The second specimen,

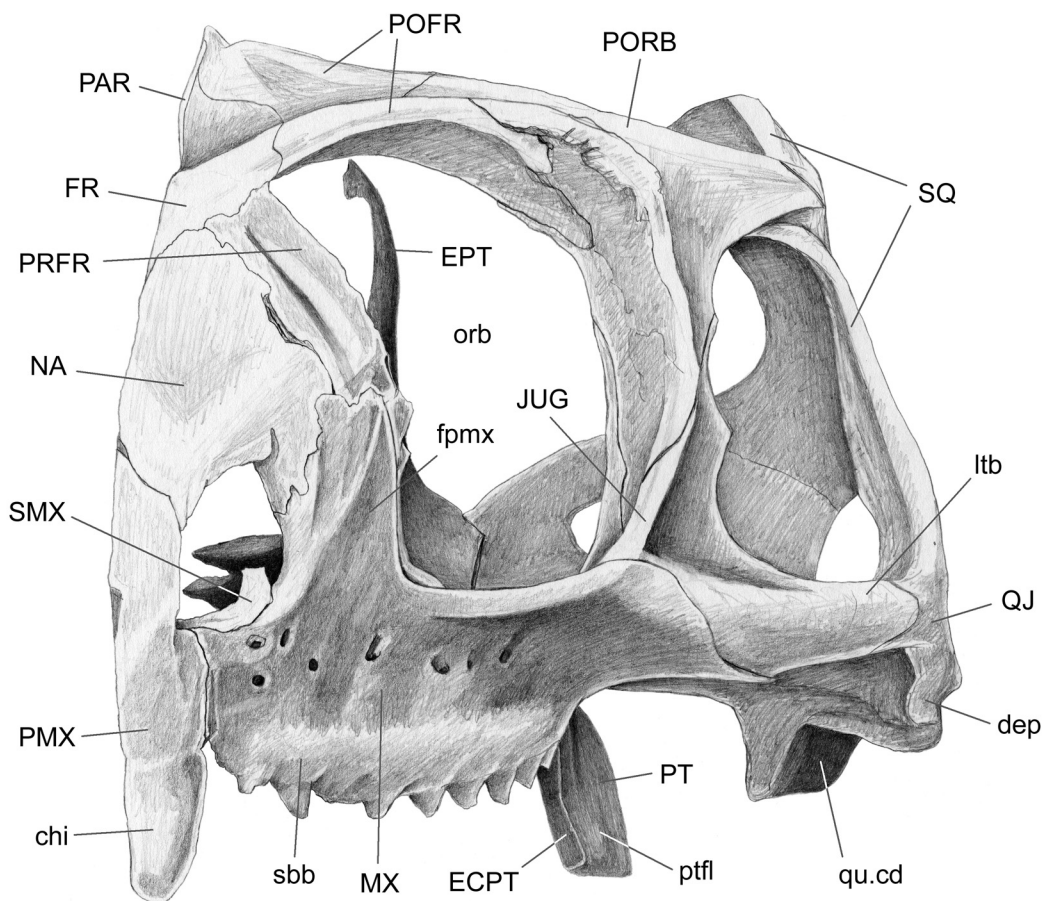


FIGURE 6. *Sphenodon* skull DGPC1 prior to disarticulation in anterior view. Skull length approximately 61 mm.

LDUCZ x036, was segmented at UCL using AMIRA (Visualization Sciences Group, Burlington MA, USA) after micro-CT scanning at the University of Hull, UK.



















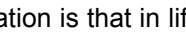
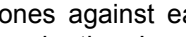
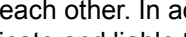
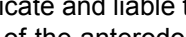
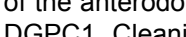
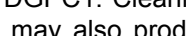
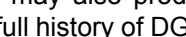
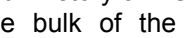




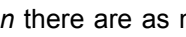
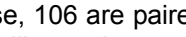
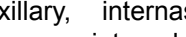
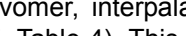
The descriptions are organised joint by joint rather than bone by bone (following Herring [1972] and Weishampel [1984]). Each joint is also categorised depending on its general location within the skull (roughly following Weishampel [1984]). Descriptions of each joint generally progress from anterior to posterior and include location; basic joint type e.g., butt, overlap, interdigitated; length and shape of the seam; exact shape and orientation of facets; type and degree of overlap at the joint; texture of the facets; tightness of fit (may relate to the extent of soft tissue); and movements that are prevented or permitted (without soft tissue).

Digital imaging software, 'Adobe Photoshop 2.0' (Adobe Systems, San Jose, California), was used to combine drawings of bones with the

"ghosts" of overlying or underlying bones. Once all the sutures had been assessed in detail, summary diagrams were produced. These include outlines of the skulls in lateral, ventral, dorsal, and occipital view with the inferred areas of underlying bone superimposed (e.g., Bolt and Wassersug 1975; Busbey 1995; Clack 2002; Jenkins et al. 2002). In addition, diagrammatic cross-sections were produced. A consistent colour code is used throughout for each bone (Table 3).

A small problem requiring consideration is the slight distortion of bone shape caused by dehydration (Tyler 1976, p. 6), particularly in long and thin bones or processes. Together with loss of soft tissue this is probably why bones in articulated dry skulls may separate slightly (e.g., maxillae in LDUCZ x343). This distortion can make rearticulation difficult. The anterior superior process of the squamosal in DGPC1, for example, has split, probably due to the loss of the organic component and subsequent dehydration. Another factor inhibiting

TABLE 3. Key to bone overlap and underlap diagrams and also schematic cross-sections.

Bone	Colour	Colour at 40%
premaxilla		
maxilla		
nasal		
prefrontal		
frontal		
palatine		
vomer		
pterygoid		
ectopterygoid		
epipterygoid		
jugal		
postorbital		
postfrontal		
parietal		
squamosal		
quadratojugal		
quadrate		

accurate rearticulation is that in life soft tissue may push individual bones against each other or pull bones away from each other. In addition, small thin processes are delicate and liable to breakage, e.g., the triangular tips of the anterodorsal processes of the squamosal in DGPC1. Cleaning and disarticulation of the skull may also produce artificial surface texture. The full history of DGPC1 is unknown, including how the bulk of the soft tissue was removed and whether solvents were used to clean the surface.

RESULTS

In *Sphenodon* there are as many as 113 cranial joints. Of these, 106 are paired and 7 are mid-line (interpremaxillary, internasal, interfrontal, interparietal, intervomer, interpalatine and interpterygoid) (Figure 7, Table 4). This number does not include the symphyseal joint between the lower jaws, joints between the braincase bones, and paired jaw joints between the quadrate and articular. The joints of the skull are divided between seven categories or units, depending on their location within the skull (Figure 7): rostral joints (20 in all), palatal joints (21 to 25), roofing joints (16 plus), temporal joints (14 plus, 2 mainly fused), metakinetetic joints (14), intraoccipital joints and mandibular joints (14 plus 4 fused). The latter two categories will not be discussed in detail here. The joints of

most individual bones are restricted to one unit but those of the pterygoid and prefrontal are distributed between three.

Rostral Joints

The rostral (or facial) joints include those joints surrounding the anterior part of the skull. The rostral unit is connected to the roofing unit by the nasals and prefrontals and to the palatal unit by the maxillae, prefrontals and vomers.

Interpremaxillary

In *Sphenodon* the premaxillae contact one another along their longest axis. In external view the dorsal portion of the joint has a seam that is sagittally orientated and generally straight, although a slight sigmoid kink is often visible (e.g., LDUCZ x036, LDUCZ x343, LDUCZ x723). This sigmoid kink is particularly large in the juvenile specimen LDUCZ x1176. In the ventral portion of the joint the external seam widens to form an ovoid gap between the anterior edges of the two premaxillae (e.g., DGPC2). In life this is filled by a plug of soft tissue (e.g., LDUCZ x036) (Figure 8). The premaxilla does not have a palatal shelf and therefore the seam is short in ventral view, limited to the alveolar rim. The joint is generally a butt joint (e.g., YPM 11419) but some texture is apparent, consisting of dorsoventrally directed striations. In AIM LH0617 there is a more obvious groove running the length of the facet surface (Figure 9), and CT scans of LDUCZ x036 demonstrate that the kink in the external seam corresponds to an overlap between the two bones. Examination of this joint is not possible in DGPC1.

Premaxilla-maxilla

In *Sphenodon* the anterior end of the maxilla loosely overlaps the lateral process of the premaxilla below the naris, with a 'recessed scarf' joint (Figure 2.10). In dorsal view, the seam runs posteromedially from near the anterolateral corner of the external naris. In lateral view the seam is generally straight, running dorsoventrally from the ventral margin of the naris to the ventral edge of the tooth row (e.g., LDUCZ x036). However, the anterior process of the maxilla is often curved anteroventrally (e.g., DGPC1, LDUCZ x343, LDUCZ x723, YPM 11419), widening the seam between the two bones. Disarticulated specimens demonstrate that there is an initial butting contact anteriorly (a vertical wall at about 90° to the outer cranial surface and about 25% of the mediolateral thickness of the premaxilla). Posterior to this, there is a scarf joint

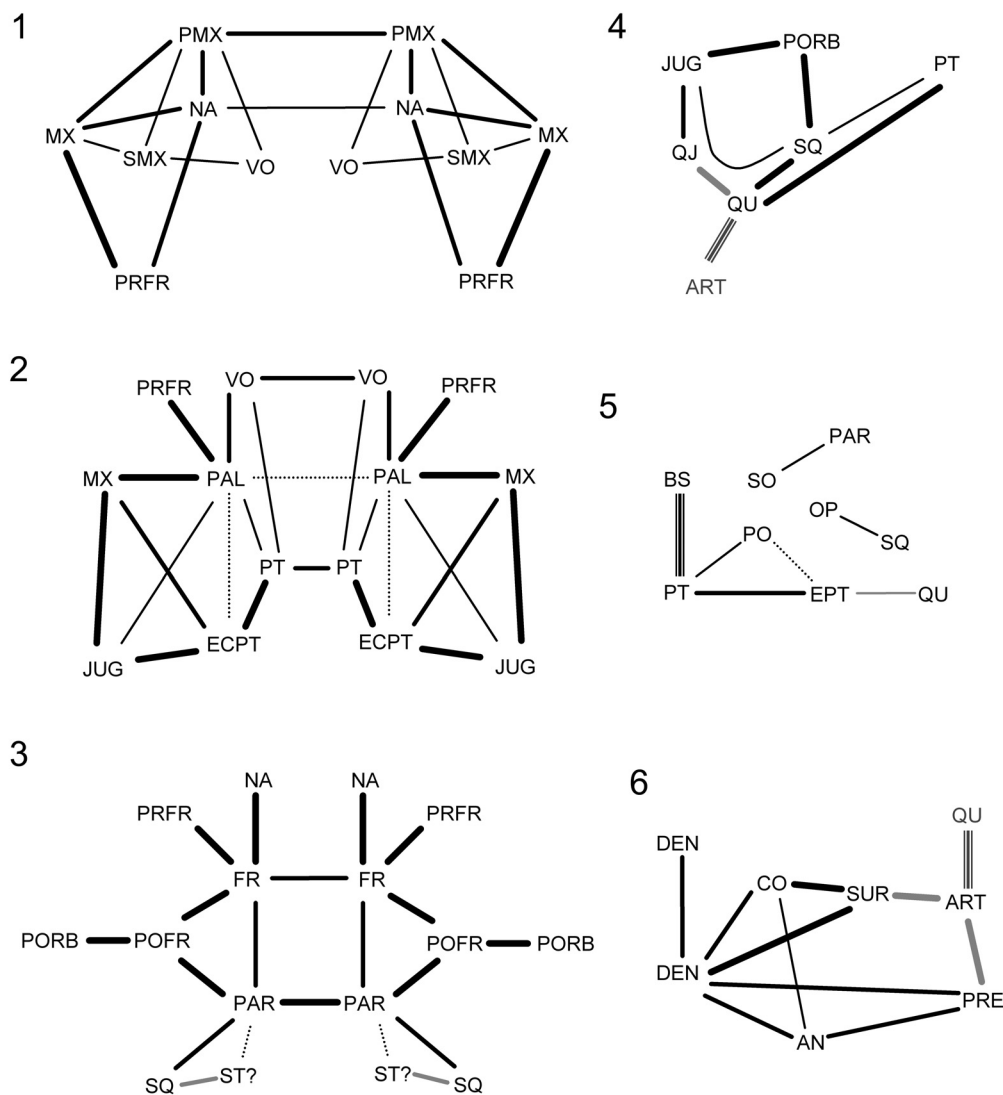


FIGURE 7. Joint relationships within *Sphenodon*. 1. rostral, 2. palatal, 3. roofing, 4. temporal, 5. metakinetic joints. 6. joints of the lower jaw. Braincase joints not shown. Dotted line = occasional contact, thin line = minor contact, medium line = intermediate contact, thick line = major contact, grey line = fusion, triple line = synovial joint.

where the angle of overlap approaches 45° . The facet on the premaxilla is generally flat although there is vertical fluting in specimen BMNH.K without corresponding fluting on the maxilla. The posterior process of the premaxilla is relatively long but tapers symmetrically reducing the area of contact with the maxilla (Figure 10). The joint does not seem to be closely apposed, and in life probably involves a substantial amount of soft tissue, particular at its ventral portion. Examination of the joint in CT section of YPM 9194 and LDUCZ x036 confirms this observation.

Without considering soft tissue, this joint shape appears to restrict the posterior part of the premaxilla from rotating laterally, and the anterior end of the maxilla from rotating medially. In the articulated skull, the paired premaxillae are held between the maxillae, but not firmly. This joint (without soft tissue) would not restrict anterior movement of the premaxilla or posterior movement of the maxilla and neither would it prevent vertical or downward movement of either bone. Because movement of the maxilla is restricted by several other bones (nasal, prefrontal, palatine, jugal, ectopterygoid) freedom at this joint has greater

TABLE 4. Summary of the relationship between skull bones in *Sphenodon*.

Bone	Number of joints	Most substantial joint	Bones
premaxilla	4	nasal	premaxilla, nasal, maxilla, vomers
maxilla	6	jugal	premaxilla, nasal, prefrontal, palatine, ectopterygoid, jugal
septomaxilla	3	maxilla	premaxilla, maxilla, vomer
nasal	4	frontal	premaxilla, nasal, prefrontal, frontal
prefrontal	4	frontal	nasal, prefrontal, maxilla, palatine
frontal	5	postfrontal	frontal, nasal, prefrontal, postfrontal, parietal
palatine	6	maxilla or prefrontal	maxilla, prefrontal, vomers, pterygoid, ectopterygoid (very weak), jugal
vomers	4	palatines	premaxilla, vomer, palatines, pterygoid
pterygoid	7	ectopterygoid	vomers, palatines, quadrate, ectopterygoid, pterygoid, squamosal, braincase (basisphenoid)
ectopterygoid	3	pterygoid	pterygoid, maxilla, jugal
epipterygoid	3	pterygoid	pterygoid, quadrate, braincase (prootic)
jugal	7	maxilla	maxilla, ectopterygoid, postorbital, quadratojugal, squamosal, palatine
postorbital	3	jugal	jugal, postfrontal, squamosal
postfrontal	3	frontal	parietal, frontal, postorbital
parietal	5	postfrontal	frontal, postorbital, squamosal, parietal, braincase (supraoccipital)
squamosal	7	quadrate	jugal, quadratojugal, postorbital, parietal, quadrate, pterygoid, braincase (opisthotic)
quadratojugal	3	quadrate	quadrate, jugal, squamosal
quadrate	3	pterygoid	pterygoid, quadratojugal, squamosal
braincase	3	parietal	parietal, pterygoid, squamosal

implications for the premaxilla although the maxilla is sometimes found to be displaced in dried specimens (e.g., LDUCZ x343).

Premaxilla-nasal

The premaxilla overlaps the anterior process of the nasal in a 'recessed scarf' joint (Figure 2.10) in which the anterior end of the nasal process slots into a 'pocket' in the back of the premaxilla (at least in DGPC1). In dorsal view, the nasal processes of the paired premaxillae appear to be pinched between the nasals with seams that run postero-medially from the dorsal margin of the naris toward the midline. The internal structure of the joint is complex (e.g., LDUCZ x343, YPM 11419, DGPC1, AUP 11883). First, the anterior process of the nasal, which extends beneath the premaxilla, is triangular and directed anterolaterally, so the hidden anterior processes of the nasals do not meet along the midline but diverge (Figures 11, 12, 13). Sec-

ond, the facet on the nasal is sunk or recessed as in a 'recessed scarf' joint. It is deep medially but shallows laterally (Figures 11.2, 12.1). As a result the paired premaxillae are wedged against each other. Third, the anterior tip of the pointed nasal process fits into a pocket in the posteroventral surface of the premaxilla (Figures 10.4, 12.4, 12.5). Hence, the nasal has both dorsal and ventral facets for the premaxilla (Figure 12.2, 12.7). The posterior wall of the pocket is fairly low, and the interior contains five pits that are probably related to nutrient supply (Figure 12.4).

Due to bisection of the skull only the lateral half the premaxilla-nasal joint is known for DGPC1. However, the available portion shows the presence of three gutters on the anterior process of the nasal that run parallel to the long axis of the process itself (anterolaterally). The posterior ends of the lateral and medial gutters are visible on the dorsal surface but excavate the surface laterally and medially,

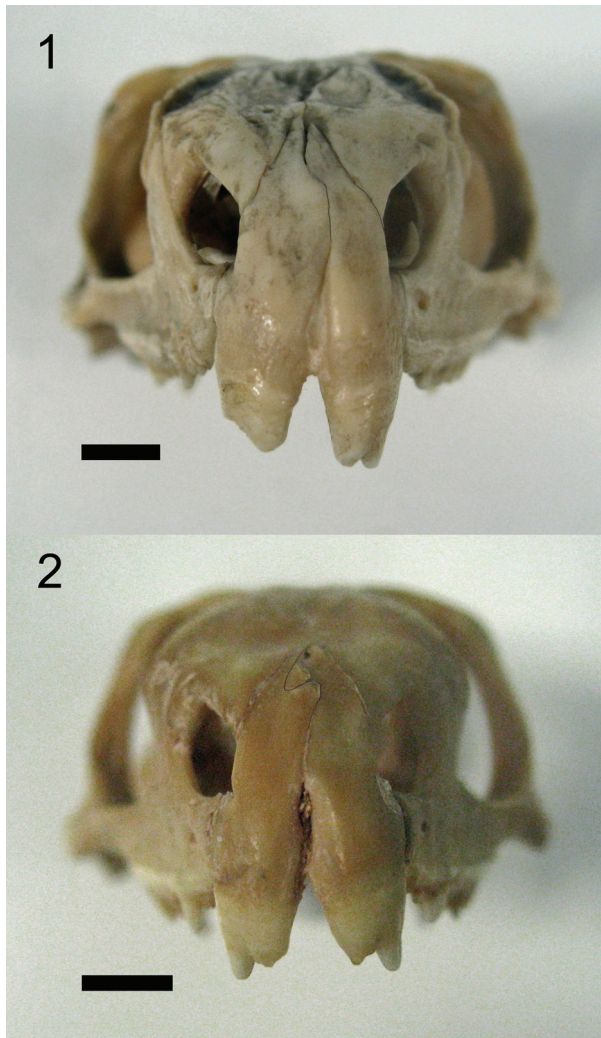


FIGURE 8. An anterior view of the skull. 1. LDUCZ x036. 2. DGPC2. Scale bar equals 5 mm.

respectively. The central gutter is more visible ventrally and terminates at the tip of the anterior nasal process. On the ventral surface of the process the three gutters are separated by a shallow groove and a concavity. The largest and most lateral of the gutters (Figure 12.1, 12.2) corresponds to a tubercle on the ventral surface of the premaxilla above the pocket (Figures 10.2, 10.4, 12.5, 12.6). The two smaller gutters on the nasal also interlock with ridges inside the pocket of the premaxilla. The medial parts of the facets, as seen in BMNH.K, bear longitudinal grooves and ridges (Figure 13). In the juvenile *Sphenodon*, LDUCZ x1176, the nasals appear to abut the edge of the premaxillary pocket but do not enter it.

This joint would prevent the posterior end of the premaxilla from rotating posteroventrally but

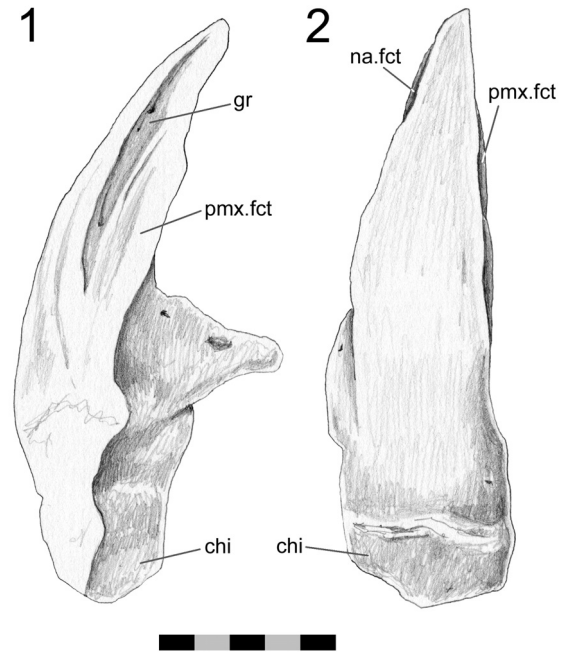


FIGURE 9. Isolated right premaxilla (AIM LH0617). 1. medial, 2. anterior views. Scale bar equals 5 mm.

some anterior rotation would be possible without soft tissue (again as seen in LDUCZ x343). The butting wall of the 'recessed scarf' and edge of the premaxillary pocket would obstruct posterodorsal movement of the premaxilla but would not restrict anteroventral movement. The small grooves and gutters on the facets, and the shape of the premaxillary pocket would inhibit mediolateral movement and increase surface area for soft tissue. The change in depth of the scarf joint would also discourage sideways movements between the nasal and premaxilla. Moreover, in an articulated skull, medial movement of one premaxilla would be prevented by the other premaxilla.

Internasal

The nasals meet along the midline between the premaxillae and frontals. The external seam is usually straight (LDUCZ x343, LDUCZ x723, NMNZ RE0385) but it can also be curved (LDUCZ x1176), irregular (LDUCZ x146) or slightly sigmoid (LDUCZ x343; BMB 100225). The length of the seam also varies in comparison with the posterior extent of the premaxillae or interorbital width; it may be relatively long (LDUCZ x721, BMB 101668, LDUCZ x343) or short (LDUCZ x723, KCL x12, BMNH 1972.1499) (Figure 14; Jones and Lappin 2009, figure 4D). The medial edge of the anterior

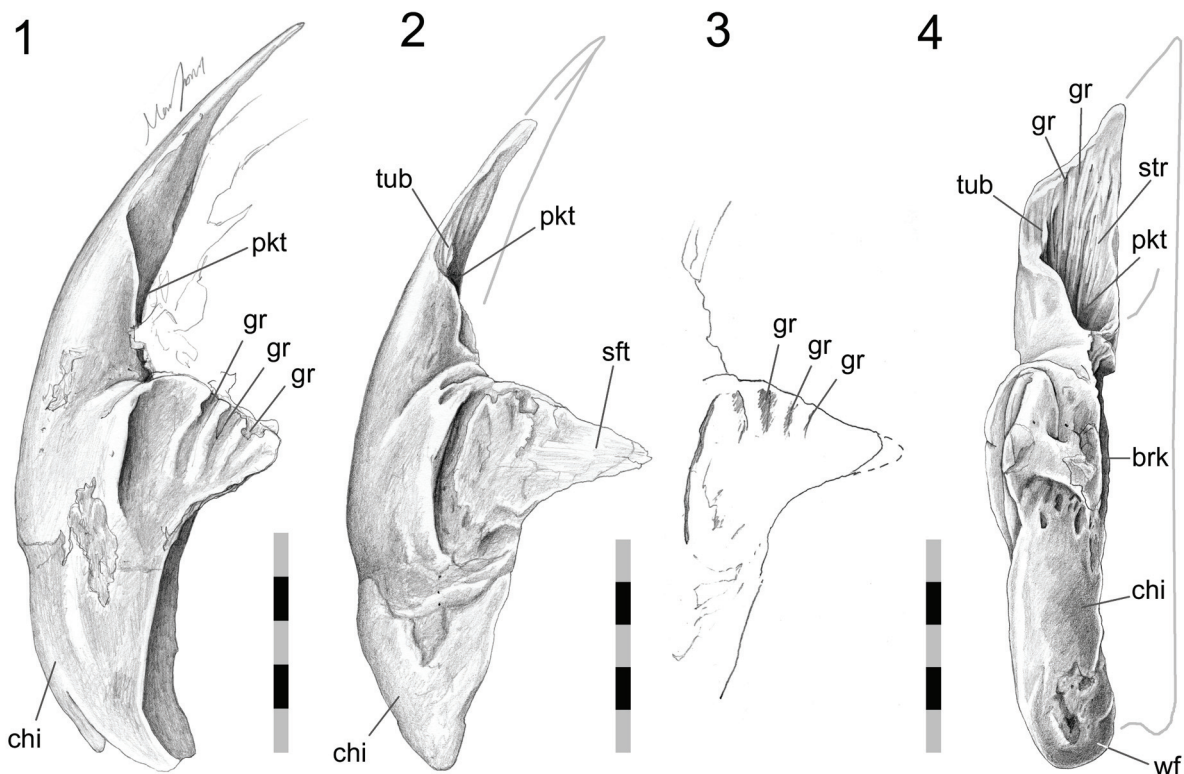


FIGURE 10. Isolated left premaxillae. 1. BMNH.K in lateral view. 2. DGPC1 in lateral view. 3. lateral process of DGPC1 ignoring soft tissue. 4. DGPC1 in posterior view. Scale bar equals 5 mm.

process for the premaxilla, seen only in disarticulated specimens, provides further contact area between the nasals (Figure 13.1). Nevertheless, contact with the premaxillae and frontals occurs across a far greater surface area. In general the internasal is a butt joint although very small shelves of bone may ‘invade’ the adjoining nasal ventrally. In one specimen (BMNH 1985.1212) the centre of the left nasal exhibits a large pathological hole from which seams extend anteriorly and posteriorly. Possibly as a response, the midline internasal seam has partially fused (Figure 15). Alternatively the right nasal may have grown to compensate for the left and a suture subsequently developed within it. In hatchling skulls there is a fontanelle between the nasals and frontals (Howes and Swinnerton 1901; Rieppel 1992; Jones and Lappin 2009, figure 4). As previously reported remains of it can be found in a number of adult skulls, and it may be over 1 mm in diameter (e.g., MANCH C120649, AMPC1, UCMZ 2614, KCL x12) (Jones et al. 2009).

Nasal-prefrontal

In dorsal view the external seam of this joint is sub-parallel to the premaxillary-nasal joint, being anterolaterally directed and generally straight before it disappears under the maxilla (Figures 5.2, 6, 14, 15). In lateral view (with the maxilla removed) the seam continues between the ventrolateral process of the nasal and lateral process of the prefrontal, travelling at first anterolaterally and then ventrally. This ventral part of the seam (hidden in articulated skulls by the facial process of the maxilla) exhibits some intraspecific variation; it may be sigmoid as in DGPC1 (Figures 16, 17.1) or almost straight as in YPM 11419. The form of the nasal-prefrontal joint changes substantially along its distance, and it seems logical to divide it into two parts; a posterior portion (best seen in dorsal view) and an anterior portion (best seen in lateral view with the maxilla removed).

The posterior portion of the joint consists of a weak slot joint (Figure 16). In DGPC1, the posterior edge of nasal overlaps a short shelf or lappet of bone from the prefrontal. This shelf in turn meets the large anterior process of the underlying frontal.

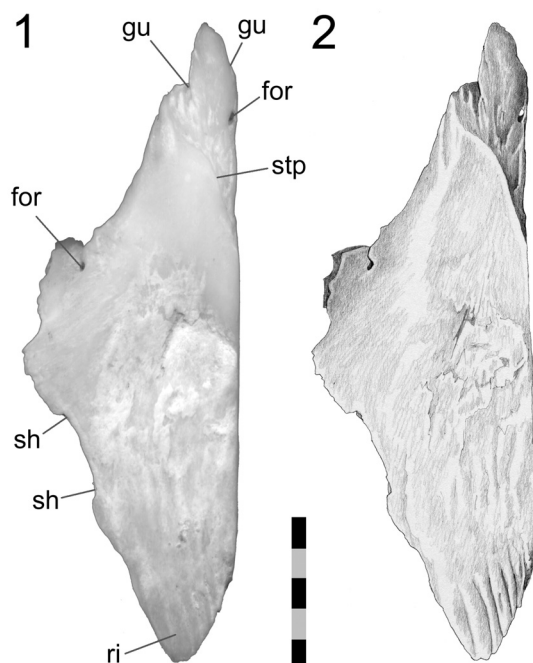


FIGURE 11. Isolated left nasal bone in anterodorsal view (DGPC1). 1. labelled photograph. 2. drawing. Scale bar equals 5 mm.

A smaller longitudinal nasal shelf also projects under the prefrontal shelf for a small distance, creating a small narrow slot joint posteriorly. Midway along the posterior portion of the joint in DGPC1 the seam is wide, and contact between the two bones is lost. These facts are not evident in LDUCZ x036, LDUCZ x343 or DGPC2 where externally the prefrontal may appear to encroach upon the nasal. In BMNH.K, nasal-prefrontal contact is also retained, and there appears to be a much longer shelf from the nasal underlapping the prefrontal. Medial to the facial process of the maxilla the nasal overlaps a triangular shelf on the prefrontal. This shelf is continuous with the lateral process of the prefrontal that continues ventrally. Overall the posterior section of the joint is not very strong, but would resist some dorsoventral movement between the bones.

The anterior portion of the nasal-prefrontal joint is associated with the maxilla-nasal joint. In a lateral view (with the maxilla removed), the lateral wing of the prefrontal can be seen to overlap about a third of the lateral wing of the nasal (Figures 16, 17, 18). The dorsal portion of this overlap is a 'recessed scarf' joint (Figure 16) but more ventrally the abutting wall on the nasal diminishes so that

the contact more closely resembles a lap joint (Figure 16). At this same point in DGPC1, two small projections (tabs) from the nasal facet increase the overlap distance. Ventral to this, the edge of the prefrontal bears a medially directed fold on to which an expanded foot-like part of the nasal process sits, effectively overlapping the prefrontal and producing a small anteroposteriorly directed butt joint. The ventral tips of the nasal and prefrontal lateral facets barely touch.

The naso-prefrontal joint, although complicated, does not appear strong even when the overlap is substantial. The bone is fairly thin and unbuttressed, and some of the detail may be subject to intraspecific variation. Nevertheless the joint would obstruct downward movement of the nasal relative to the prefrontal and lateral rotation of the posterior end of the nasal. Consequently, the joint would also obstruct upward movements of the prefrontal and medial rotation of its posterior end. Anterolateral and posteromedial movements along the joint would also be inhibited (at least in DGPC1). It would not prevent upward or medial movement of the nasal and correspondingly neither would it prevent downward or lateral movement of the prefrontal.

Maxilla-septomaxilla

In *Sphenodon* the septomaxilla is a small curved bone. Its posterolateral surface rests against the dorsomedial edge of the maxilla at the base of the nares (e.g., DGPC1, LDUCZ x036).

Premaxilla-septomaxilla

A small anterior portion of the septomaxilla rests against the dorsal surface of the premaxillary lateral process. No obvious facet can be found on either bone.

Vomer-septomaxilla

The anterior portion of the vomer has a dorsally expanded lateral edge. The anterior border of this raised edge bears a C-shaped embayment, making a hook-like process that accepts the anteromedial end of the septomaxilla or at least soft tissue associated with it (Figure 19).

Maxilla-nasal

The external seam of this joint occurs between the lateral part of the nasal and the anterodorsal edge of the facial process of the maxilla. In lateral view the posterior part may initially be directed anteriorly but after a short distance it turns

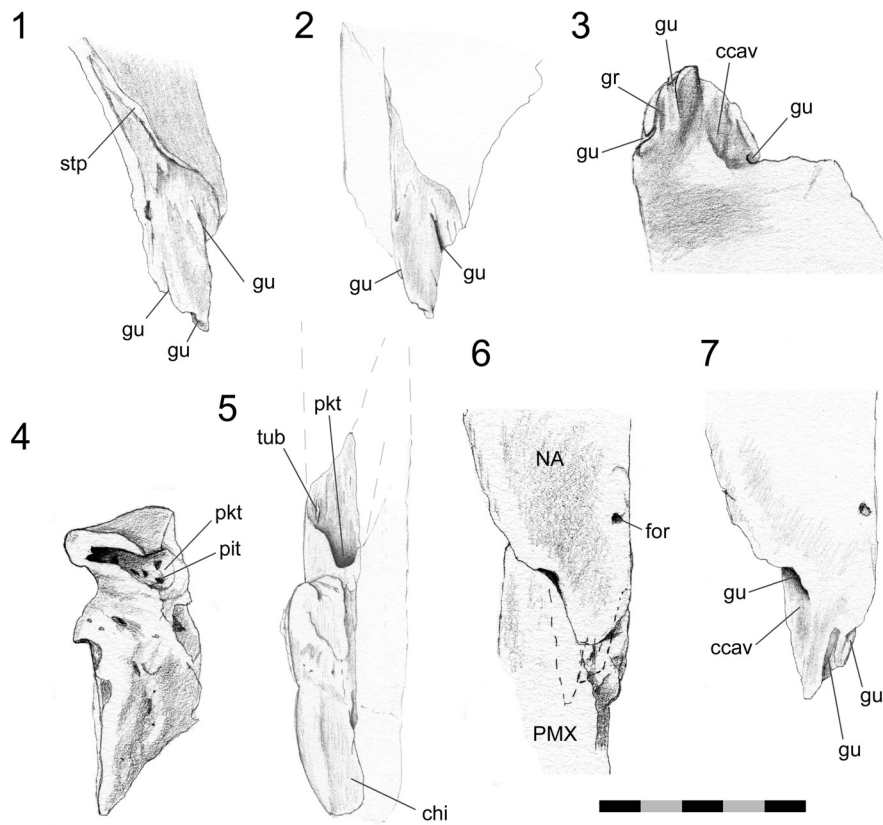


FIGURE 12. Premaxilla-nasal joint in specimen DGPC1. 1. anterior tip of the left nasal in anteromedial view. 2. dorsal, 3. ventral, 4. posterodorsal, 5. posterior view, 6. the left premaxilla and nasal in articulation in posteroventral view from DGPC1, 7. The anterior tip of the left nasal in posteroventral view without the premaxilla (DGPC1). Scale bar equals 5 mm.

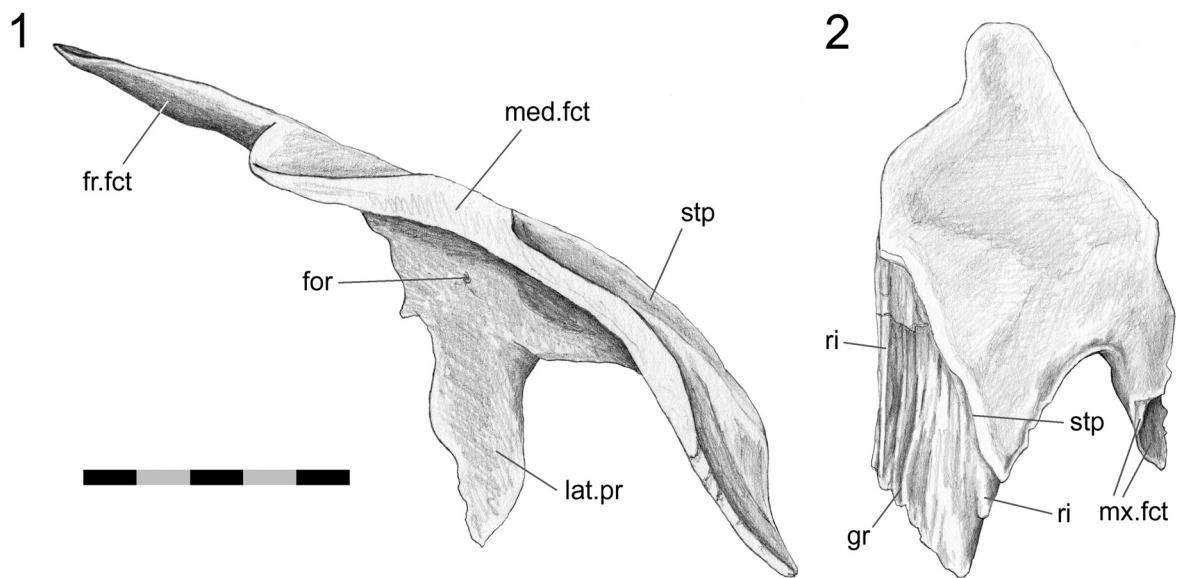


FIGURE 13. Isolated nasal bone (specimen BMNH.K). 1. lateral, 2. anterior views. Scale bar equals 5 mm.



FIGURE 14. Variation of internasal seam length 1. LDUCZ x723. 2. LDUCZ X721. Both in anterodorsal view with seams outlined in black. Scale bar equals 5 mm.

ventrally as the facial process curves toward the base of the naris (e.g., Figure 5).

As described above, the long ventrolateral process of the nasal is partly overlain by the prefrontal but the remaining part of the faceted process is overlain by the facial process of the maxilla (Figures 17, 18). Hence, the variation in the degree and shape of the maxilla-nasal contact is related to that found in the prefrontal-nasal overlap, for example in DGPC1 the maxilla-nasal contact is greatest ventrally whereas in YPM 11419 it is more evenly distributed. Anterodorsally there is also a slot arrangement peripheral to the main overlap (Figure 17.3). Here a short but wide, posteriorly-directed projection from the nasal slots into a dorsoventrally directed groove on the anterior edge of the maxilla facial process. This arrangement results in a triple overlap, from the medial to lateral surface: nasal-maxilla, maxilla-nasal, nasal-maxilla. In a lateral view of DGPC1, with the maxilla removed, the lateral surface of the nasal is slightly recessed compared to that of the prefrontal (Figure 17.3), creating a dorsoventrally orientated trough. Correspondingly the anterior portion of the facial process has a medial bulge. The maxillary facet of the nasal bears parallel striations directed posterovertrally but similar striations are not obvious on the medial facet of the maxilla. This joint restricts anterior movement of the maxilla and to some extent would restrict lateral or medial rotation of the tooth row. Posteroventral movement of the maxilla is not prevented by this joint alone.

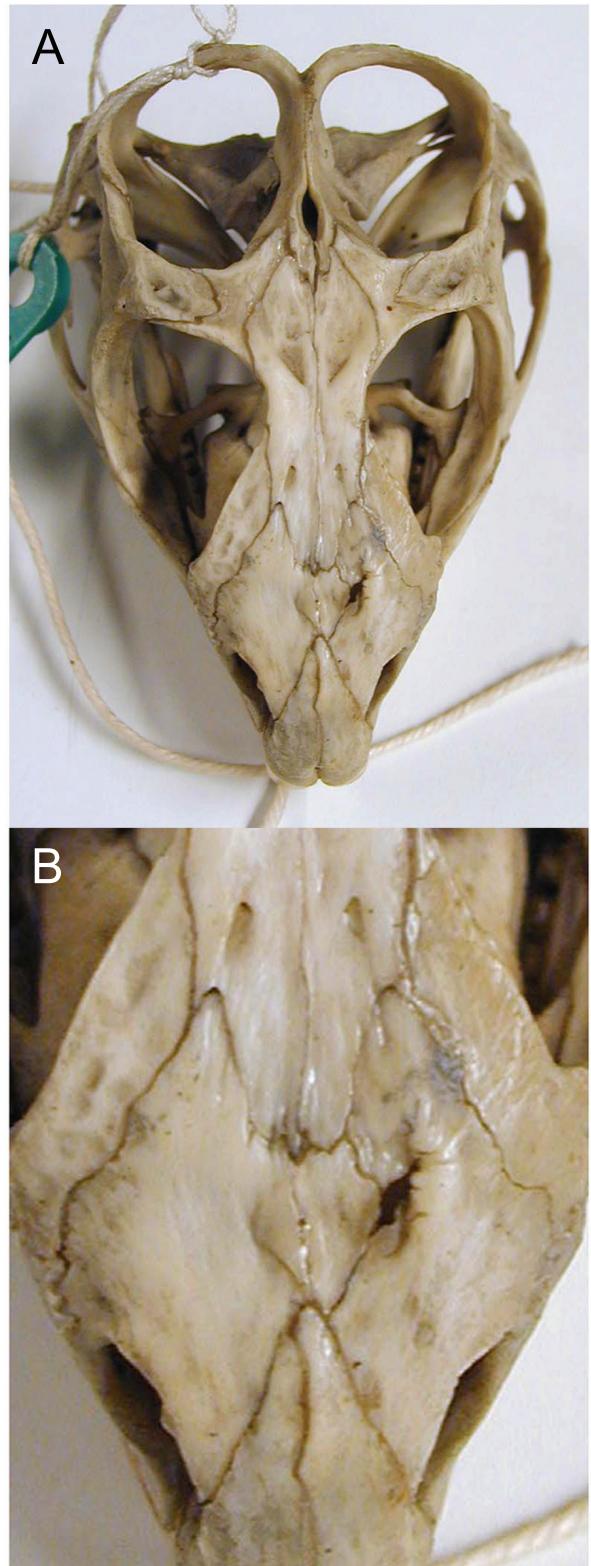


FIGURE 15. Skull (BMNH 1985.1212) with a pathology on the left nasal. 1. anterodorsal view. 2. close up of the snout. Skull length approximately 59 mm.

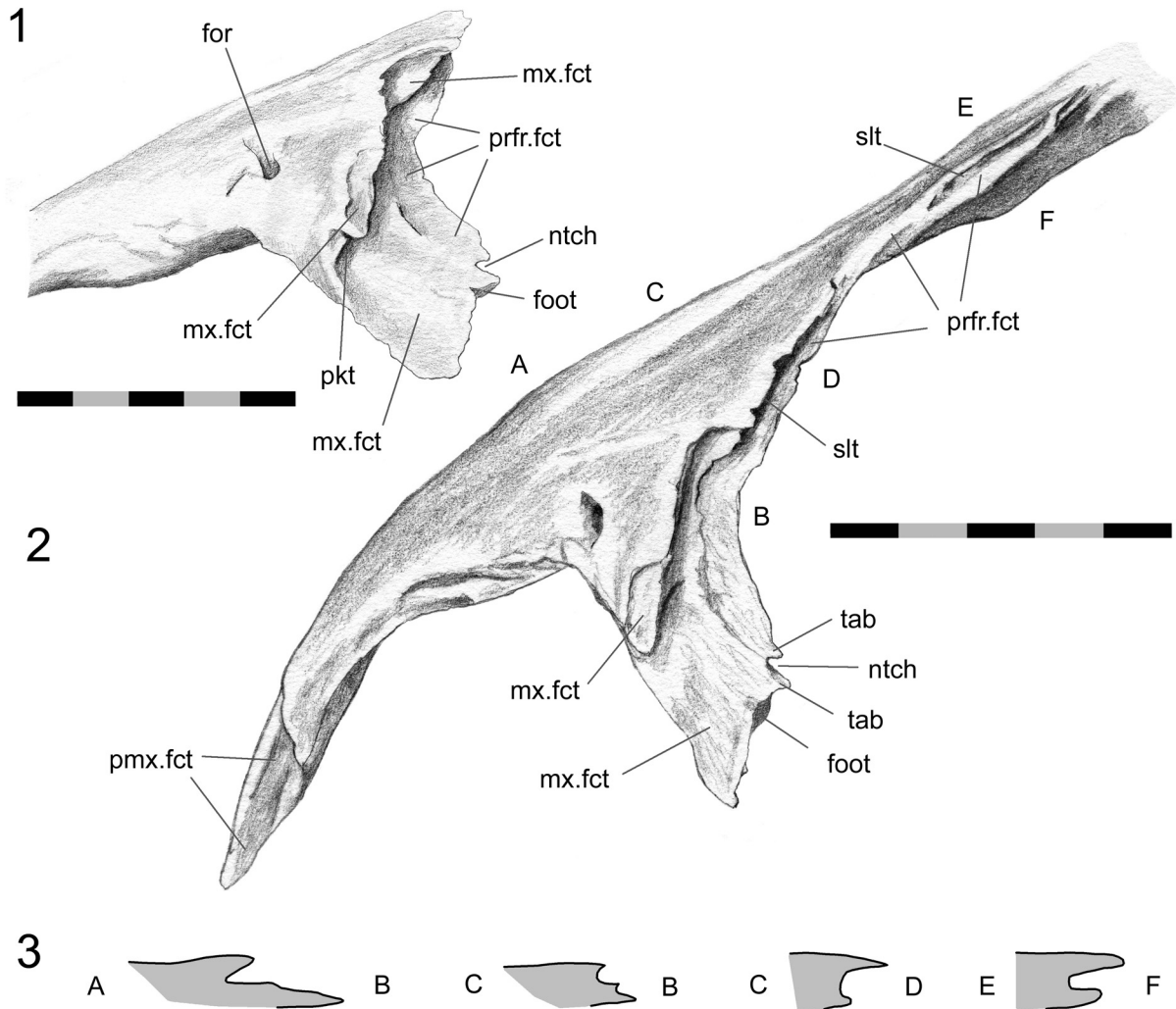


FIGURE 16. Left nasal (DGPC1). 1. dorsolateral, 2. lateral view. 3. schematic representations of the facet profile as seen in section between the points A, B, C, D, E and F. Scale bar equals 5 mm.

Maxilla-prefrontal

There are two points of contact between the maxilla and prefrontal, one on either side of the large foramen with a sloping ledge that accommodates the lacrimal canal. The most anterior seam begins at the anterior margin of the lacrimal foramen and follows the curved, but occasionally crenulated, outline of the facial process of the maxilla until it reaches the nasal. The second more posterior seam is essentially straight and runs between the posterior margin of the lacrimal duct and the junction with the palatine.

The anterior contact involves a large lateral facet on the prefrontal, which is overlapped by the majority of the facial process of the maxilla (Figures 17, 20). As mentioned above the prefrontal itself overlaps a portion of the nasal lateral facet and hence contributes to a triple bone overlap at this junction, although the skull is not exceptionally thick here. The prefrontal's lateral facet has anteroventrally directed striations, and one of these ends in a foramen. Similarly orientated, but less obvious, striations are visible on the facet of the maxilla (Figure 20). These internal striations parallel the anteroventrally directed grooves that can sometimes be seen on the external surface of the

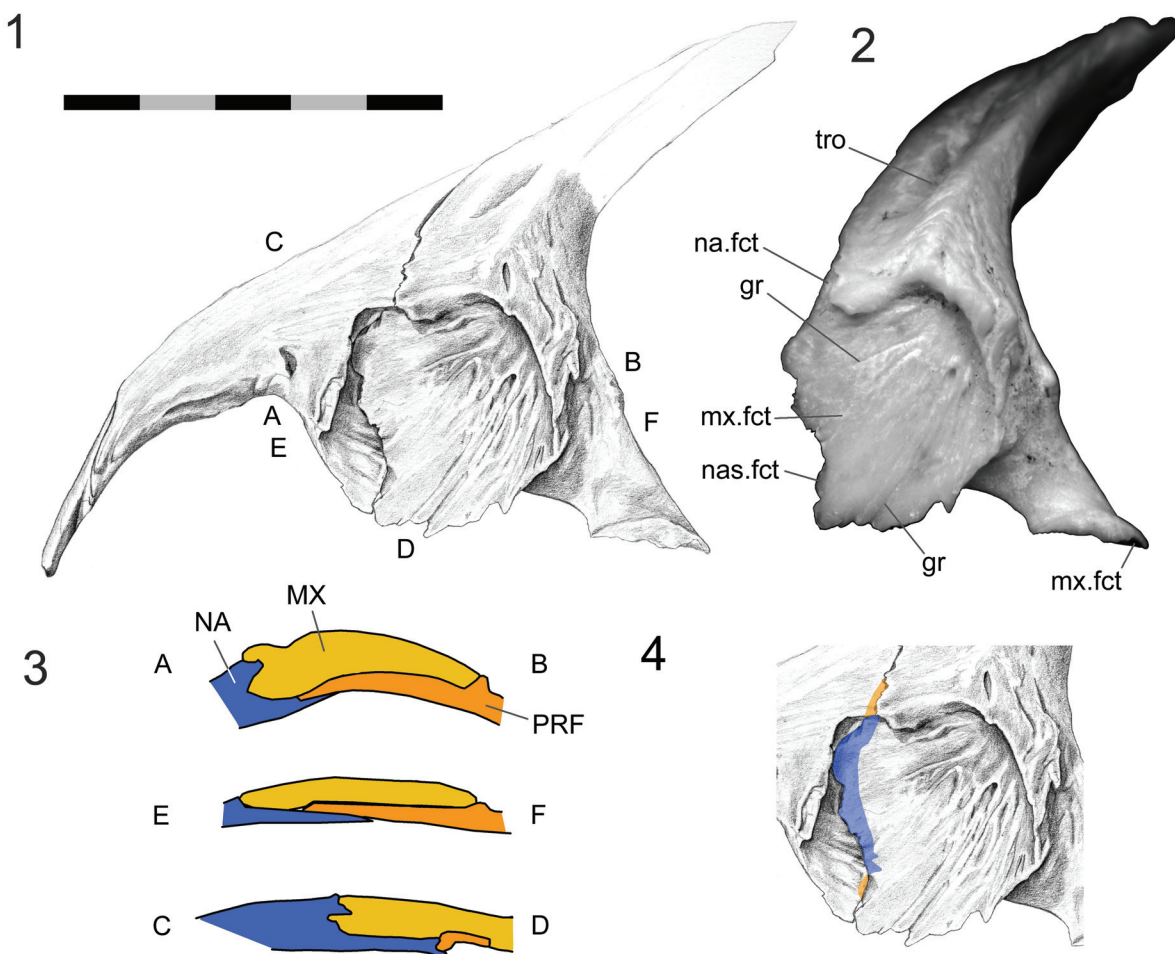


FIGURE 17. Prefrontal-nasal joint (DGPC1). 1. left nasal and prefrontal in articulation showing the combined maxillary facet. 2. lateral process of the prefrontal in lateral view. 3. schematic cross-sections across the nasal-prefrontal-maxillary facial process complex. Numbers correspond to the position of the cross-sections. Blue = nasal, orange = prefrontal, gold = maxilla. Scale bar equals 5 mm.

facial process of the maxilla. The ventral margin of the lateral facet (prefrontal) is dentate (Figures 17.1, 21.1), bearing planar triangular projections which fit into corresponding depressions and recesses on the medial surface of the maxilla (Figures 20, 21.1). The posterodorsal margin of the prefrontal facet is a deep wall which abuts and may occasionally overlap the dorsal margin of the maxilla very slightly. The external seam may also appear “slightly interdigitated” (*sensu* Herring 1972, figure 1). In cross-section the joint most closely resembles a ‘stepped joint’ (Figure 2.3) but the seam’s morphology and facet texture in some individuals also indicates some subtle Type-B interdigitation. This joint would prevent the facial process of the maxilla from rotating medially and would also restrict any posterodorsal movement.

The posterior maxilla-prefrontal joint involves the posteroventral process of the prefrontal, which is associated with the maxilla-palatine and prefrontal-palatine joints (Figure 21). The ventrolateral edge of this process sits in a short groove on the dorsal surface of the maxilla just behind the facial process. The surface of the groove is not smooth in DGPC1 but bears two tubercles and two foramina (Figure 21.2). The groove is bounded medially by a small ridge (Figure 22). The fit is not tight and so may involve substantial soft tissue.

Premaxilla-vomer

The right and left premaxilla-vomer joints can effectively be treated as a single horizontal joint between the paired premaxillae and paired vomers. The posterior surface of the conjoined premax-

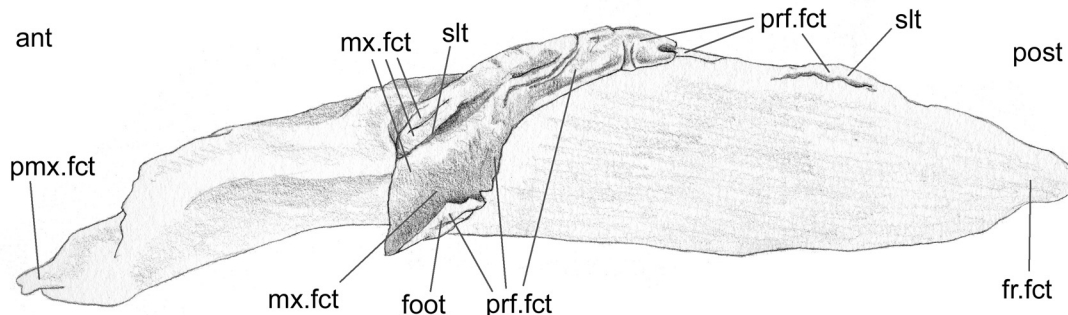


FIGURE 18. Left nasal in ventrolateral view (DGPC1). Scale bar equals 10 mm.

illae, cleaned of soft tissue, bears little evidence of its relationship with the vomers (e.g., DGPC1, DGPC2), and no facet is visible. The anterior end of each vomer bifurcates into two prongs but can be separated from the premaxilla by a notable distance (occasionally equal to the width of the vomerine anterior process e.g., NMNZ RE0385) (Figure 23.1). However, as seen in uncleaned skulls (e.g., LDUCZ x343, LDUCZ x1176) and CT data (YPM 9192), the posterior surfaces of the premaxillae and anterior tips of the vomers are connected by a thick sheet of soft tissue (Figure 23.2). This observation demonstrates the problems associated with inferring soft tissue from fossils. Each vomer also has a more posteriorly placed lateral prong that articulated with the small septomaxilla.



FIGURE 19. Vomers in ventral view (UMZC 2612). Scale bar equals 5 mm.

Palatal Joints

This palatal unit is the largest in the skull and is linked to the rostral unit by the paired maxillae, prefrontals and vomers, to the roofing unit by the prefrontals and to the temporal unit by the jugals and pterygoids.

Vomer-palatine

The anterior tongue-like edge of the palatine overlaps the posterodorsal surface of the vomer (Figure 24). The facet on the vomer is scarfed with the slope directed anteromedially (Figures 25, 26). The amount of overlap depends on the vomer's posterior extent (which can be seen in ventral view). In some specimens the overlap is small with a vomerine-palatine ventral seam that runs anteromedially from the edge of the choana before turning posteromedially (LDUCZ x343 left; LDUCZ x036, left). In other specimens the overlap is larger where the ventral seam travels medially before turning sharply posteriorly to be parallel with the midline (e.g., LDUCZ x1176); larger again when the entire course is roughly posteromedial (LDUCZ x343; LDUCZ x146; LDUCZ x036, right; LDUCZ x343 right); and most extensive when the seam runs posteromedially before turning posteriorly to reach the junction with the pterygoids (DGPC2, NMNZ RE0385 Jones et al. 2009, figure 3.1). The facet on the vomer also includes a slot or pocket that accommodates the lateral edge of the anterior palatine process. The vomer laps the palatine early in ontogeny when the skull is no more than 6 mm in length (Howes and Swinnerton 1901, skull length = about 5.6 mm; Werner 1962, about 6 mm, 5.4 mm according to Bellairs and Kamal 1981, p. 118).

Vomer-ptyergoid

In *Sphenodon* the anterior tips of the paired pterygoids overlap the posterior ends of the paired

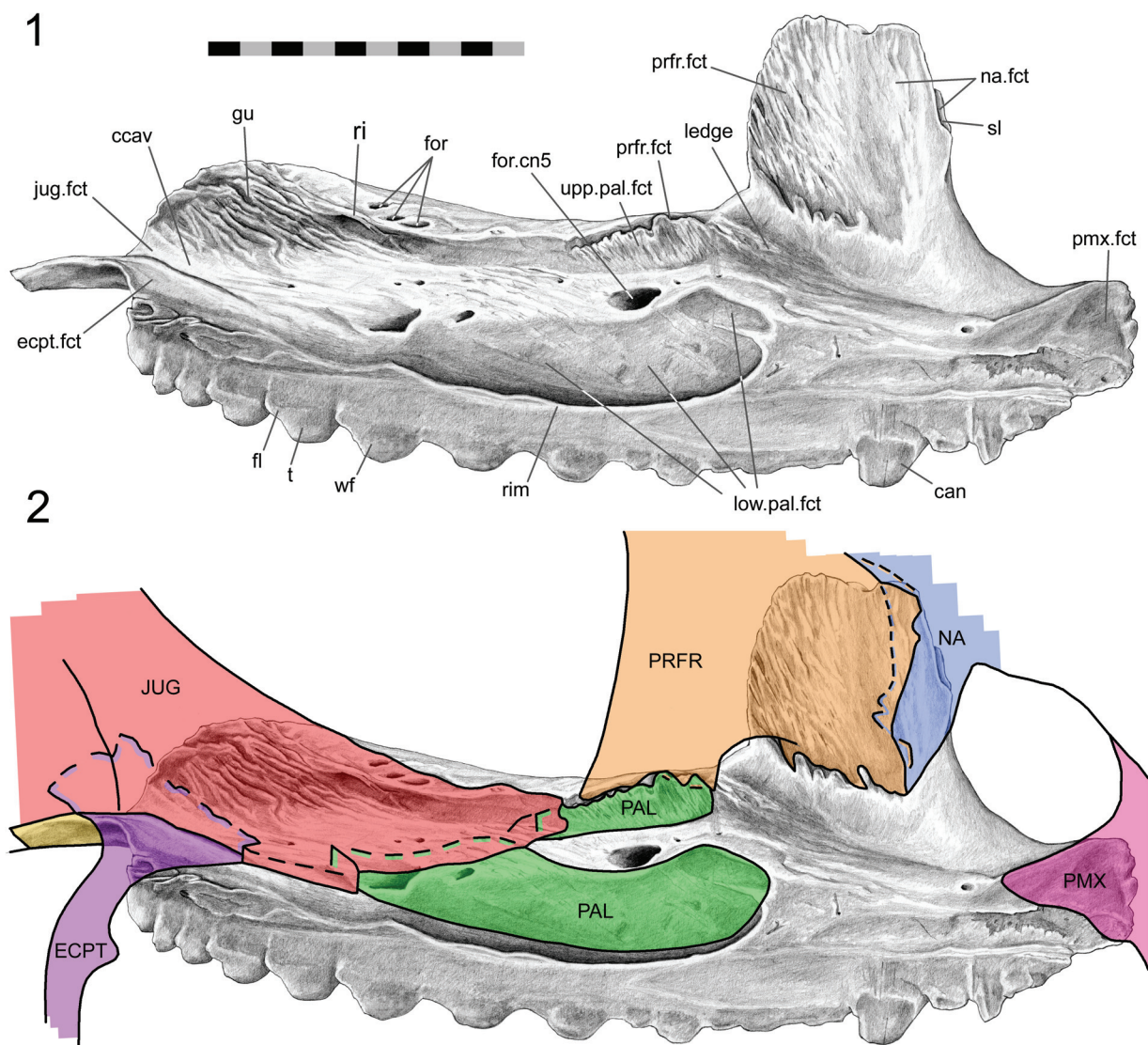


FIGURE 20. Left maxilla (DGPC 2). 1. medial view. 2 medial view overlain with the ghosts of other bones. Pink = premaxilla, blue = nasal, orange = prefrontal, green = palatine, red= jugal, purple = ectopterygoid. Scale bar equals 10 mm.

vomers medially (Figure 25; Jones et al. 2009, figure 3.2). This joint is separated from the vomer-palatine joint by a small ridge of bone (e.g., AIM LH0617; AUP 11883) but the posterior part underlies the palatine-pterygoid joint. In ventral view the vomer and pterygoid are separated by a short seam, which may be parallel to the coronal plane (LDUCZ x143), oblique to the sagittal plane (DGPC2) or 'V' shaped (LDUCZ x036).

Intervomerine

The ventral and dorsal seams for this midline joint are generally straight suggesting a simple butt

joint (e.g., Jones et al. 2009). However, disarticulated material shows that, at least in some cases, it can be more complex. In specimen AIM LH0617, a small anteromedial shelf from the left vomer slots into a groove in the right vomer, centrally the medial edge of the left is overlapped slightly by the medial edge of the right, and posteriorly the medial edge of the right is overlapped by the left (Figure 25). In the central portion of the joint the medial margins of the vomers are dorsoventrally expanded, increasing the contact area between them.

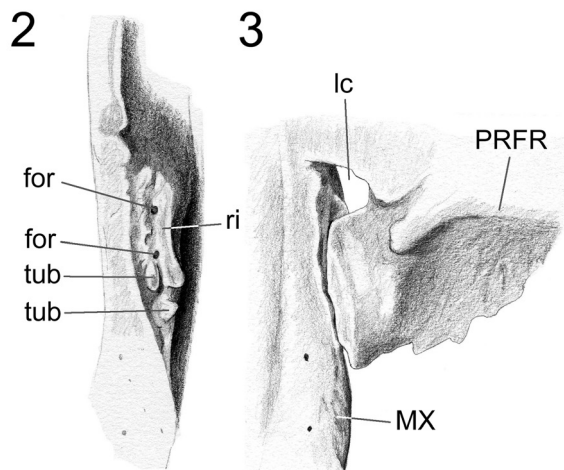
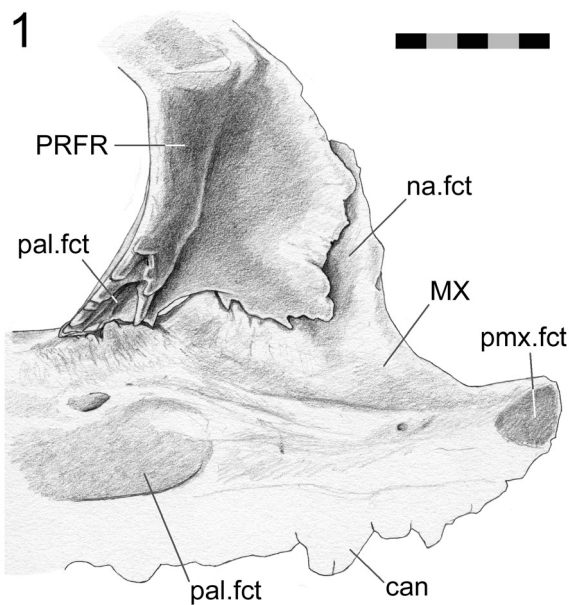


FIGURE 21. Left maxilla-prefrontal joint (DGPC1). 1. in articulation viewed in medial view. 2. facet for the prefrontal on the dorsal surface of the maxilla. 3. maxilla and prefrontal articulated in dorsal view. Scale bar equals 55 mm.

Prefrontal-palatine

As previously reported the ventral process of the prefrontal meets the palatine with a wide joint (Bolt 1974). Viewed in posterodorsal aspect (through the orbit) this seam travels from its junction with the maxilla in a primarily dorsomedial direction. It is often interdigitated (e.g., LDUCZ x036) although not always (e.g., DGPC 2). Isolated bones demonstrate that this joint is extremely complex (Figures 27, 28). The anterolateral end of the palatine bears a facet facing posterodorsally at an

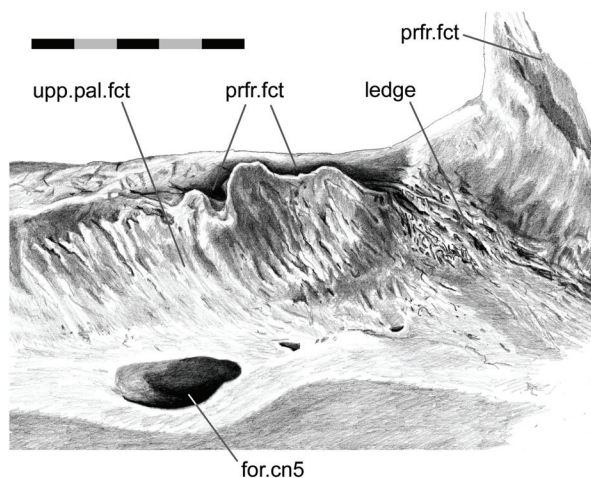


FIGURE 22. Close up of the maxilla (DGPC1) in medial view showing the site for articulation with the posterior end of the prefrontal and for the upper part of the lateral palatine process. Scale bar equals 5 mm.

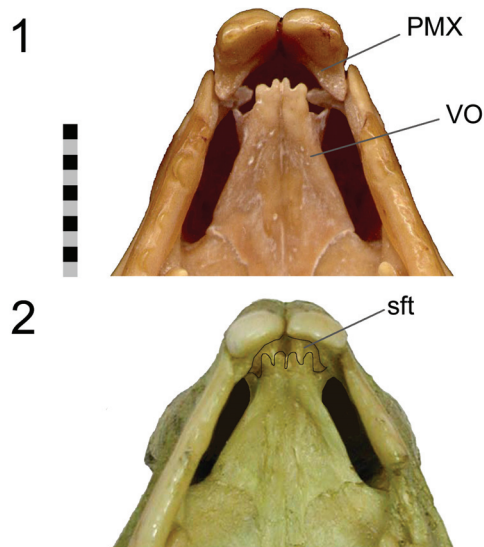


FIGURE 23. Premaxilla-vomer joint. 1. NMNZ RE0382 cleaned of vom-pmx soft tissue. 2. UMZC 2582 with soft tissue present. Scale bar equals 10 mm.

angle of approximately 45° from the horizontal plane (level with the long axes of the maxillary tooth rows) (Figure 28). The posterior edge of the facet is recessed with a stepped (Figure 2.3) and jagged (zig-zagged) border (Type-B interdigitation, Figure 2.4). The posterior process of the prefrontal sits in this sloping depression with a broadly corresponding posterior edge (Figure 27.1, 27.2). The anterior part of the facet on the palatine is also jagged, and this sits against a step on the underside of the prefrontal (Figure 27.6, 27.7). Visible in

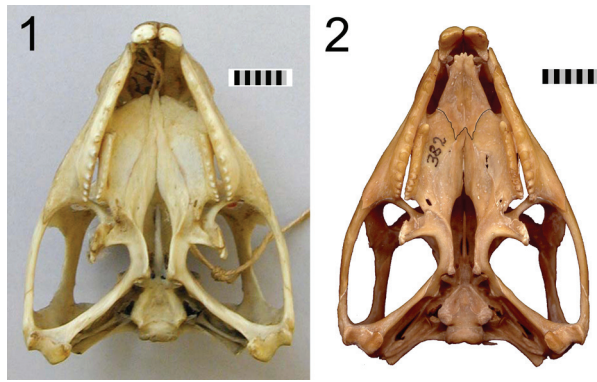


FIGURE 24. Vomer-palatine joint. 1. skull (OMNH 908) without vomers in place. 2. skull (NMNZ RE0382) with vomers present and vomerine-palatine seam outlined in black. Scale bar equals 10 mm.

anteroventral view, a process from the prefrontal sits in a notch on the palatine medial to three projections from the latter (Figure 27.6, 27.7). The ventrolateral part of the ventral process of the prefrontal (that articulates with the maxilla) wraps around the palatine to form a longitudinal slot (Figure 27.6, 27.8). The facet on the prefrontal is somewhat striated laterally (Figure 27.8).

The prefrontal would be restrained from moving anteroventrally or medially and the palatine from moving posterodorsally or laterally. This joint would also stop the lower end of the prefrontal rotating anteriorly and the medial edge of the palatine from rotating laterally. The interlocking processes are not tight and would therefore allow some movement but the arrangement would provide a large surface area for soft tissue in many

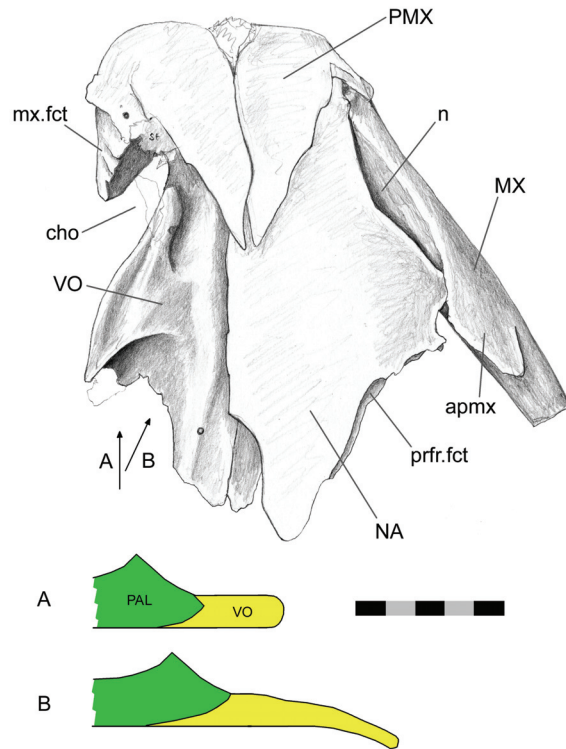


FIGURE 26. Partially articulated rostrum (BMNH.K) in dorsal view that demonstrates the facet on the vomer for the palatine. Schematic cross-sections (A and B) through the palatine-vomerine joint are also shown. Scale bar equals 10 mm.

potential orientations. Overall this joint could be described as a stepped overlap with some Type-B interdigitation but some of the interlocking parallel

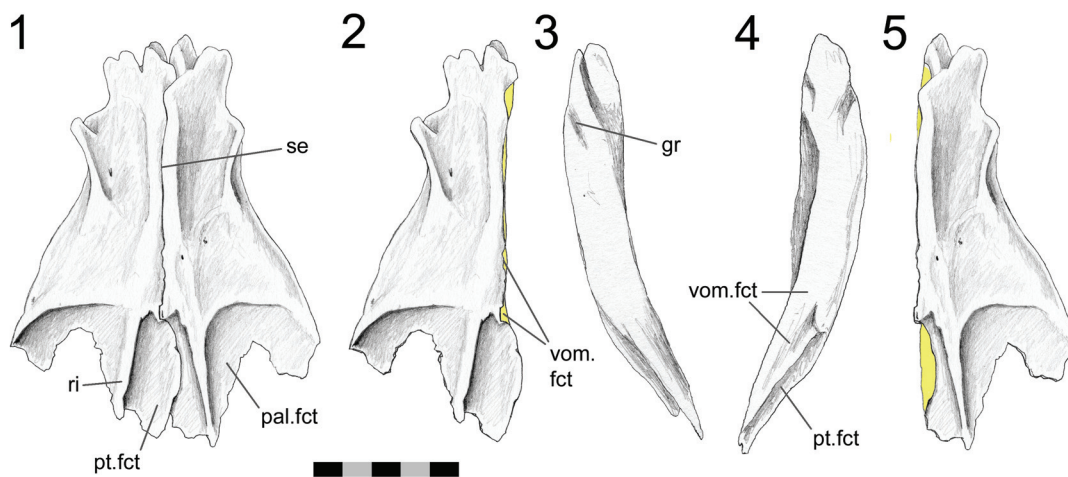


FIGURE 25. Intervomerine joint (AIM LH0617). 1. articulated vomers in dorsal view. 2. left vomer in dorsal view. 3. left vomer in medial view. 4. right vomer in medial view. 5. right vomer in dorsal view. Scale bar equals 5 mm.

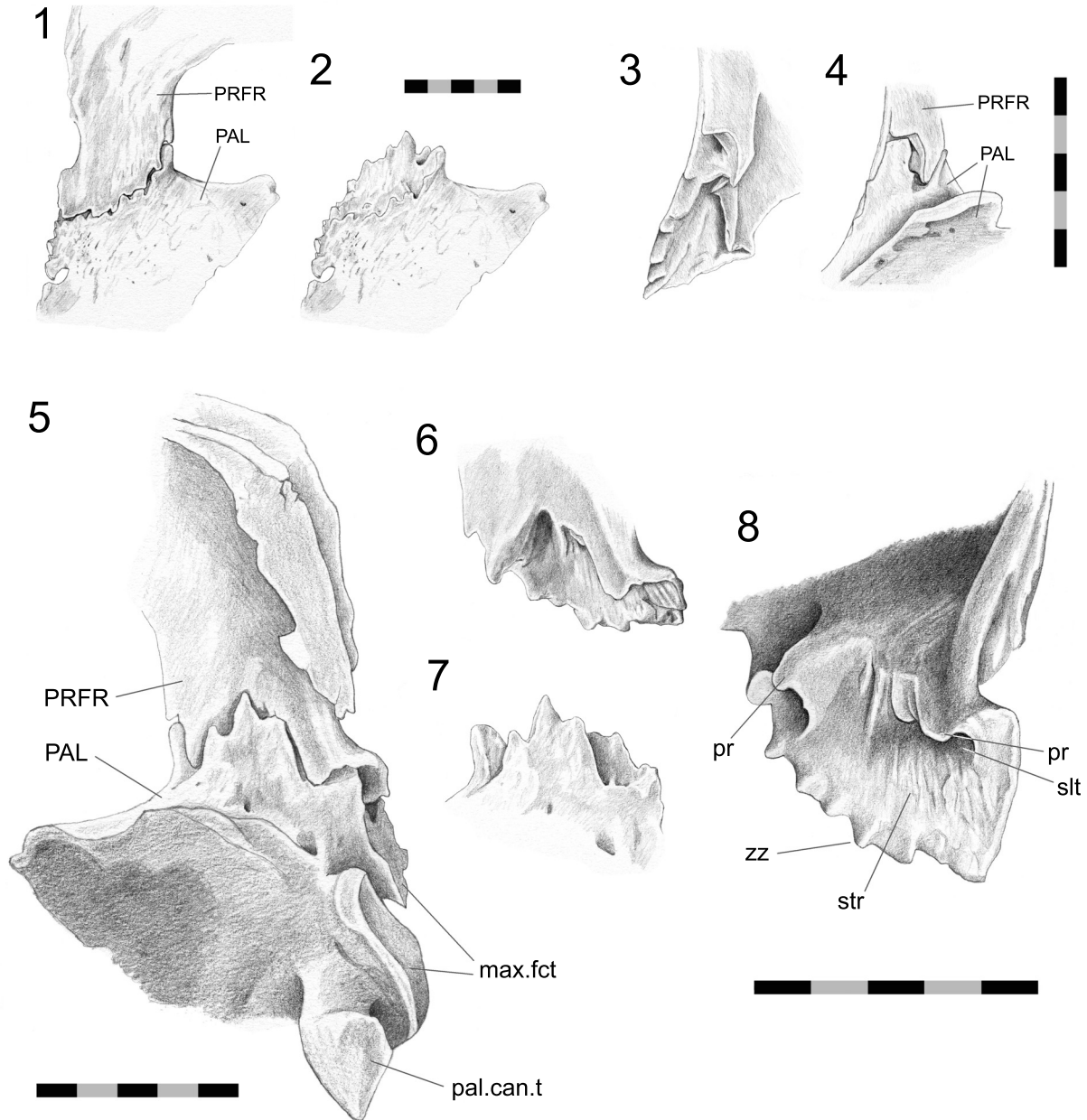


FIGURE 27. Left prefrontal-palatine joint (DGPC1). 1. in articulation and in posterodorsal view. 2. left palatine facet for the prefrontal in posterodorsal view. 3. ventral process of the left prefrontal in medial view. 4. left prefrontal and palatine in articulation and in medial view. 5. left prefrontal and palatine in articulation and in anteroventral view. 6. ventral process of the left prefrontal in anteroventral view. 7. facet on the left palatine in anteroventral view. 8. ventral process of the prefrontal in anteroventral view. Scale bar equals 5 mm.

to the bone surface also resembles a slot joint or Type-A interdigitation.

Maxilla-palatine

In *Sphenodon* the palatine has two lateral processes separated by a foramen for the maxillary division of the trigeminal nerve (cranial nerve 5)

and associated blood vessels. This foramen is marked “mf” in Jones et al. (2009, figure 3.2). Both of these processes are involved in the joint with the maxilla (Figures 20, 28, 29).

The upper maxilla-palatine joint is a loose butt contact with some very weak vertical Type-B interdigitation. In lateral view (disarticulated) the upper

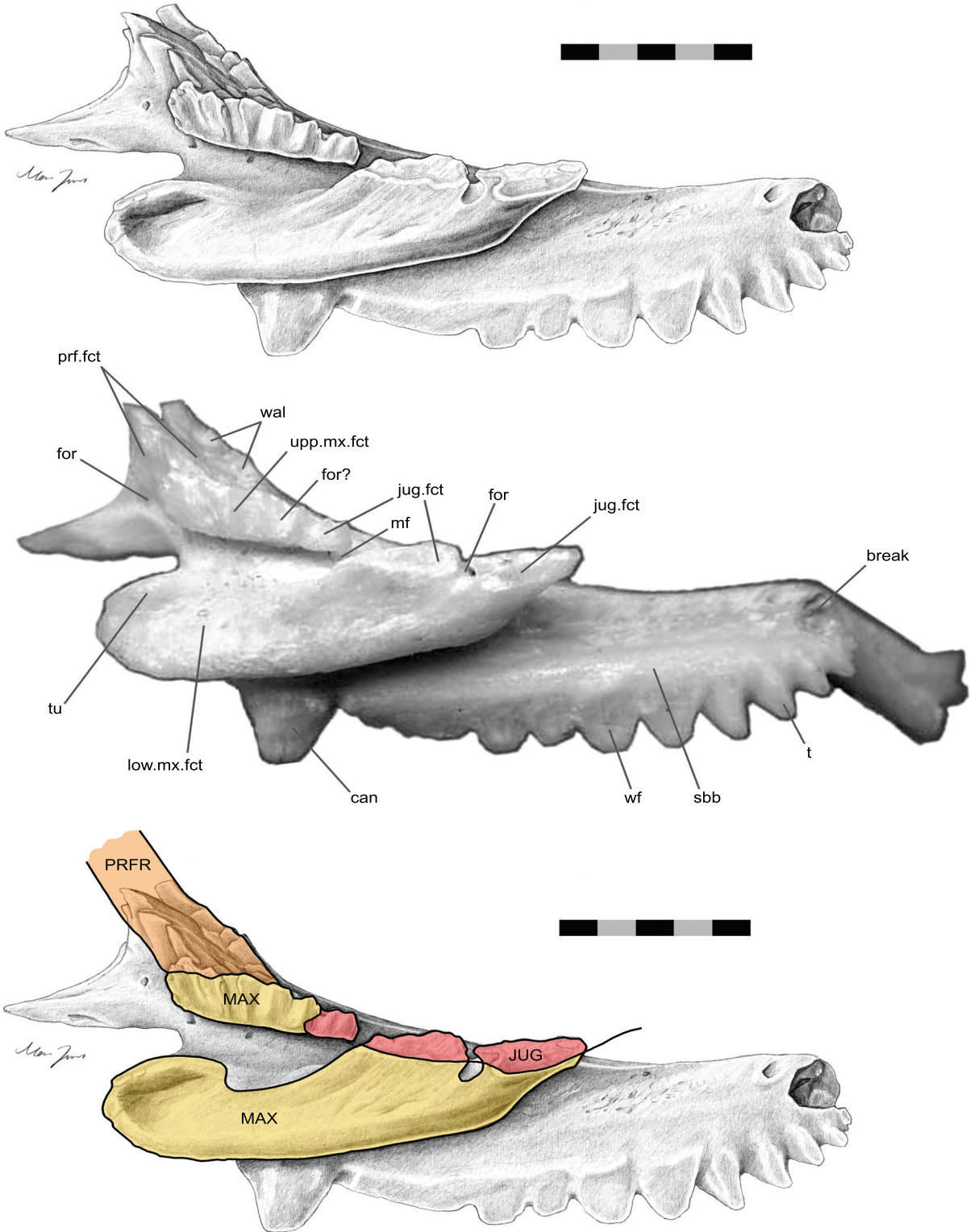


FIGURE 28. Left palatine (DGPC1) in lateral view. Gold = maxilla, orange = prefrontal and red = jugal. Scale bar equals 5 mm.

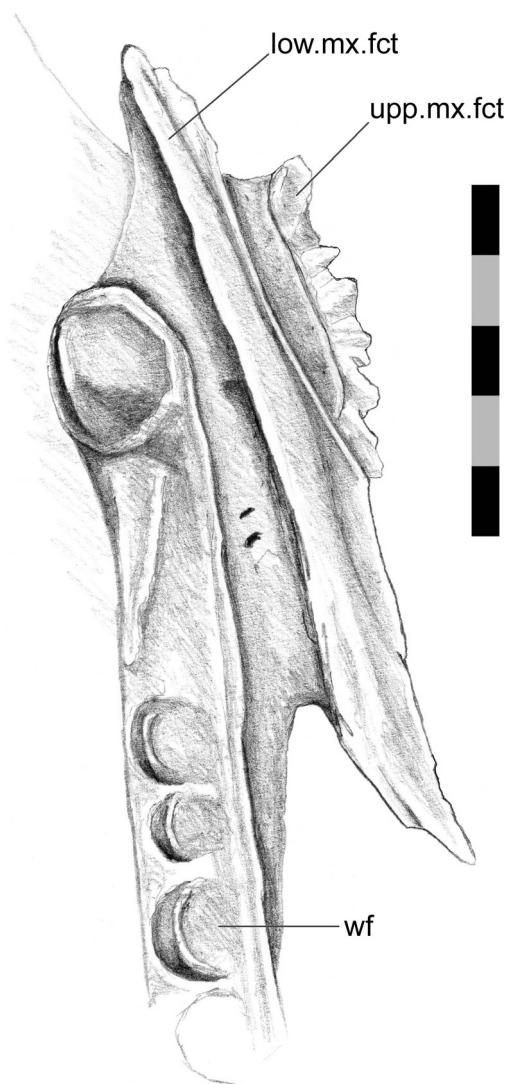


FIGURE 29. Anterolateral corner of the palatine (DGPC1) in ventral view. Scale bar equals 5 mm.

process of the palatine is rectangular and fluted, in DGPC1 this comprises five or six ridges which are directed posteroventrally in the anterior part and anteroventrally in the posterior part (Figure 28). Two grooves in this fluting probably relate to the presence of foramina. The corresponding facet on the maxilla for the upper lateral process of the palatine bears subtle anteroventrally directed striations (Figure 22). These striations are not obviously reflected on the palatine's maxillary facet.

The lower maxilla-palatine joint is primarily a loose butt joint. The lower lateral process of the palatine stems from a point above the anterior half

of the palatine tooth row (Figure 29). It expands anterolaterally and posteriorly to form a large process with an anterolaterally facing ovoid facet. This broad facet sits loosely against a depression in the maxilla almost dorsal to the maxillary tooth row so that the majority of the facet is orientated in between the long axis of the maxilla and long axis of the maxillary tooth row (Figures 5, 30). Ventral to the facet on the maxilla is a trough with a slight rim which is particularly distinct anteriorly (Figure 30). In life the space between the trough and lower palatine process is filled with soft tissue and the joint appears to be very well supported (e.g., LDUCZ x723). There is a distinct lack of sculpture on either the maxilla or palatine for the lower maxilla-palatine joint but anterodorsally the lower facet on the palatine bears a shallow tubercle and depression that corresponds to a depression and ridge on the maxilla (Figures 20, 28). The posterodorsal corners of both palatine processes contact the jugal and are discussed below.

Maxilla-jugal

In dorsal view the seam arcs posterolaterally from the junction with the palatine to the margin of the orbit. In lateral view, the seam is sigmoid: running posteriorly from the edge of the orbit, turning first posteroventrally and then posteriorly again along the base of the lower temporal bar. In ventral view the seam is 'V'-shaped, running posteromedially and then anteromedially before meeting the ectopterygoid.

The jugal slots into a long concavity in the maxilla that broadens posteriorly and is bounded laterally by the sub-orbital margin (Figure 30). The long axis of the cavity is directed anteromedially but it is asymmetrical with a greater lateral component. At the posterior end of the concavity the lateral wall flexes medially and then laterally thus producing a longitudinal ridge (Figure 20) that slots into a wide groove along the lateral surface of the jugal (Figure 31). The ridge and groove are less pronounced in LDUCZ x1176 than in DGPC1 (Figure 32). Posteriorly this ridge has a rugose surface with convoluted striae and gutters directed anterodorsally, anteriorly and anteroventrally. Anteriorly the ridge is more sharply defined (at least in DGPC1) and shelf-like. Above it, anteriorly, there are three distinct slits (elongate foramina) (Figure 20). In dorsal view the base of the maxillary concavity can be seen to possess small gutters that are generally orientated anteromedially, particularly on the lateral side (Figure 30). Correspondingly the maxillary facet of the jugal is roughened, particu-

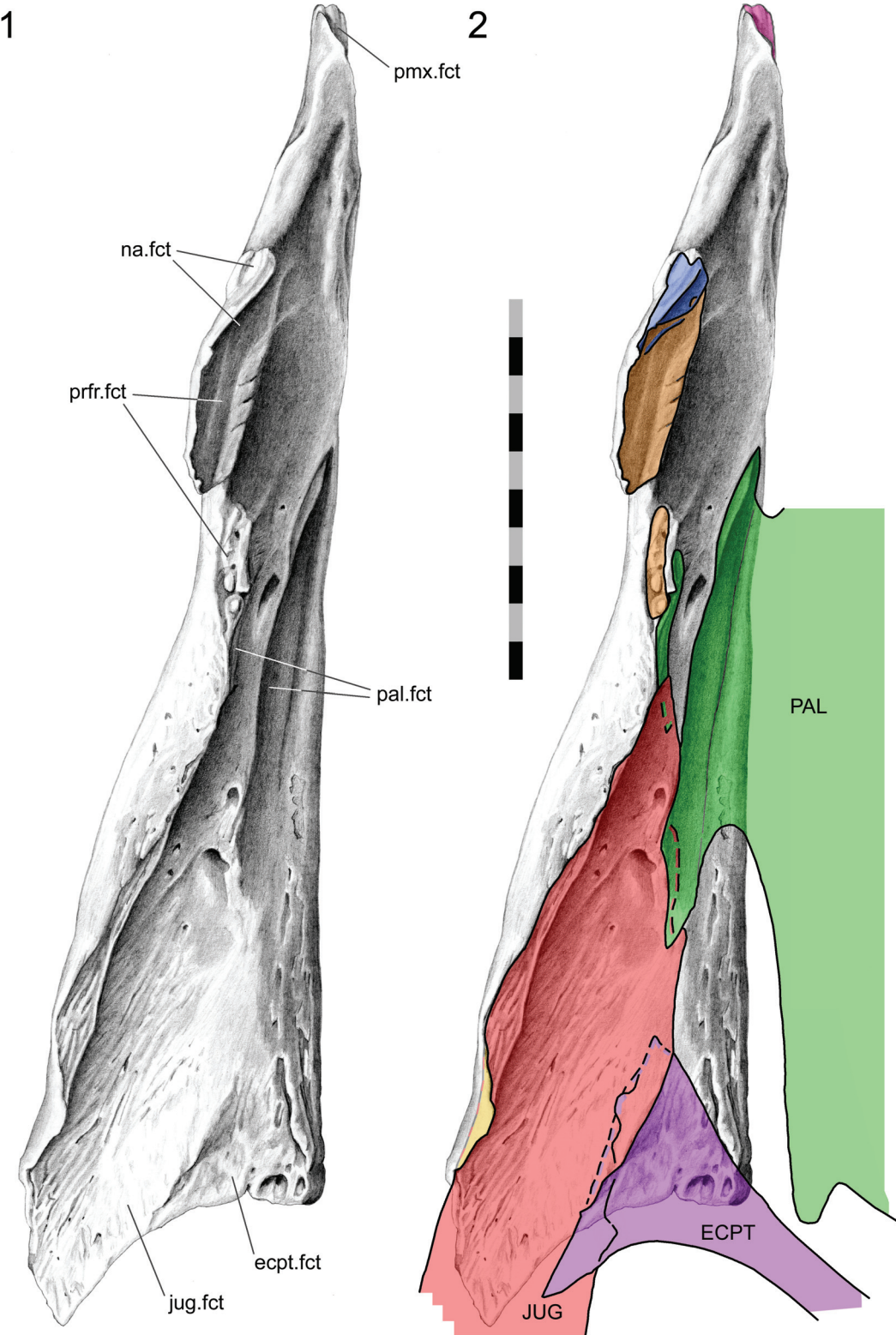


FIGURE 30. Left maxilla (DGPC1). 1. dorsal view. 2. dorsal view overlain with the ghosts of other bones. Pink = premaxilla, blue = nasal, orange = prefrontal, green = palatine, red= jugal, purple = ectopterygoid. Scale bar equals 10 mm.

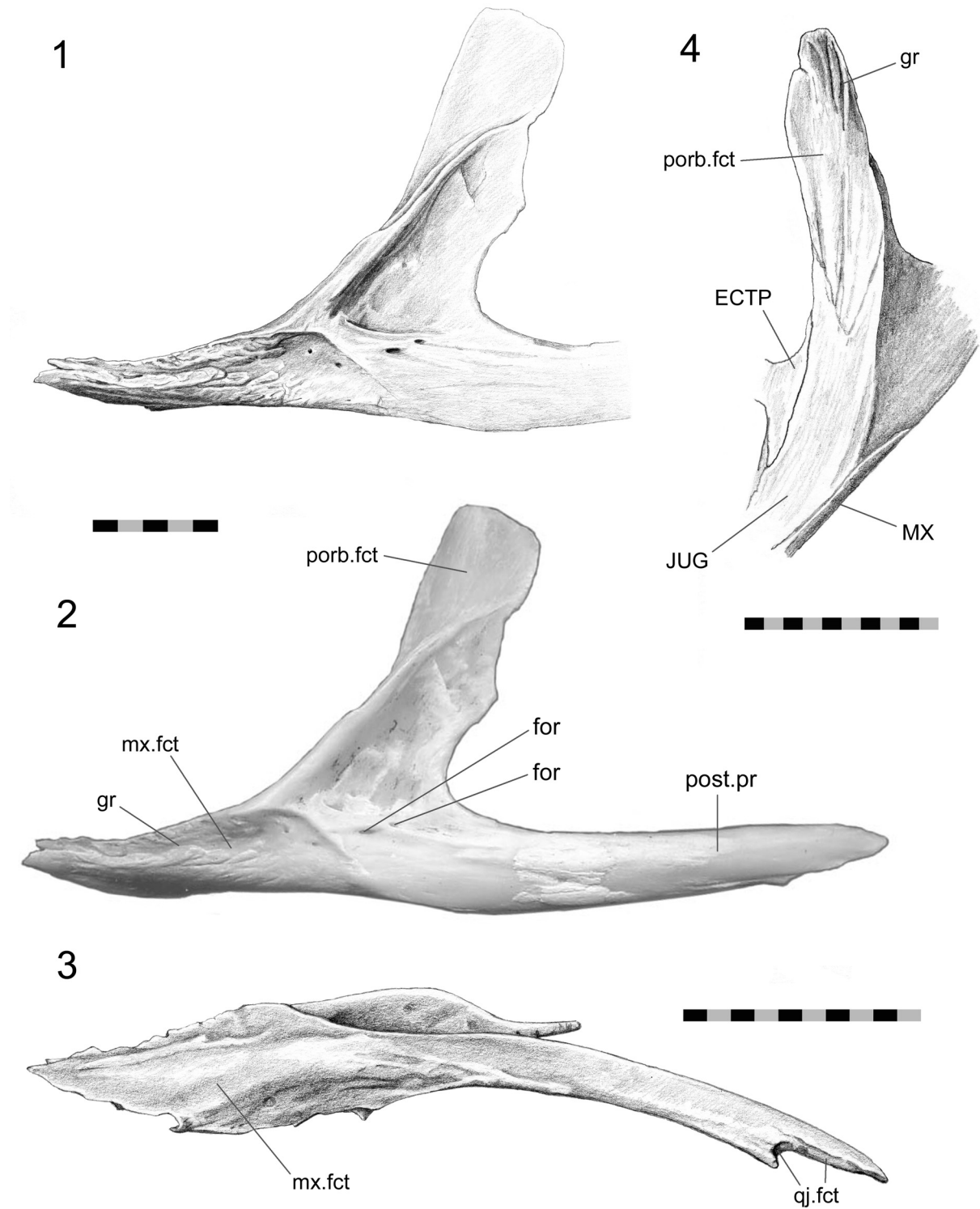


FIGURE 31. Left jugal. 1. Drawing of DGPC1 in lateral view. 2. DGPC1 in lateral view labelled. 3. DGPC1 in ventral view. 4. anterodorsal process of the jugal in LDUCZ x1176 without the postorbital in place. Scale bar equals 5 mm (1), 10 mm (2-4).

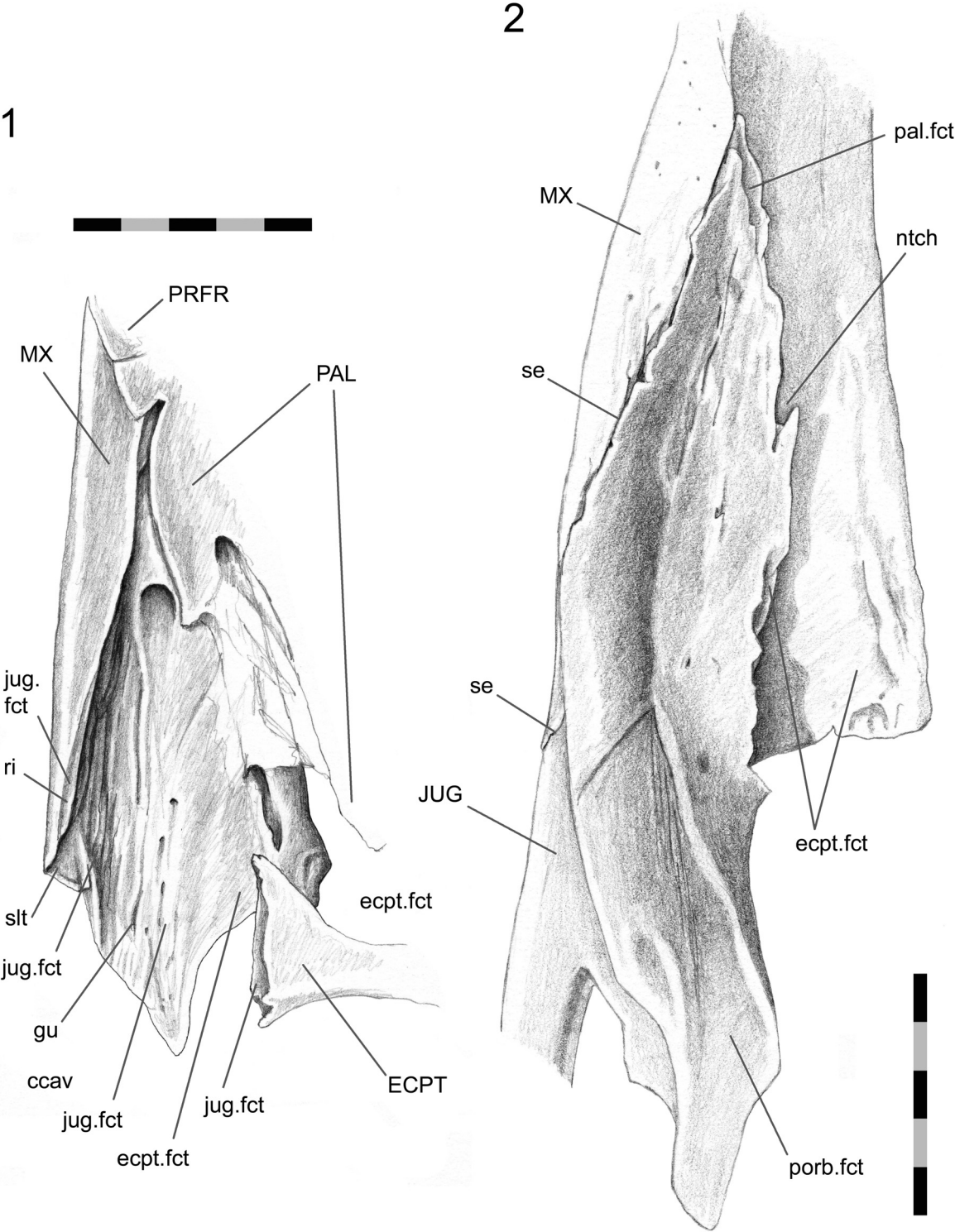


FIGURE 32. Maxilla-jugal joint. 1. skull without the jugal in place (LDUCZ x1176). 2. maxilla and jugal in articulation (DGPC1). Scale bar equals 5 mm.

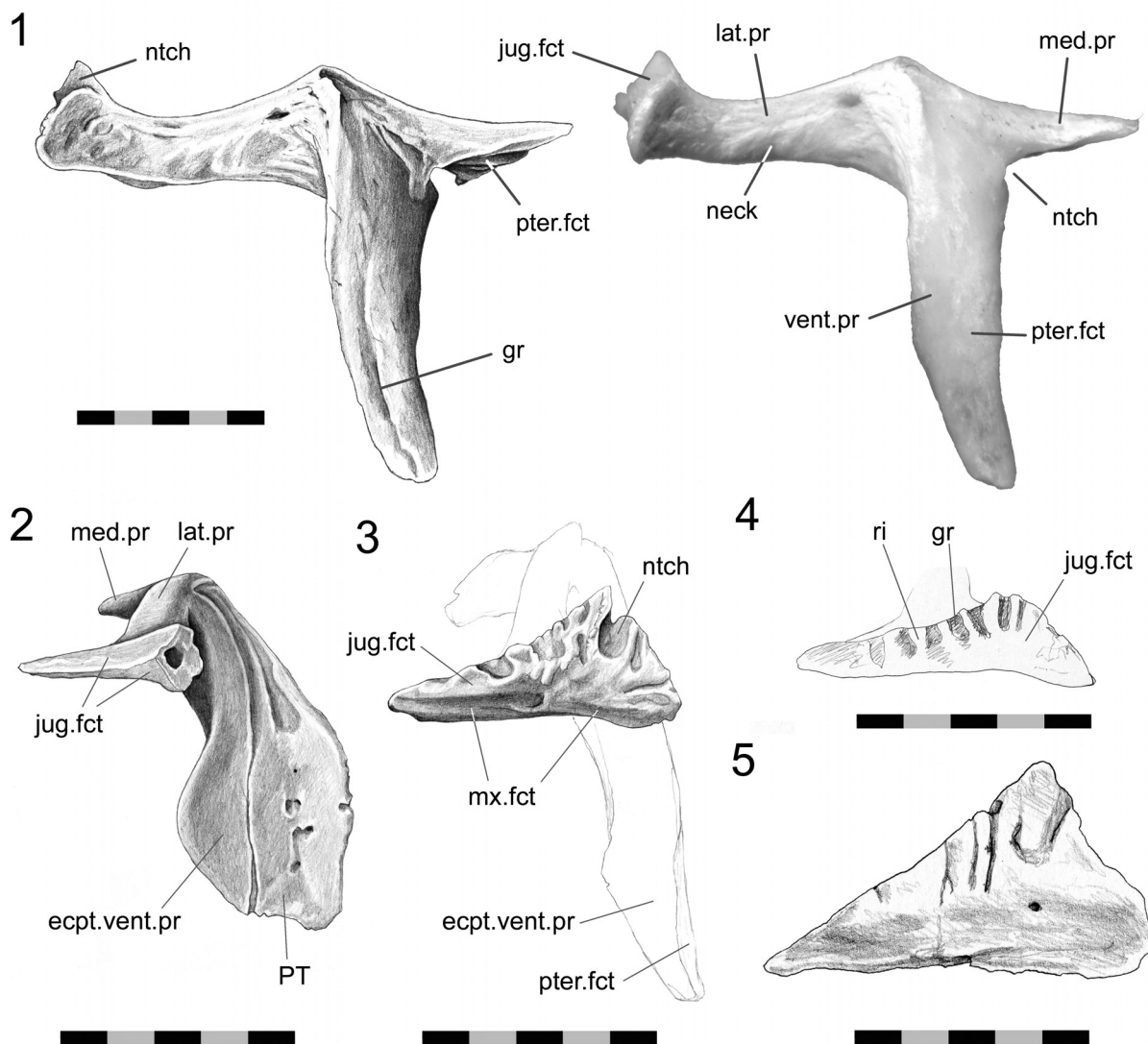


FIGURE 33. Ectopterygoid. 1. posterodorsal view of DGPC1. 2. anterolateral view of LDUCZ x1176 (pterygoid flange also visible). 3. anterolateral view of DGPC1. 4. Anterolateral view of BMNH.K. 5. anterolateral view of AIM LH0671 (reversed for comparison). Scale bar equals 5 mm.

larly in lateral view (Figure 31). The facet also displays several neuro-vascular foramina, some of which are at the anterior end of gutters. Two of these foramina, situated at the anterior end of the concavity, are very large (Figure 30). This joint would prevent anterior, lateral and ventral movement of the jugal and posterior, medial and dorsal movement of the maxilla. In a hatchling (e.g., FMNH 65905) the maxilla overlaps the jugal less extensively (Rieppel 1992).

Jugal-ectopterygoid

The ectopterygoid is a 'T'- shaped bone composed of a long ventral process, a slightly shorter

lateral process and an even shorter medial process (Figure 33). The proximal portion of the lateral process was termed the 'neck' for the fossil rhyngocephalian *Gephyrosaurus* by Evans (1980). The lateral process expands to become two-thirds the width of the neck and ends in a triangular face but there is variation in its exact dimensions as well as the surface texture. The face tends to be shallower in smaller individuals (Figure 33) and the dorsal edge may be ribbed and complex.

This lateral process of the ectopterygoid plugs into a shallow depression on the medial surface of the jugal above the edge of the maxilla-jugal seam (Figure 34). The apex of the facet on the jugal coin-

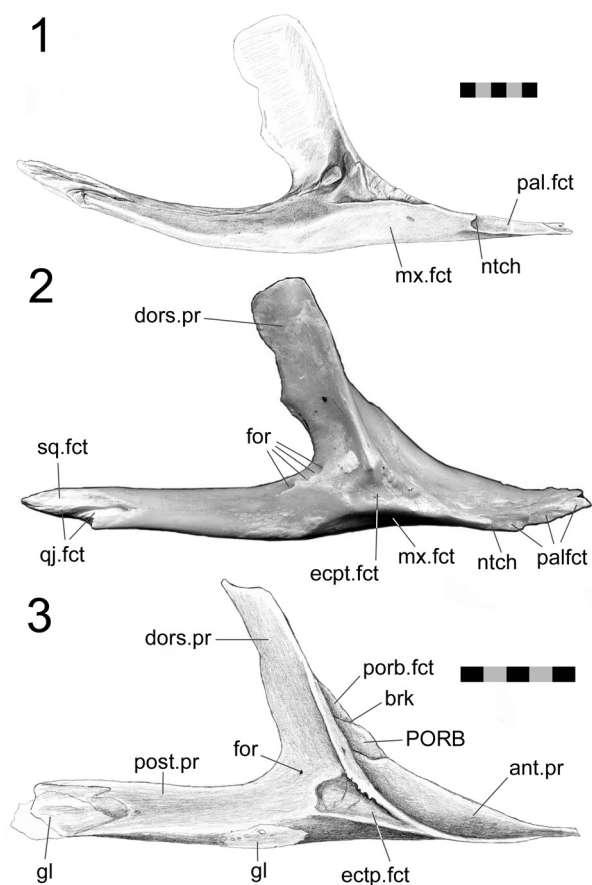


FIGURE 34. Left jugal. 1. DGPC1 in ventromedial view. 2. DGPC1 in medial view. 3. LDUCZ x1176 in medial view. Scale bar equals 10 mm.

cides with the medial ridge of the postorbital bar (Figure 34). In DGPC1, the apex of this facet bears a small process that coincides with a groove on the ectopterygoid. As inferred from seam morphology this feature is also found in DGPC2, LDUCZ x146 (left) but not in LDUCZ x343, LDUCZ x036, or LDUCZ x146 (right). In a dorsal view of the articulated skull, the slightly crenulated seam extends posterolaterally from the anterior junction with the maxilla, and its posterior tip may turn ventromedially (DGPC1; DGPC2; LDUCZ x146, left). In posterior view, the seam passes ventrolaterally before turning ventromedially and meeting the maxilla. The section of seam visible in posterior view may also be interdigitated (e.g., LDUCZ x146, right).

This joint would resist medial and dorsoventral movement of the jugal and conversely lateral and dorsoventral movement of the ectopterygoid. The contact appears strong with a large contact surface relative to the size of the ectopterygoid, anteriorly there is some slight interdigitation.

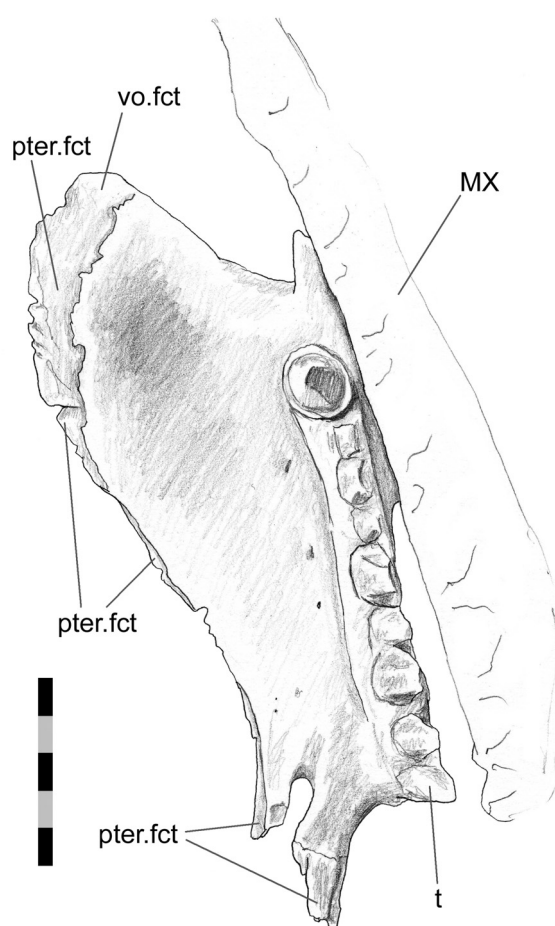


FIGURE 35. Left palatine (DGPC1) in ventral view. Scale bar equals 5 mm.

Palatine-jugal

This joint primarily involves the anteromedial edge of the jugal abutting against the posterodorsal edge of the lower lateral palatine process (Figures 28, 32). In addition the tip of the jugal extends anteriorly beyond the maxillary foramen contacting the upper lateral palatine process (e.g., DGPC1, LDUCZ x723, LDUCZ x343 and possibly LDUCZ x1176) for a relatively short distance. Viewed dorsally, the majority of the seam runs posterolaterally but the posterior extremity of this seam turns medially.

The joint is essentially a perpendicular butt contact resisting medial movement of the jugal and lateral movement of the palatine. However, in DGPC1 (Figures 32.2, 34) the facet on the jugal is slightly concave and, as reflected in the seam, the posterior end of the joint is notched so that the jugal hooks behind the palatine (Figure 32). This

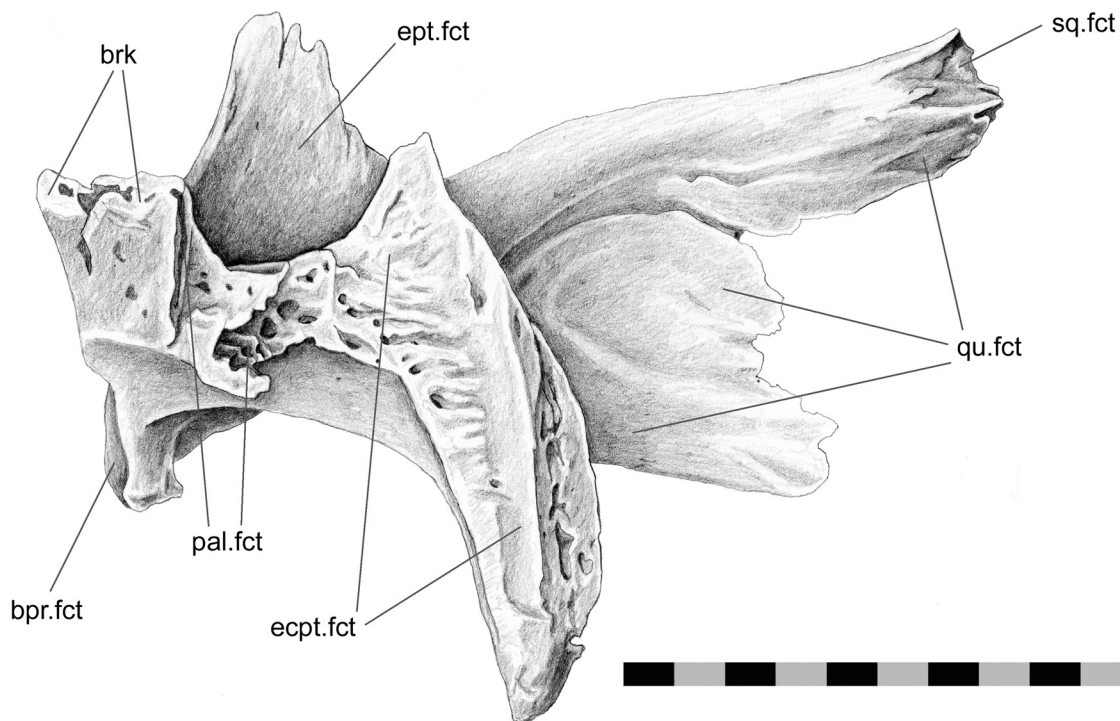


FIGURE 36. Left pterygoid (DGPC1) in anterior view. Scale bar equals 10 mm.

arrangement of the bones would restrict posterior movement of the palatine and anterior movements of the jugal as well as some mediolateral movements. Apart from the upper facet of the palatine, which bears two vertical ridges, the facets involved lack obvious sculpture (Figure 28).

Palatine-ptyerygoid

This joint is associated with the intervomerine, vomer-palatine, and vomer-ptyerygoid joints. In ventral view the seam generally runs posterolaterally from the junction with the vomer, although its anterior and posterior ends maybe more sagittally directed (Jones et al. 2009). In dorsal view the anterior end of the seam can be slightly convoluted and in posterior view the small posterior section of the joint has an 'S' shaped seam.

This joint can be divided into three parts. The anterior part involves the palatine overlapping the anterior processes of the pterygoid with a shallow scarf joint (Figures 2.5, 35) so that both palatines meet in the midline on the dorsal surface of the palate (e.g., DGPC2; Sharrell 1966). However, the tips of the pterygoids remain exposed anteriorly (Jones et al. 2009, figure 3.2). The central part of

this joint involves the mediolateral edge of the palatine overlapping the lateral edge of the pterygoid but contact is generally minimal (Figure 35) and may even be lost entirely leaving an elongate fontanelle (e.g., LDUCZ x036 left side). In the posterior part of the joint the lateral pterygoid margin expands dorsoventrally and bears two slot-like recesses running oblique to the midline (Figure 36). Two posterior processes from the palatine insert against these recesses (Figure 37). The contact lies just in front of the pterygoid-ectopterygoid joint and is related to the minor (or even occasional) palatine-ectopterygoid joint. The joint between the more medial process and slot is almost a simple butt contact (Figure 37.4). The joint between the more lateral process and slot is more complicated, in that the posterior tip of the process ends in a cup that wraps around the ventral edge of the slot (Figure 37.4).

In hatchlings the palatines do not appear to overlap the pterygoid extensively (Werner 1962) but the two posterior palatine processes are present in hatchling or near hatchling specimens (Howes and Swinnerton 1901; Werner 1962).

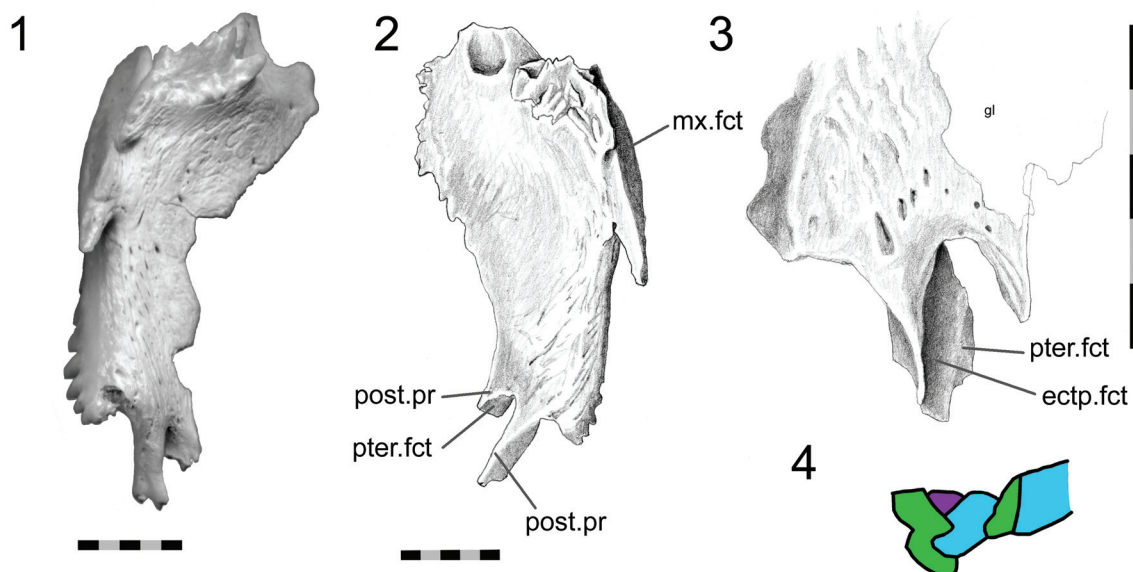


FIGURE 37. Palatine-pterygoid joint. 1. left palatine (DGPC1) in anterodorsal view. 2. right palatine (YPM11419) in dorsal view. 3. close up of the two posterior processes which articulate with the pterygoid and sometimes the ectopterygoid. 4. cross-section through the two posteromedial processes of the palatine in articulation with the pterygoid and ectopterygoid. Green = palatine, purple = ectopterygoid, blue = pterygoid. Scale bar equals 5 mm.

Interpterygoid

In *Sphenodon* the paired pterygoids are connected anteriorly along a midline seam which is less than half the total length of the bones (Figure 24.1). In ventral view the seam tends to exhibit low amplitude and long wavelength meandering (e.g., LDUCZ x036). The dorsal view is similar but the waveform may have greater amplitude. The internal structure can be clearly seen in BMNH.K and YPM11419. A medial view of a disarticulated pterygoid reveals long slots and flanges that are anterodorsally inclined from the long axis (Figure 38). These slots and flanges interlock as in Type-A interdigitation (Figure 2.2) but because the bones are relatively thin, contact seems small relative to the overall size of the bones. Therefore, despite being very distinct the joint is not necessarily strong. The meandering of the external seams corresponds to some Type-B interdigitation (Figure 2.4) but it is very subtle by comparison to the obvious Type-A interdigitation.

Interpalatine

The thin dorsomedial edges of the paired palatines meet along the midline above the vomer-pterygoid junction (Sharrel 1966, p. 29; Jones et al. 2009, figure 3). This arrangement can be appreciated with a dorsal view of the palate, provided the

specimen is cleaned of soft tissue (e.g., in DGPC2; Jones et al. 2009). In ventral view the joint is hidden by the underlying vomers and pterygoids.

Pterygoid-ectopterygoid

The contact surface is relatively large (described as “extensive” by Günther [1867]), and involves both the ventral and medial processes of the ectopterygoid. The posterior surface of the ectopterygoid ventral process sits in a cavity in the descending process of the pterygoid to form the pterygoid flange (Figure 39). The ectopterygoid medial process is smaller than the lateral process but is expanded anteriorly and sits in a triangular recess on the dorsal surface of the pterygoid (Figure 40). The dorsal part of the joint is related to both the palatine-pterygoid joint and the negligible palatine-ectopterygoid joint.

Separating the medial process and the longer ventral process of the ectopterygoid is a small notch that accepts a small sill from the pterygoid. The ventral facet on the pterygoid is curved and bears both pitting and transverse ridging, particularly on its laterally facing surface. The ventral process of the ectopterygoid is curved and exhibits a subtle groove running along its length (Figure 33). Nevertheless the joint between the ectopterygoid and pterygoid is tightly apposed. It would resist anteroventral movements of the pterygoid and pos-

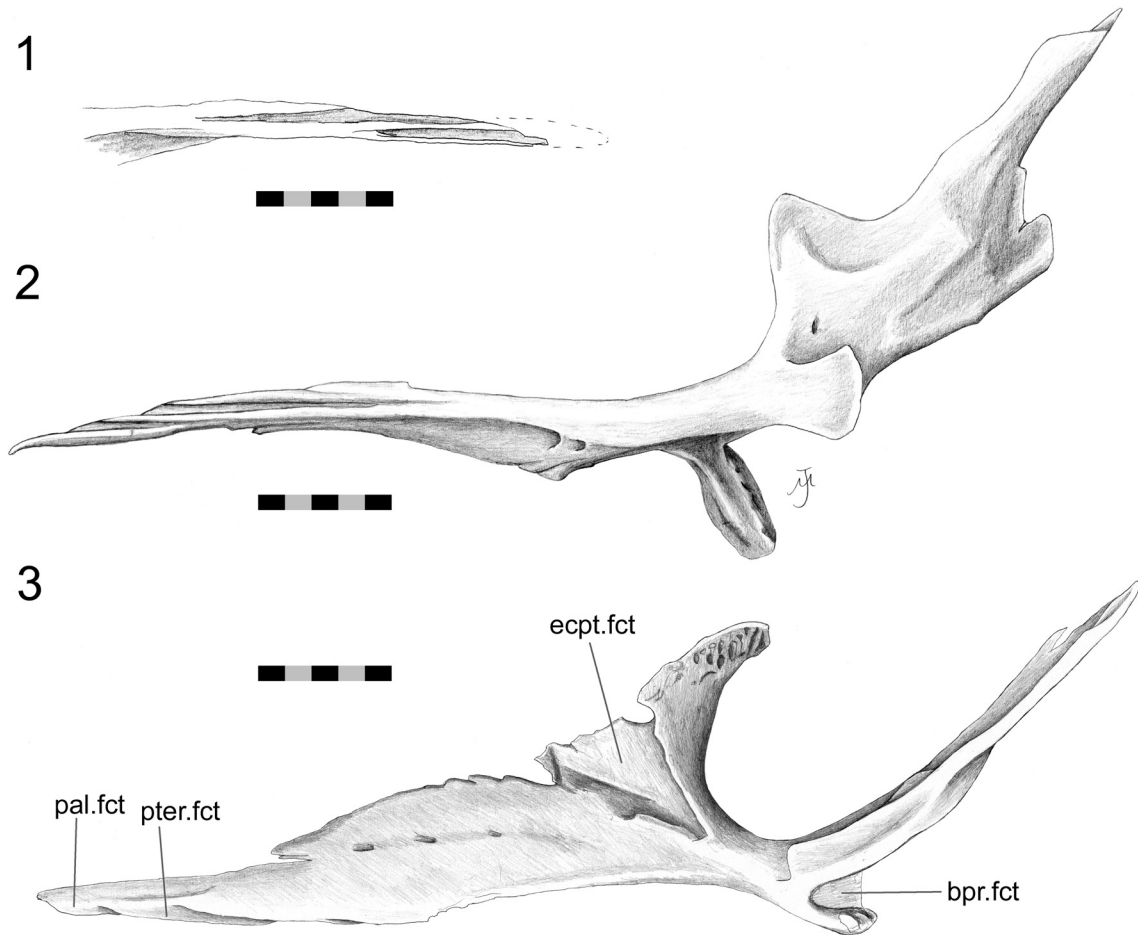


FIGURE 38. Pterygoid (BMNH.K). 1. anterior tip of the left pterygoid in medial view. 2. right pterygoid in medial view. 3. right pterygoid in dorsal view. Scale bar equals 10 mm.

terodorsal movements of the ectopterygoid. This arrangement would prevent the lateral ectopterygoid process from rotating posteriorly and the medial ectopterygoid process from rotating anteriorly but it would not prevent the opposite from occurring (i.e., anterior rotation of the lateral process and posterior rotation of the medial process).

Palatine-ectopterygoid

In DGPC2, the anterior tip of the ectopterygoid's medial process rests against the dorsolateral surface of the lateral-most palatine projection. Consequently, small slivers of the ectopterygoid (laterally) and pterygoid (medially) are held between the two posterior projections of the palatine (Figures 35, 37). Only the tips of the posterior palatine projections are involved leaving a space between the bases (Figure 24.2; Jones et al. 2009, figure 3). In specimen DGPC1 contact between the ectopterygoid and palatine is less certain but may

have occurred indirectly through soft tissue related to the pterygoid-palatine joint.

Maxilla-ectopterygoid

The expanded lateral process of the ectopterygoid sits on the dorsal surface of the maxilla above the posterior end of the tooth row (Figures 20, 30). In dorsal view the seam travels posteromedially from the edge of the jugal. In disarticulated specimens the edges of the facet on the maxilla are not clearly delimited but within the location of the facet the surface bears pitting and ridges suggesting ligamentous tissue. However, this sculpture is not reflected on the ventral facet of the ectopterygoid which is smooth and may have occurred during preparation (Figure 30). This joint prevents the ectopterygoid from moving ventrally and the posterior end of the maxilla from any dorsal movement.

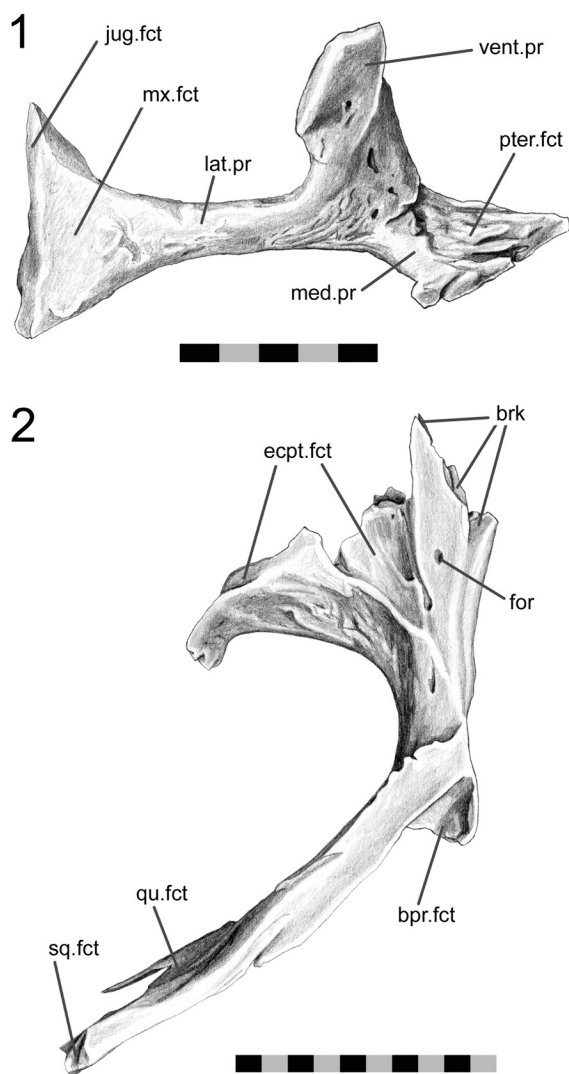


FIGURE 39. Pterygoid-ectopterygoid joint (DGPC1). 1. left ectopterygoid in posterodorsal view. 2. left pterygoid in dorsal view. Scale bar equals 5 mm (1), 10 mm (2).

Roofing Joints

The roofing joints are situated dorsally on the skull and mainly include those of the frontal, post-frontal and parietal. The roofing unit is linked to the rostral unit by the nasal and prefrontal, the palatal unit by the prefrontal, the temporal unit by the post-orbital and squamosal, and the metakinetic unit by the parietal.

Nasal-frontal

The naso-frontal seam generally runs posterolaterally from the midline to the junction with the prefrontal (e.g., Jones and Lappin 2009, figure 4; Jones et al. 2009, figure 2). There is some varia-

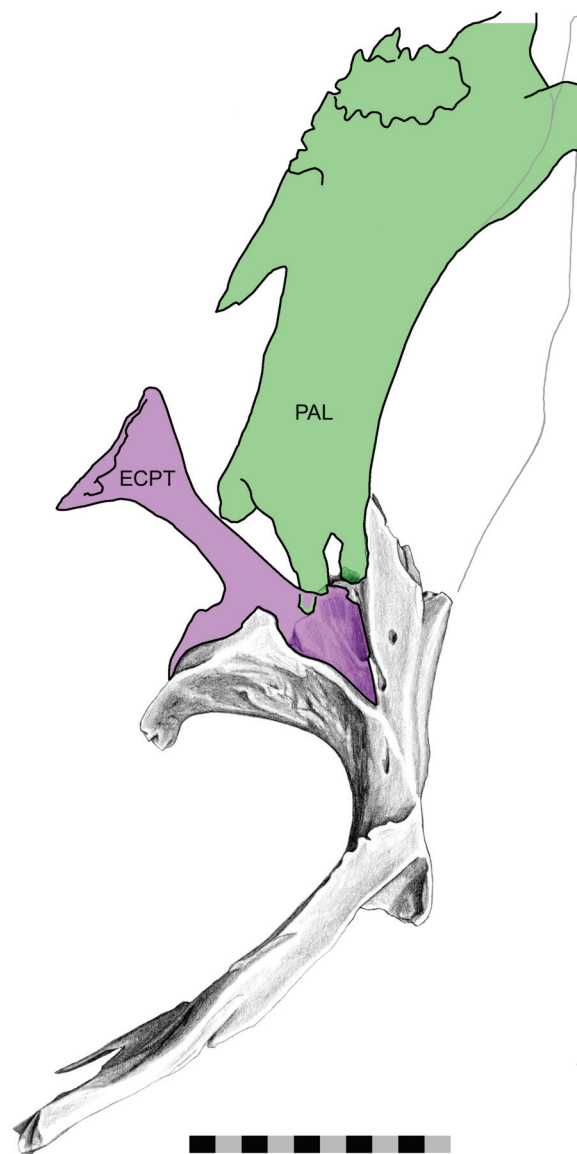


FIGURE 40. Left pterygoid (DGPC1) overlain by ghosts of neighbouring bones. Purple = ectopterygoid, green = palatine. Scale bar equals 10 mm.

tion in the exact shape of this seam as it may be nearly straight (e.g., BMNH 1844.102911; PCDG2 left side, LDUCZ x723 left side) or more sigmoid (e.g., LDUCZ x036, BMNH.K) travelling from the midline anterolaterally, posterolaterally, laterally and anterolaterally again. Correspondingly, in dorsal or ventral view, the posterior edge of isolated nasals may be either "V" shaped (e.g., PCDG2) or lobate (BMNH.K).

The posterolateral ends of the nasals overlap the anterolateral processes of the frontals with a scarfed tongue-in-groove joint (Figures 2.13, 41,

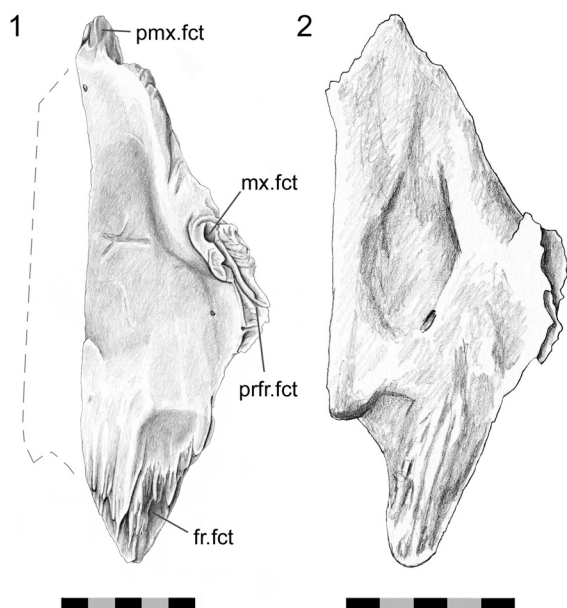


FIGURE 41. Left nasals in ventral view. 1. BMNH.K. 2. DGPC1. Scale bar equals 5mm.

42, 43, 44). In the disarticulated DGPC1 the medial portions of the bones are not available for study but the structure has been observed in other specimens (e.g., BMNH.K). The contact is particularly extensive along the junction with the prefrontal but diminishes medially (Figures 42, 44). Of 42 skulls examined, a notable midline fontanelle was present between the nasals and frontals in nine (21.4%: specimens AMPC 1, BMNH 1844.102911, KCL x12, LDUCZ x146, MANCH C.1206.49, NMNZ RE0382; OMNH 4911; UMZC 2613, UMZC 2614; Jones and Lappin 2009; Jones et al. 2009). In specimen MANCH C.1206.49 (skull length = 54.8 mm) this fontanelle is 2.8 mm long and 1.5 mm wide.

The anterolateral nasal facet on the frontal is generally scarfed, but it is also concave across its width so that the joint resembles a tongue-in-groove joint (Figures 42, 43, 44). Correspondingly the posterior process of the nasal is scarfed and convex across its width (Figure 13.1, 41). In DGPC1 the facet on the frontal possesses several long gutters and ridges that reflect similar texture on the facet of the nasal (Figure 41.1). These are generally orientated sagittally although they have some lateral inclination. Among the gutters there are also two large foramina. Other disarticulated nasals (e.g., BMNH.K, YPM 11419) possess a much smoother facet surface (Figure 41.2).

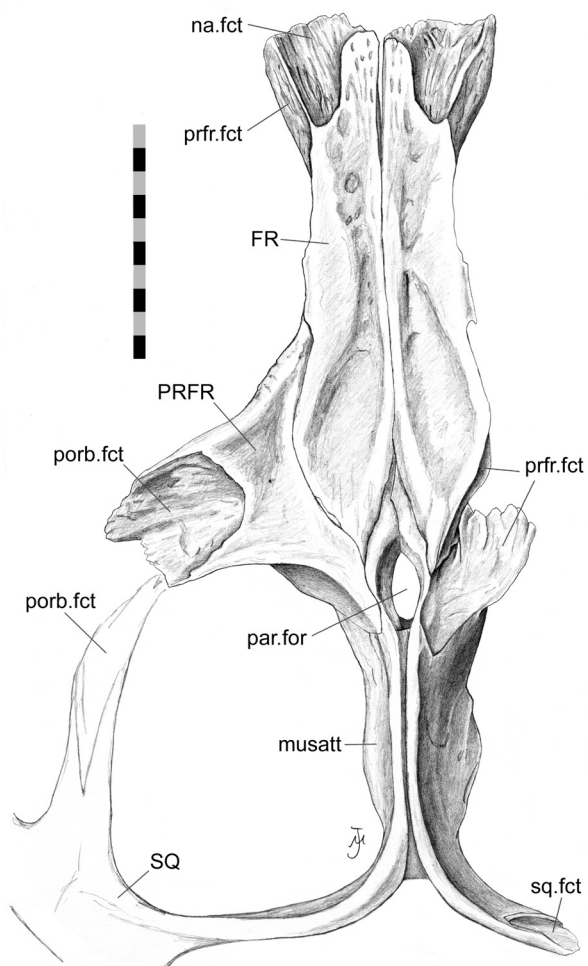


FIGURE 42. Partial skull roof (BMNH.K) in dorsal view. Both frontals, both parietals and left postfrontal present. Nasals, prefrontals and right postfrontals are absent. Scale bar equals 5 mm.

This joint would resist dorsal or anterior movements of the frontal and ventral or posterior movements of the nasal. The mediolateral movements of both bones would also be inhibited by the concave shape of the frontal facet and also the sagittally orientated gutters. According to Rieppel (1992), the nasals overlap the frontals extensively even in the hatchling.

Frontal-prefrontal

In dorsal view the seam travels posteriorly from the nasal to the orbital margin along a roughly parasagittal line with a slight lateral inclination. In lateral view the seam travels posteroventrally before folding back anteroventrally in a “V” shape. The frontal-prefrontal joint has two components, an anterior part and a posterior part (Figures 42, 44,

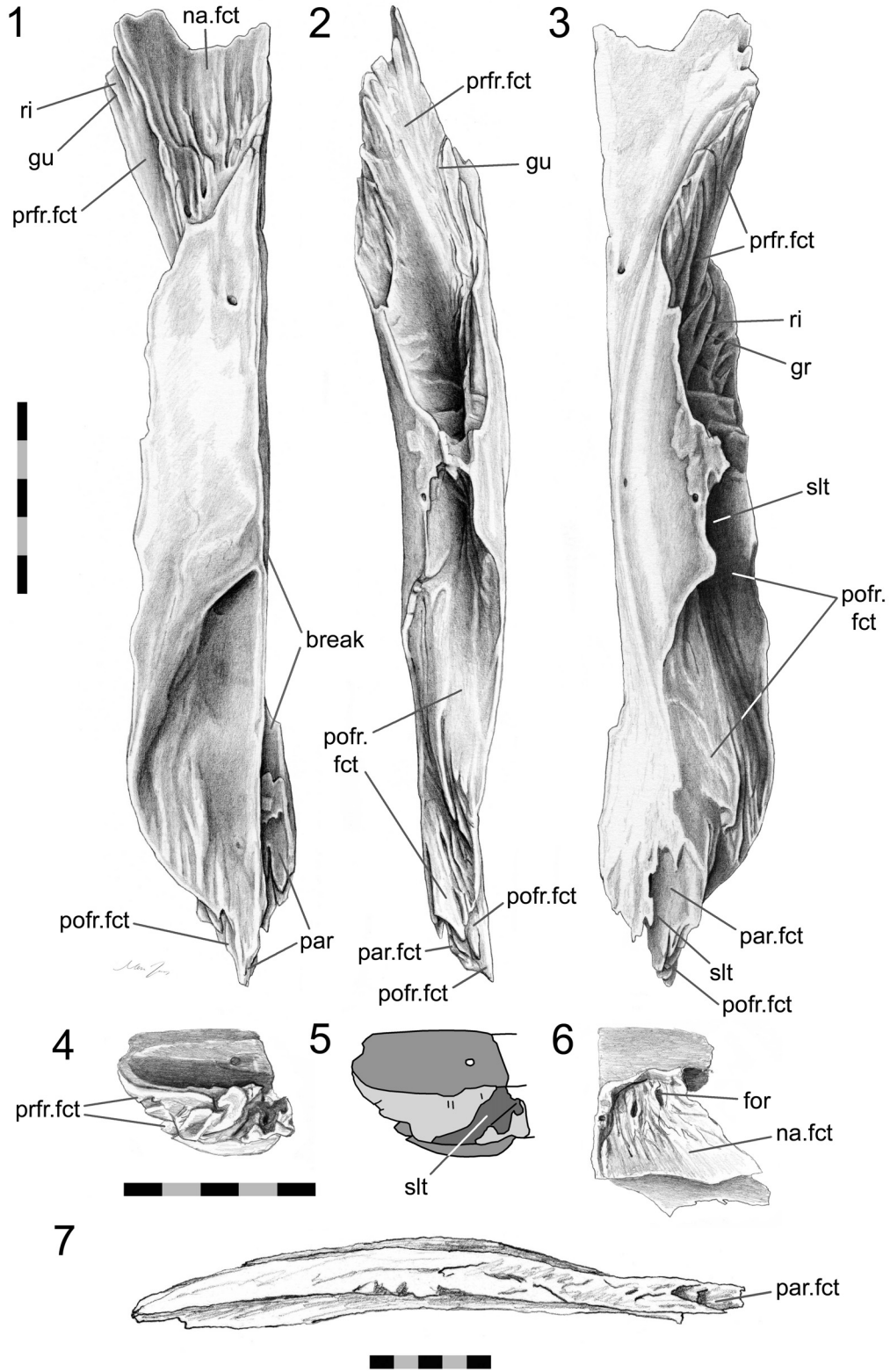


FIGURE 43. Left frontal (DGPC1, except 7, which is YPM 11419). 1. dorsal, 2. lateral, 3. ventral, and 4. posterior views. 5. posterior view with less detail showing the oblique slot in a darker shade of grey. 6. anterior view. 7. medial view of a right frontal. Medial edge of DGPC1 is broken. Scale bar equals 5 mm.

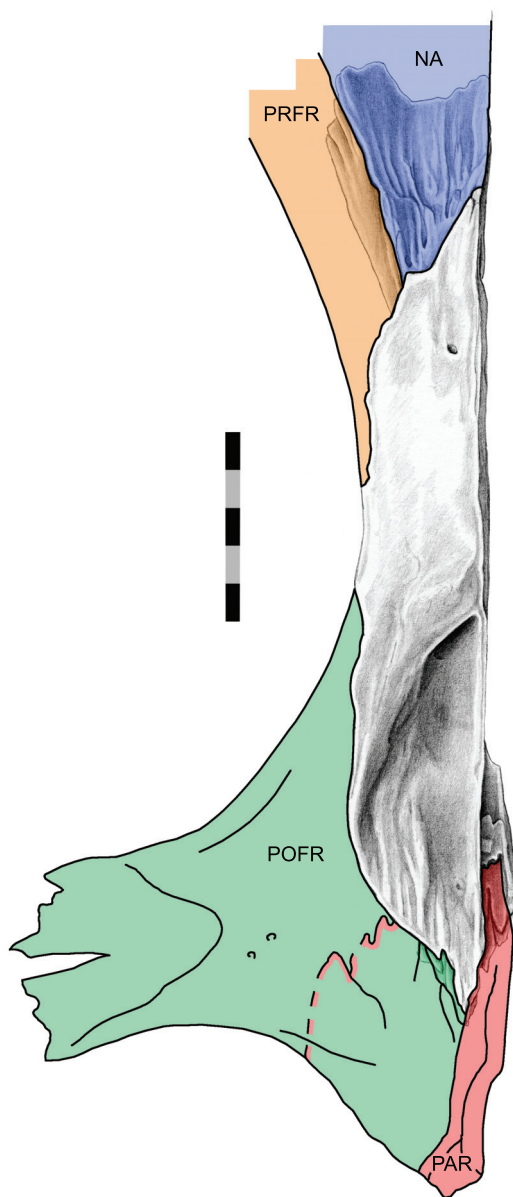


FIGURE 44. Left frontal (DGPC1) in dorsal view overlain by ghosts of the neighbouring bones. Blue= nasal, orange = prefrontal, green = postfrontal. Scale bar equals 5 mm.

45, 46, 47). In the anterior part, the anterolateral process of the frontal fits inside a deep 'V'-shaped slot in the medial surface of the prefrontal posterior process (Figures 42, 44, 45, 46.3-4). In the posterior part, the posterior process of the prefrontal inserts into a deep cavity in the anterolateral surface of the frontal bone (Figures 45, 46.1-2, 47, 48). Longitudinal ridges can be found dorsally in both parts of this joint (Figures 43.1, 43.3, 45.1). Anteriorly the joint is associated with the nasal-pre-

frontal and nasal-frontal joints (Figure 46). Both components of the joint combine to form an alternating slot joint. This joint would resist anterior movement of the frontal and posterior movement of the prefrontal but would also prevent differential dorsoventral movements between the bones.

Interfrontal

In *Sphenodon* the frontals generally contact each other sagittally with a long butt joint. Ventrally the seam is generally straight except where it exhibits low amplitude interdigitation centrally between the orbital margins (e.g., LDUCZ x1176, BMNH K, UCMZ2614; AUP 11883) (Figures 48, 49). Correspondingly, in medial view the mid ventral portion of the facet bears ridges oblique to the long axis of the bone (Figure 43.7) representing some degree of Type-B interdigitation (YPM11419). The interfrontal suture fully closes in hatchlings between stages S and T when the skull is 9–14 mm long (Howes and Swinnerton 1901; Schauinsland 1903; Werner 1962; Rieppel 1992; Jones and Lappin 2009).

Frontal-postfrontal

In dorsal view the seam for this joint can vary dramatically between specimens (Figure 50). From the anterior border of the orbit, the seam travels posteromedially toward the junction with the parietal but may do so in a straight line (e.g., LDUCZ x036), a broad 'V'-shaped line (e.g., UMZC 2583, LDUCZ 1176), a gentle curve (e.g., UMZC 2614) a broad curve (e.g., BMB 101806, BMNH 19851212, LDUCZ x146, DGPC1, BMNH.K), a sigmoid curve (e.g., UMZC 2613, BMB 100225, NMNZ0382) or a very sigmoid curve (e.g., UMZC 2593, DGPC2). In a lateral view of the whole skull, the anterior segment of the seam travels anterodorsally from the orbital margin before turning posterodorsally at mid length.

This joint primarily involves the medial surface of the postfrontal slotting into the lateral surface of the frontal (Figures 47, 48, 49, 50, 51, 52, 53, 54) but it can be divided into three sections. In the anterior section, the anterior process of the postfrontal (Figures 51, 52.2) inserts into a deep slot in the frontal (Figures 43, 47, 48, 49, 54). This slot exhibits gutters and ridges running along its axis (Figures 43, 48). In the central and largest section the frontal sits in a deep concavity on the postfrontal (Figure 52.2), and some specimens possess a small shelf on the frontal that enters the postfrontal (BMNH K) (Figure 42). The posterior section is related to the anterior joints of the parietal. In

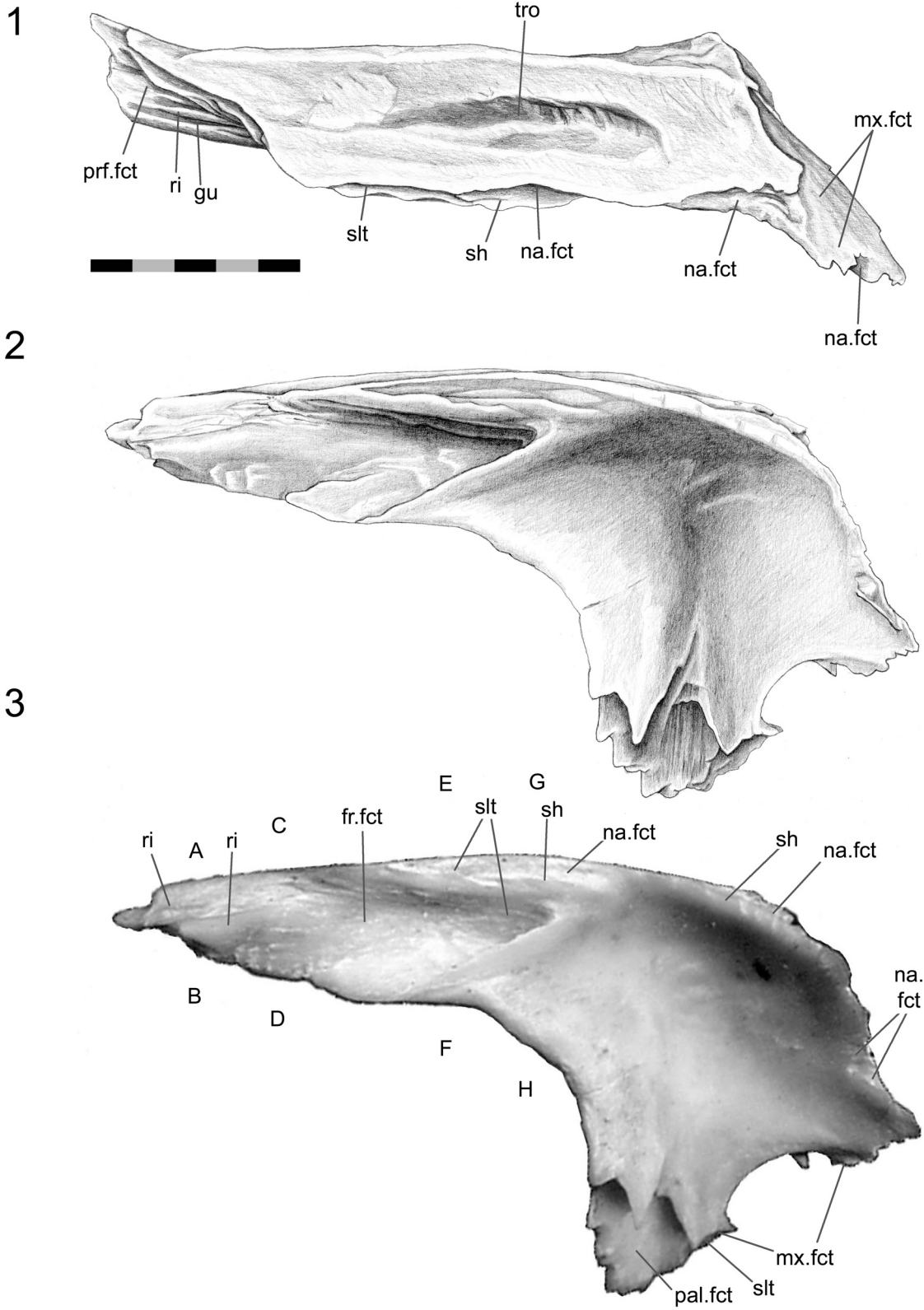


FIGURE 45. Left prefrontal (DGPC1). 1. dorsal, 2. and 3. medial views. Letters correspond to cross-sections in Figure 46. Scale bar equals 5 mm.

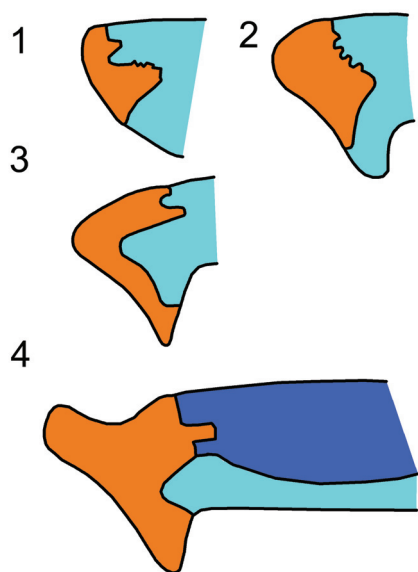


FIGURE 46. Schematic coronal cross-sections through the left prefrontal-nasal-frontal joint. 1. section between A and B in Figure 45.3. 2. section between C and D in Figure 45.3. 3. section between E and F in Figure 45.3. 4. section between G and H in Figure 45.3.

LDUCZ x1176 this involves a thin flat process from the frontal slotting into the postfrontal (Figure 55). Alternatively, as in DGPC1, the postfrontal may overlap a small posterolateral sliver of the frontal (Figures 43.1, 44, 51.1) and posteriorly the posterior tip of the frontal overlaps a small triangular shelf extending medially from the postfrontal (Figures 43.3, 54).

Frontal-parietal

Elsewhere this cranial joint suture is sometimes referred to as the coronal suture, reflecting human terminology (e.g., Moss 1954, 1957; Markens and Oudhof 1980; Opperman 2000). The joint is complex and is associated with the medial joints of the postfrontal. Primarily this joint involves an alternating overlap; laterally the frontal overlaps the parietal but medially the parietal overlaps the frontal (Figures 42, 43, 44, 48, 49, 50, 53, 54, 55, 56, 57, 58, 59).

In dorsal view the external seam is short (Figure 50; Günther 1867; Arnold 1998; Evans 2008; Jones and Lappin 2009; Jones et al. 2009). From the midline it may travel posterolaterally around the anterior margin of the parietal foramen before meeting the junction with the postfrontal (Figure 50.6; e.g., LDUCZ x036, UMZC 2613, UMZC 2611). Alternatively it may be more sigmoid, at first travelling laterally or anterolaterally before turning posteriorly and finally curving posterolaterally (Figure 50.2; e.g., LDUCZ x1176, UMZC 2582, UMZC 2610, NMNZ RE0382). The frontal has two posterior processes (Figures 43), a lateral process that overlaps the parietal (Figures 43.3, 54) and a medial process that is overlapped by the parietal (Figures 43.1, 44, 53, 55, 58, 59). The two processes are separated by an oblique slot (Figure 43.5) that may be smaller in juvenile frontals (e.g., LDUCZ x1176). Occasionally the posteriormost medial edge of the frontal is exposed dorsally (e.g., NMNZ RE0382) but otherwise the overlapping facets of both bones are scarfed, and therefore this resembles the 'birds-mouth' joint found in wood joinery (Figure 2.15; Graubner 1992). On its own,

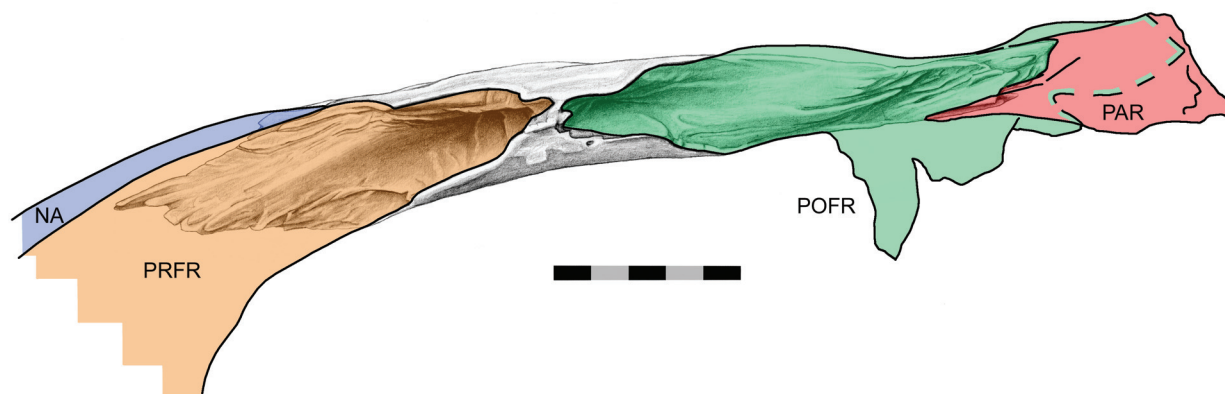


FIGURE 47. Left frontal bone (DGPC1) in lateral view overlain by ghosts of the neighbouring bones. Blue = nasal, orange = prefrontal, green = postfrontal. Scale bar equals 5 mm.

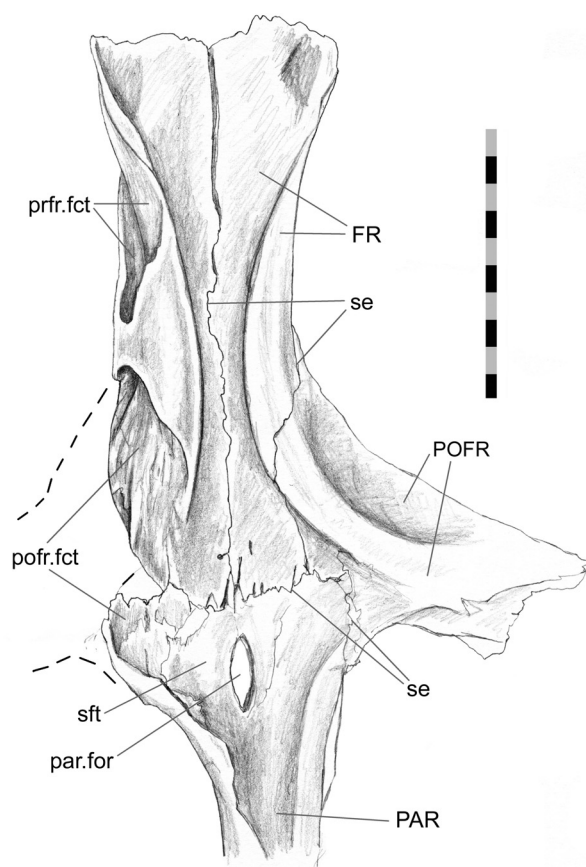


FIGURE 48. Partial skull roof (BMNH.K) in roughly ventral view as the prefrontal facet on the left is not visible. Both frontals, both parietals and left postfrontal present. Nasals, prefrontals and right postfrontal are absent. Scale bar equals 10 mm.

without soft tissue, this joint would resist all movements except perhaps anterior movement of the frontal and posterior movement of the parietal.

In hatchlings the adjoining medial portions of the frontals and parietals have not fully ossified, resulting in a fronto-parietal fontanelle (Howes and Swinnerton 1901; Rieppel 1992). It is closed in specimens with skull lengths approaching 15 mm (Howes and Swinnerton 1901; Jones and Lappin 2009).

Postfrontal-parietal

This is the largest joint of the parietal and overall involves the posterior end of the postfrontal overlapping the anterolateral part of the parietal (Figures 42, 44, 47, 48, 49, 50, 51, 52, 53, 56, 57, 58, 59). In dorsal view the seam runs posteromedially from the junction with the frontal for a short distance, occasionally reaching the anterior edge of the parietal crest at a point level with the posterior end of the parietal foramen (Figure 50). Here, it

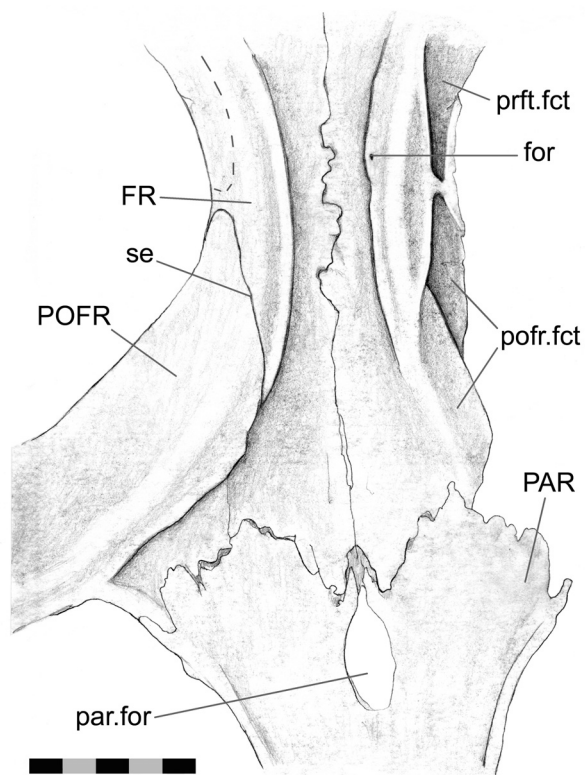


FIGURE 49. Partial skull roof (UMZC 2614) in ventral view. Left prefrontal and postfrontal are absent. Scale bar equals 5 mm.

curves around, and the seam continues anterolaterally. It may continue this course (e.g., LDUCZ x1176, LDUCZ x723 right side) or it may fold back posteriorly (e.g., LDUCZ x036; LDUCZ x343 left side, DGPC1). Variation in the posterior extent of the postfrontals can occur even within the same individual (Figure 50; e.g., DGPC2, LDUCZ x036).

Disarticulation of the skull bones demonstrates that the postfrontal overlaps the broad anterolateral expansion of the parietal (Figures 56, 57). The expansion is concave, and aligned along the contours are several gutters (Figure 57), ridges and tubercles that slot into complementary features on the postfrontal. Therefore the structure corresponds to a scarf joint (Figure 2.5) with some Type-A interdigitation (Figure 2.2). Often a splint or tab of bone from the posterolateral corner of the postfrontal (Figures 51, 52.1) underlaps the anterolateral edge of the parietal (e.g., DGPC1, LDUCZ x036) (Figure 58). This joint would resist any significant dorsal movement of the parietal and ventral movement of the postfrontal. It would also inhibit anterolateral movements of the parietal and posteromedial movements of the postfrontal.

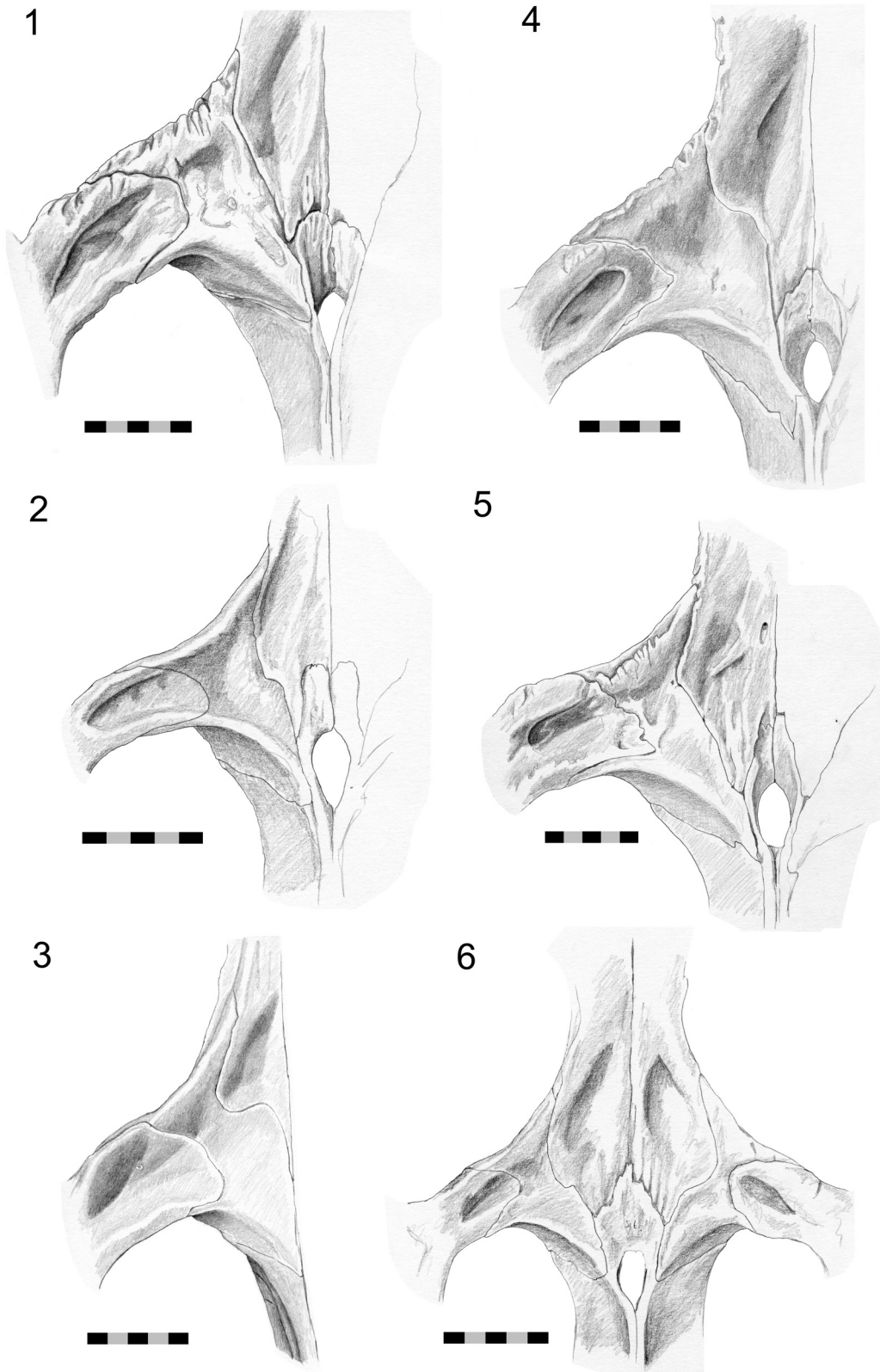


FIGURE 50. Variation in postfrontal, frontal and parietal seams. 1. UMZC 2582. 2. UMZC 2610. 3. UMZC 2593. 4. UMZC 2583. 5. UMZC 2583. 6. UMZC 2611. Scale bar equals 10 mm.

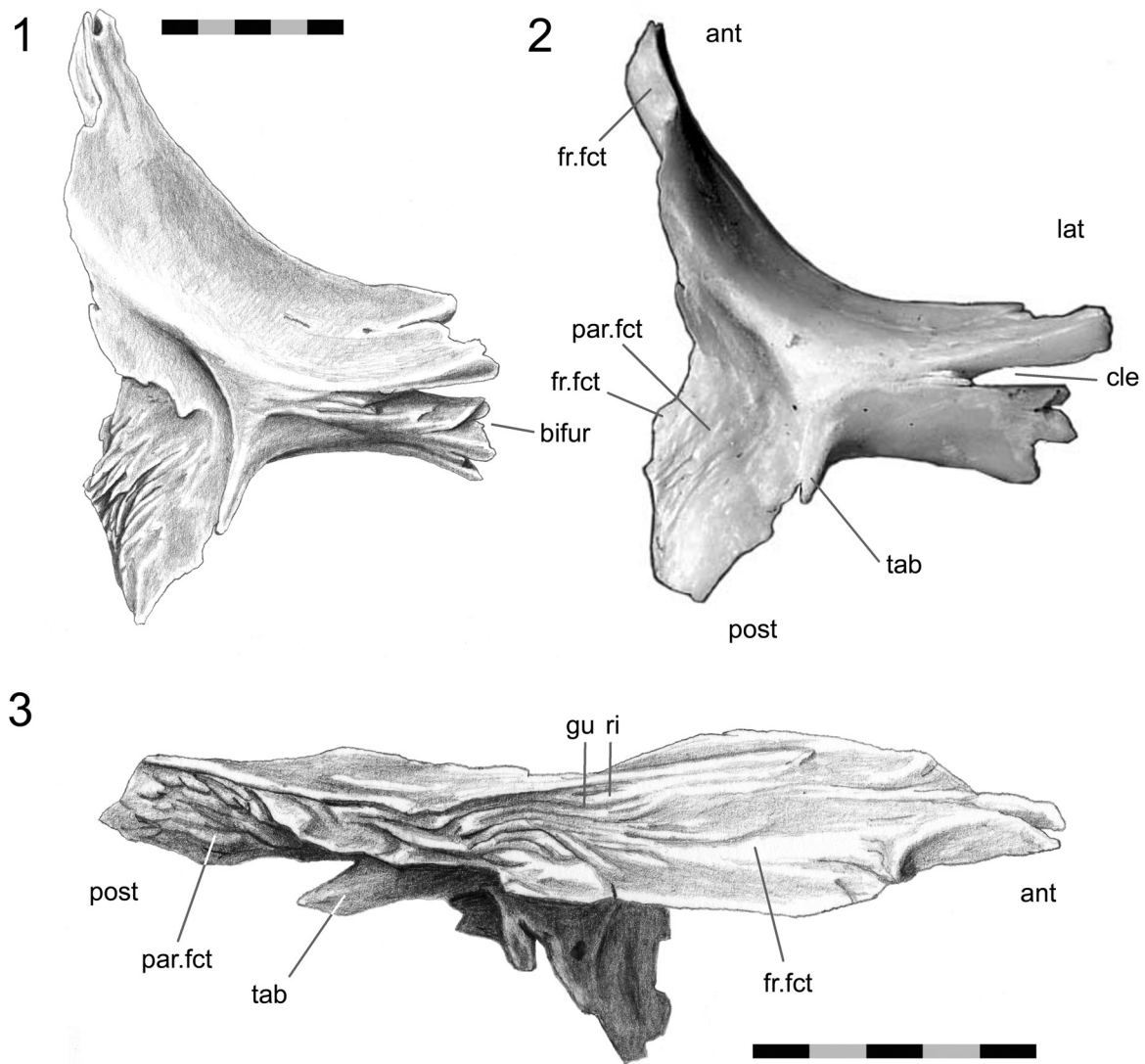


FIGURE 51. Postfrontal (DGPC1). 1. and 2. ventral views. 3. medial view. Scale bar equals 5 mm.

Postorbital-postfrontal

The postorbital and postfrontal of *Sphenodon* are both fairly robust and together form the upper part of the postorbital bar (Günther 1867; Evans 2008; Jones et al. 2009). The bar has a dorsal surface, an anteroventral surface and a posteroventral surface, with the latter two separated by the ventral ridge (Figure 53). The articulation is a complex, and tightly fitting, slot joint between the medial process of the postorbital and the lateral process of the postfrontal (Figures 42, 51, 52, 53, 60).

The seam demonstrates intraspecific variation but overall it travels around the central part of the upper postorbital bar in a zig-zag fashion. On the dorsal surface the seam arcs medially from the

edges of the upper postorbital bar. The shape of this arc is subject to variation (Figure 50); it may be broadly 'U'-shaped (Figure 50.1, 50.2, 50.3; Jones et al. 2009, figure 2.2; e.g., LDUCZ x146, LDUCZ x721, LDUCZ x723, LDUCZ x1176, NMNZ RE0382; NMNZ RE2509) or more 'V'-shaped (Figure 50.4, 50.5, 50.6; e.g., DGPC 1, LDUCZ x036, LDUCZ x343, BMNH1985.1212, YPM9194), demonstrating varying degrees of symmetry. On the posteroventral surface the seam travels ventrolaterally before folding back ventromedially in a 'V' shape (e.g., LDUCZ x1176), or more irregularly (e.g., DGPC1). The seam continues ventromedially until a point just before the ventral ridge where it turns ventrolaterally. On the anteroventral surface the seam continues ventrolaterally before redirect-

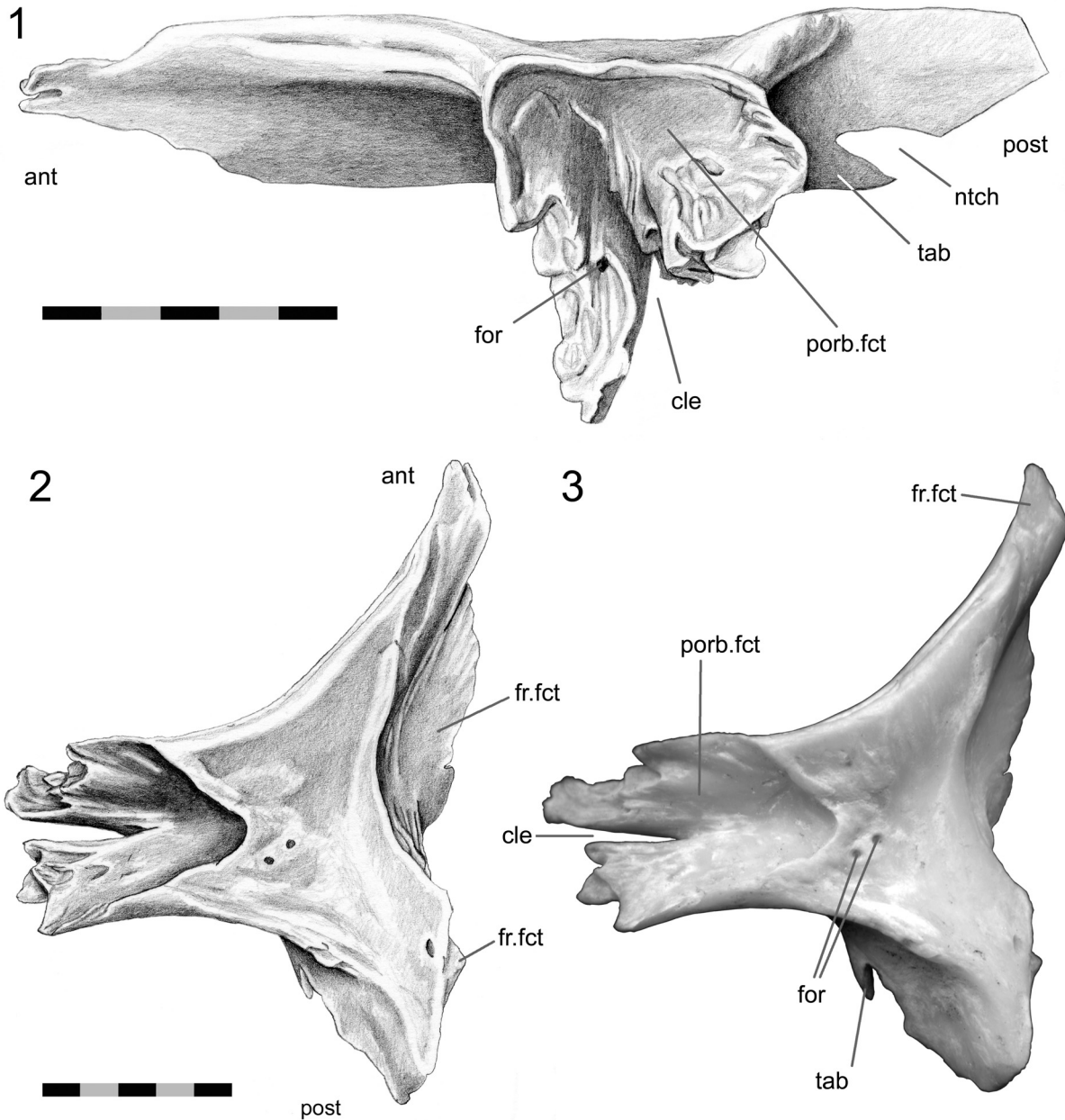


FIGURE 52. Postfrontal (DGPC1). 1. lateral view. 2. and 3. dorsal views. Scale bar equals 5 mm.

ing dorsomedially. This redirection can occur almost immediately (LDUCZ x036, LDUCZ x146, DGPC2, YPM9194), in a simple 'V' shape (e.g., LDUCZ x1176), or in a lobed curve (DGPC1, LDUCZ x723).

The internal part of the joint can be divided into a dorsal part and a ventral part. The dorsal part consists of a tongue-in-groove joint where the tongue-shaped medial process of the postorbital (Figures 60, 61) sits in a concavity on the postfron-

tal (Figures 2.13, 42, 52, 62). The ventral part of this joint consists of a triple vertical slot joint, with two slots in the postorbital (Figures 2.11, 60, 61) and one in the postfrontal (Figures 51, 52, 53). The latter slot is here referred to as the postfrontal cleft. Its exact position can vary, and it may be absent altogether (e.g., Figure 42, BMNH.K, AIM LH 833) but it is usually found at the base of the postfrontal concavity with a long axis parallel to that of the upper postorbital bar. This cleft accepts a narrow

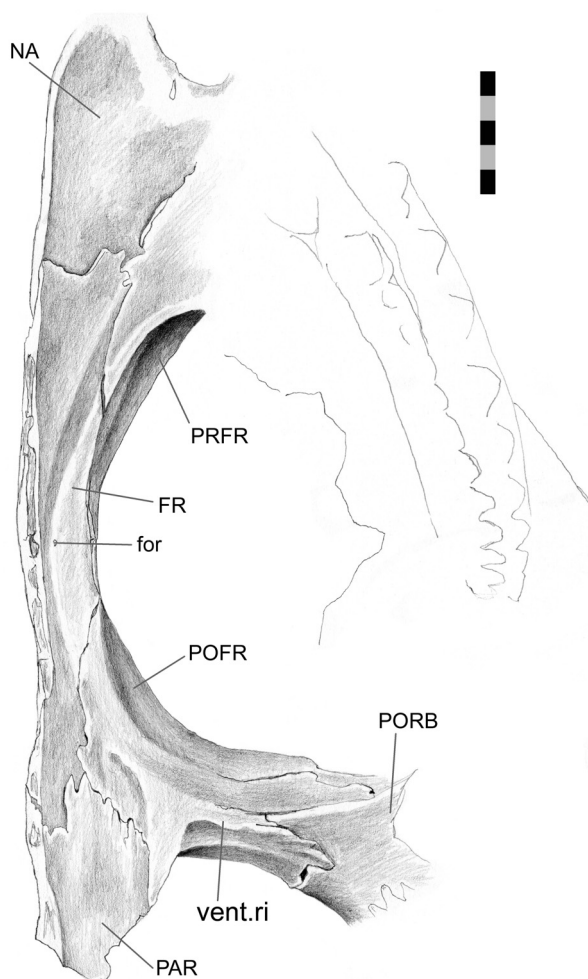


FIGURE 53. Partial skull roof (DGPC1 prior to disarticulation) in ventromedial view. Scale bar equals 5 mm.

keel of bone that projects ventrally from the postorbital (Figures 60, 61). When present the postorbital cleft divides the lateral end of the postfrontal into anterolateral and posterolateral processes as suggested by the postorbital-postfrontal seam (Figure 52). It is these two processes that insert into the two slots on the postorbital. The postfrontal anterolateral process is slightly larger than the dorsolateral process and slots into an anterior cavity against the postorbital keel. The ceiling of the cavity bears a long ridge (Figure 61) complimentary to a groove on the anterolateral process of the postfrontal (Figure 52.2). Smaller tubercles and ridges are also present. In lateral view a fairly large foramen can be seen at the proximal end of one of the gutters (Figure 52.1). The tip of the postfrontal posterolateral process also bifurcates (Figure 51.1) around a small process inside the posteromedial slot of the postorbital (Figure 60.1).

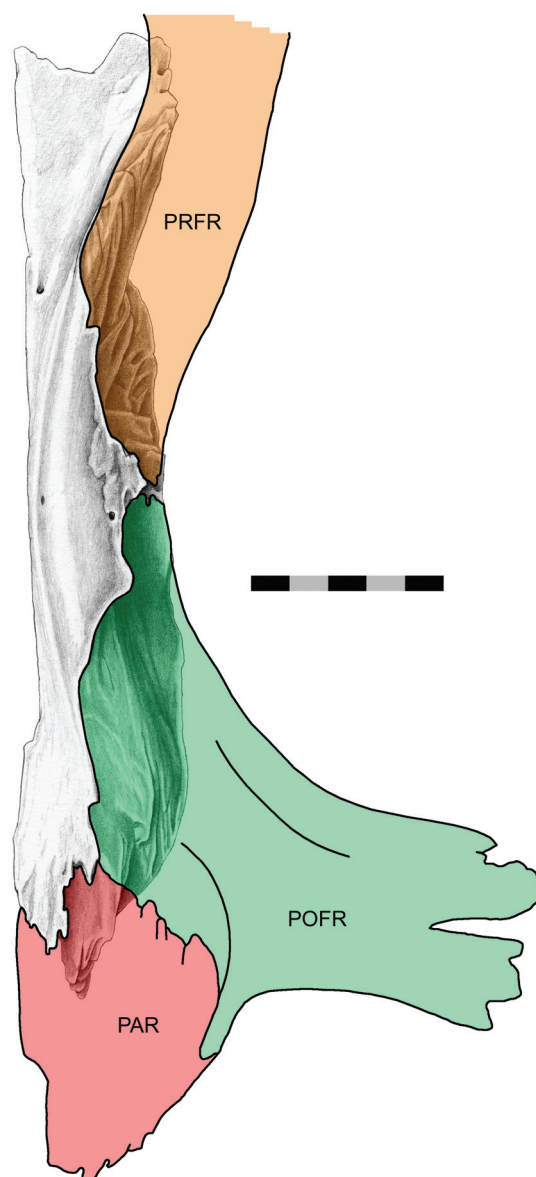


FIGURE 54. Frontal in ventral view, overlain by ghosts of the neighbouring bones. Orange = prefrontal, green = postfrontal, red = parietal. Scale bar equals 5 mm.

Even without soft tissue, the only movements permitted by this joint are medial movement of the postfrontal and lateral movement of the postorbital. The dorsal tongue-in-groove and ventral vertical slot joint would resist lateral movement of the postfrontal, medial movement of the postorbital and anteroposterior movements of either bone. Dors-ventral movements are restricted by the shape of the slots in the postorbital. In addition, the tongue-in-groove would obstruct dorsal movements of the postfrontal and ventral movements of the postor-

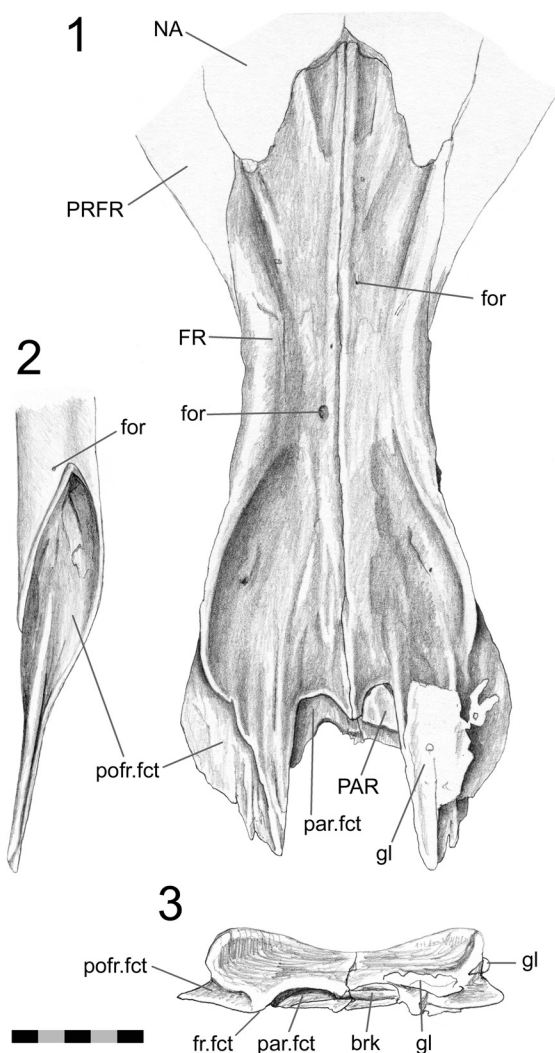


FIGURE 55. Frontal-postfrontal joint (LDUCZ1176). 1. frontals in dorsal view. 2. left postfrontal facet in lateral view. 3. frontals in posterior view. Scale bar equals 5 mm.

bital. The keel, ridges and slots would all increase the potential surface area for soft tissue attachment.

In a large hatchling *Sphenodon* (skull length = 12.3 mm) the postorbital overlaps the postfrontal to a similar extent to that found in adults (Rieppel 1992) but in smaller skulls the overlap is less extensive (Howes and Swinnerton 1901, skull length = 9 mm).

Interparietal

This cranial joint is sometimes referred to as the sagittal suture of human terminology (e.g., Moss 1954, 1957; Opperman 2000, Byron et al.

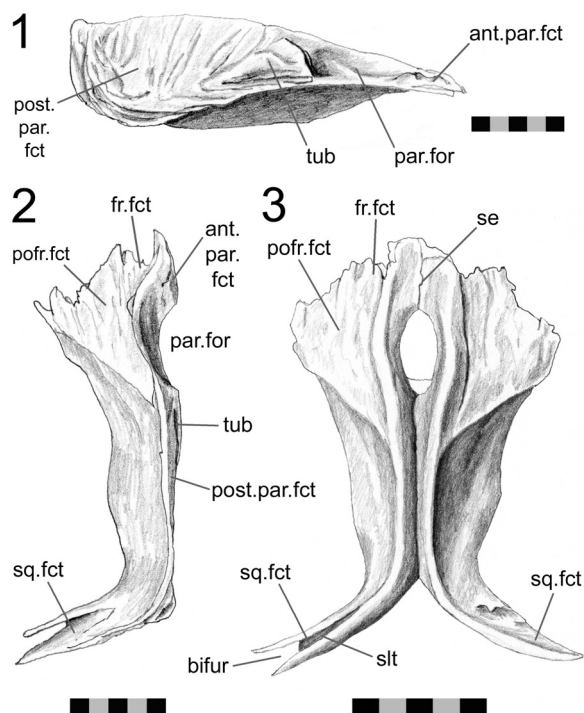


FIGURE 56. Parietal. 1. medial view of YPM 11419. 2. dorsal view of YPM 11419. 3. dorsal view of LDUCZ x1176. Scale bar equals 5 mm.

2004). In *Sphenodon*, the parietals contact each other along the midline with a straight seam either side of the parietal foramen, and form a raised crest (Figure 14). They are not necessarily fused (*contra* Evans 1980, p. 240) although they can often be very firmly apposed (Figure 14.1; e.g., DGPC2, LDUCZ x036, LDUCZ x723). In other individuals, however, the two halves of the crest are separated dorsally or bifurcated (e.g., LDUCZ x146, LDUCZ x721; LDUCZ x343). As this bifurcation can be found in small skulls (e.g., LDUCZ x1176) it is unlikely that it relates to presence or absence of the large scaly “nuchal crest” found in adult males (e.g., Gillingham et al. 1995; Parkinson 2002). In posterior view the external seam can appear sigmoid (LDUCZ x036).

Examination of isolated specimens demonstrates that this joint is essentially a large butt joint. However, the medial surface of each parietal is dorsoventrally expanded so that the contact surface is two or three times deeper than that of the interfrontal or internasal (Figure 56.1). Also, the facet surfaces are not entirely smooth. For example, the left parietal of YPM 11419 has a large anterior bony tubercle anteriorly (Figure 56.1) that inserts into a corresponding depression on the

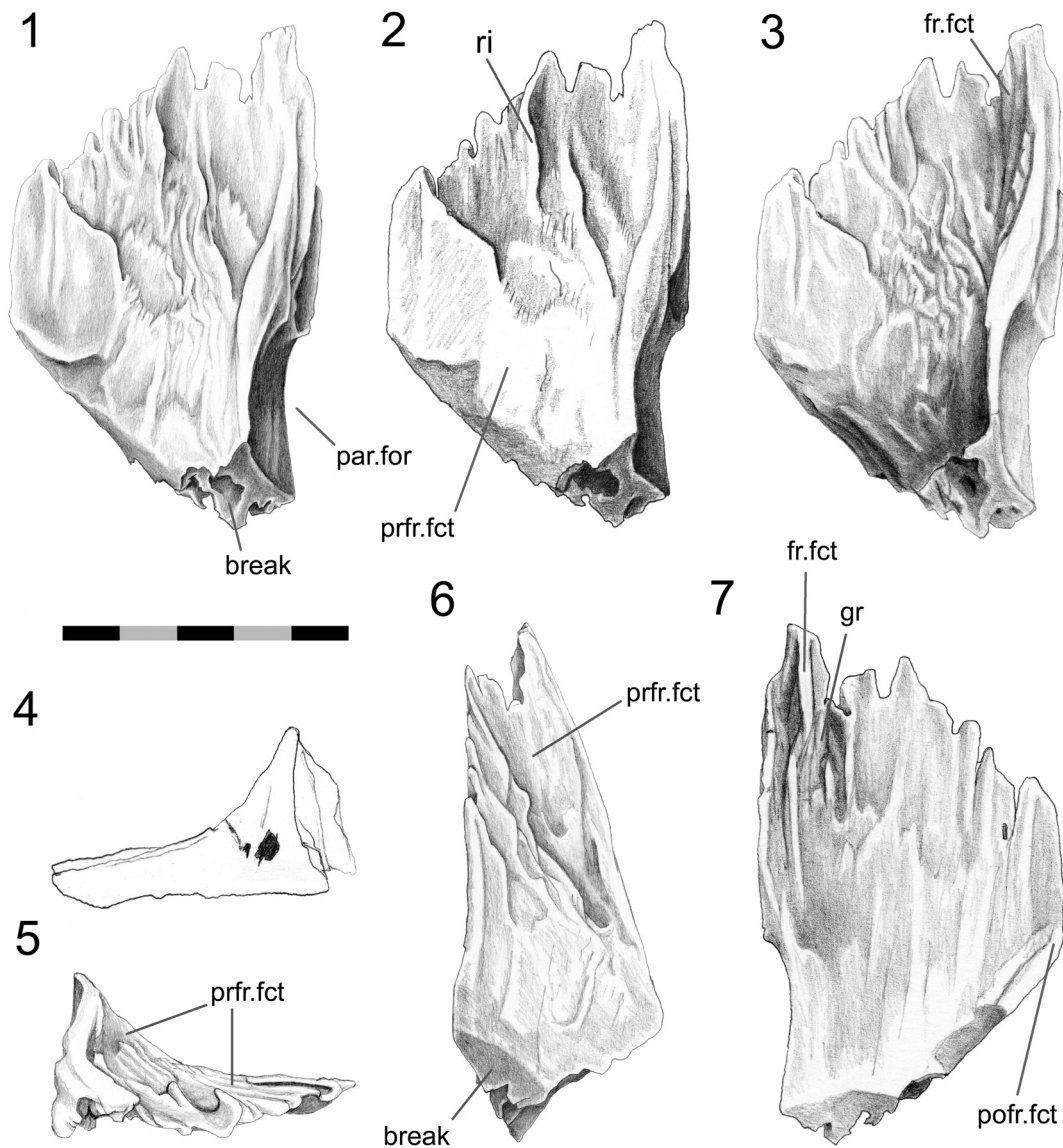


FIGURE 57. Anterior portion of the parietal (DGPC1) 1. dorsal view lit from top left corner with low angle lighting. 2. dorsal view lit from top left corner. 3. dorsal view lit from bottom right corner. 4. posterior, 5. anterior, 6. lateral, 7. ventral views. Scale bar equals 5 mm.

right parietal. Posteroventrally directed striations are also visible above the tubercle and posterior to the parietal foramen. These may serve to resist some anteroposterior movements. The sigmoid shape of the seam, often visible posteriorly, also shows that a small process from one parietal inserts into a small depression in the posterior edge of the other.

In hatchlings the parietals make contact along the midline after stage S and before stage T when the skull is about 10 mm long and most of it is ossi-

fied (Howes and Swinnerton 1901; Rieppel 1992). Before their contact, the parietals are separated by a large central space (Howes and Swinnerton 1901; Schauinsland 1903; Werner 1962).

Parietal-squamosal

The medial process of the squamosal sits in the bifurcating end of the parietal bone (Figures 56, 59). The latter is asymmetrically 'U' shaped in cross-section, with the posterior process being taller than the anterior process by about half. This

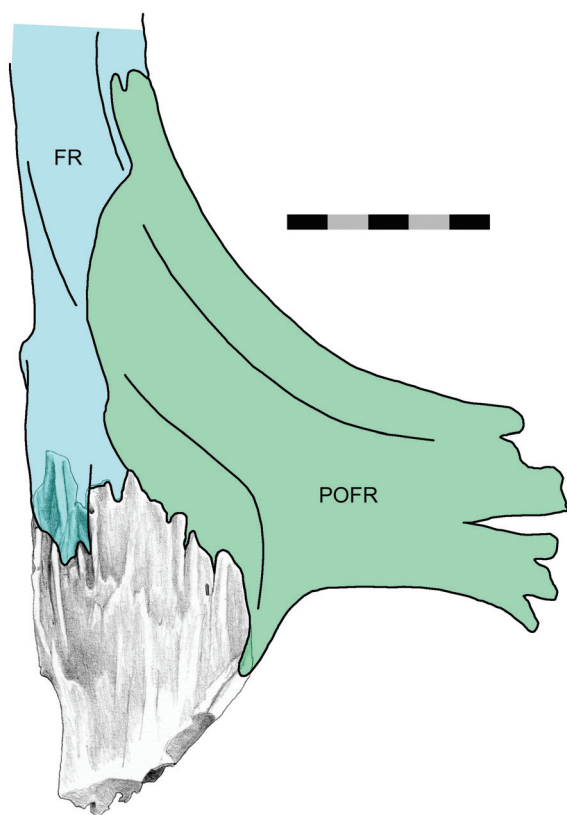


FIGURE 58. Anterior portion of the parietal (DGPC1) in ventral view overlain by the ghosts of the neighbouring bones. Light blue = frontal, green = postfrontal. Scale bar equals 5 mm.

joint resists anteroposterior movements of both bones, medial and ventral movements of the squamosal, lateral and dorsal movements of the parietal. Some very minor mediolateral movement may have been permitted to relieve local tension caused by contraction of the adductor musculature.

Parietal-supratemporal

The supratemporal is unknown in adult *Sphenodon* although a tiny sliver representing it was tentatively identified in a hatchling specimen (Rieppel 1992).

Temporal Joints

The temporal joints surround the lower temporal fenestra. The temporal unit is linked to the palatal unit by the jugal and pterygoid, the roofing unit by the postorbital and squamosal, and the metaki-netic unit by the pterygoid and quadrate.

Jugal-postorbital

The postorbital sits on top of and against the dorsal process of the jugal. In lateral view the seam

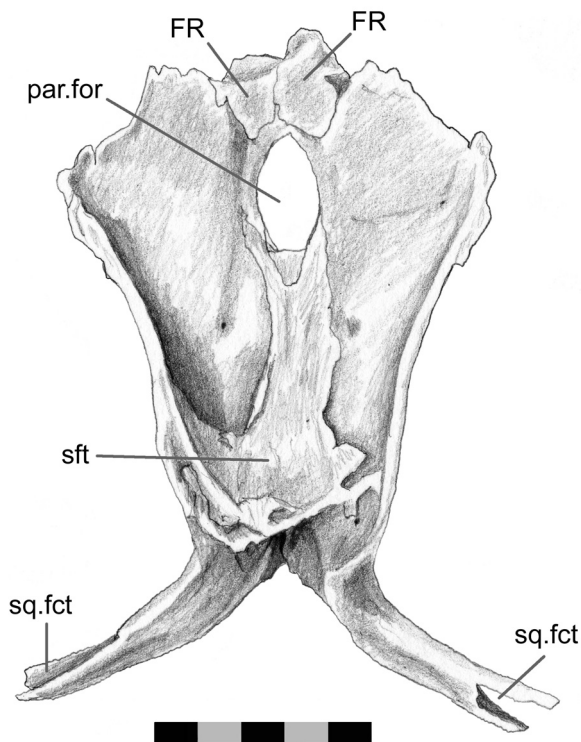


FIGURE 59. Parietal (LDUCZ x1176) in ventral view. Right side demonstrates breakage. Scale bar equals 5 mm.

is diagonal, sloping backwards with a slight sigmoid shape (Figures 62.1; Günther 1867; Evans 2008; Jones 2008; Jones et al. 2009). The joint is composed of a single but twisted articulating surface that can be separated into upper and lower parts. In the lower parts the facet on the jugal faces anteromedially (Figures 31.4, 32.2, 34.3, 62) and provides a shallow depression that accommodates the postorbital. In the upper portion of the joint the jugal expands dorsally alongside the medial surface of the postorbital (Figures 62, 63). In the juvenile LDUCZ x1176, the tip of the jugal dorsal process tapers rather than being “squared-off” as in the adult *Sphenodon* examined (Figures 32.2, 34). In DGPC1, the articulation surface bears subtle striations aligned with its long axis (Figure 31). However, the only substantial texture is located on the postorbital in the mid-part of the joint. It consists of a tubercle surrounded by gutters and ridges (Figure 60.3). Overall, the joint has an extensive surface area for soft tissue with overlap occurring along the full height of the postorbital bar. Primarily, it would restrict dorsoanteromedial movement of the jugal and ventroposterolateral movement of the postorbital. The medial seam of the joint crosses

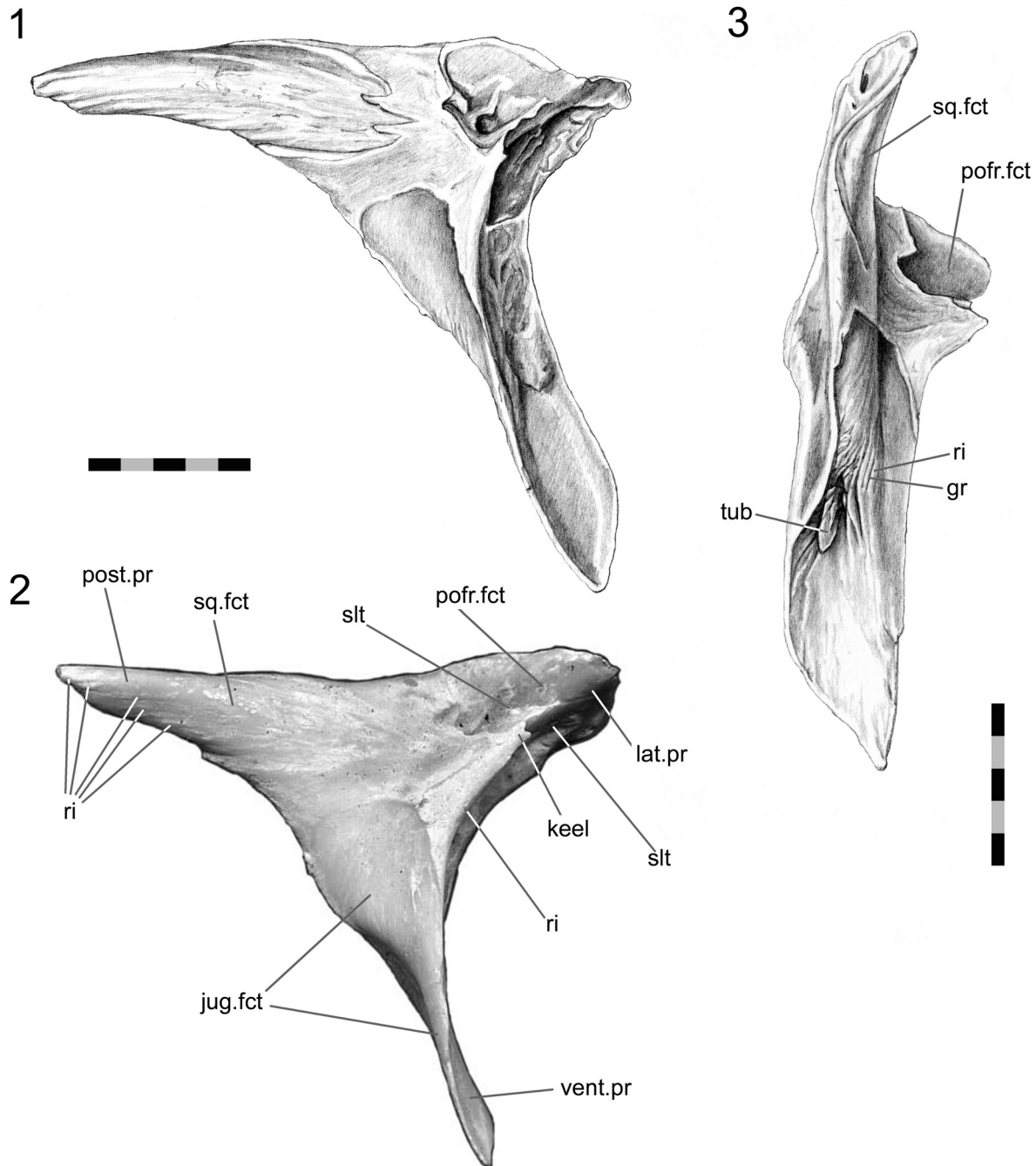


FIGURE 60. Left postorbital (DGPC1). 1. and 2. medial view following disarticulation. 3. Anterior view following disarticulation. Scale bar equals 10 mm.

the medial ridge of the postorbital and jugal which itself is a continuation of the ventral ridge found on the postfrontal.

Available images of hatchling skulls suggest there is overlap at this joint but it is not as extensive as in adult skulls (Figure 4; Rieppel 1992; Werner 1962).

Jugal-quadratojugal

In *Sphenodon* the posterior process of the jugal generally overlaps the anterior process of the quadratojugal but the exact nature of this overlap varies intraspecifically (Figure 64). In lateral view, the seam travels posterodorsally to the junction

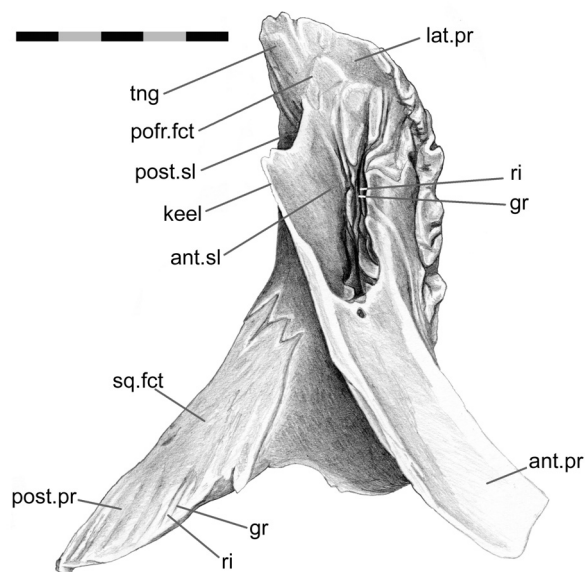


FIGURE 61. Postorbital (DGPC1) in anteroventral view. Scale bar equals 5 mm.

with the squamosal (Jones et al. 2009). In ventral view the seam is generally posterolaterally transverse. However, it is variable, and may differ in individuals between left and right sides. It may be straight (e.g., LDUCZ x723 right side, LDUCZ x1176, LDUCZ x036, LDUCZ x146), sigmoid (e.g., DGPC1, DGPC2) or 'V' shaped (e.g., LDUCZ x723

left side). In DGPC1 most of the quadratojugal lateral facet is 'L' shaped in coronal section, and the posterior process of the jugal sits on the sill of the 'L'. As a result the posterior end of the jugal overlaps the quadratojugal for a length two or three times the height of the lower temporal bar. In ventral view the quadratojugal generally overlaps the jugal but occasionally along the medial edge of the lower temporal bar, the jugal may overlap a portion of the quadratojugal (DGPC1). The joint has additional features in some larger individuals and so may change with ontogeny. The features include interlocking pegs anteroventrally (e.g., DGPC1) so that the joint as a whole can resemble an asymmetrical 'birds mouth joint' (Figure 2.15; Graubner 1998). Furthermore in DGPC1, at least, the facet on the quadratojugal bears a slight ridge that fits into a groove on the jugal. It should be noted that the shape of the jugal posterior process (and thus also the lower temporal bar) is variable; both in terms of its relative dorsoventral dimension (Jones 2008) but also its mediolateral dimension. In coronal section, the process can be twice as tall as wide (Figure 64.3; e.g., LDUCZ x146) or it may be nearly circular with equal width and height (Figure 64.4; e.g., DGPC1). Where the lower temporal bar is very circular in cross-section the posterior process of the jugal is acuminate, and the corresponding joints with the quadratojugal and squamosal

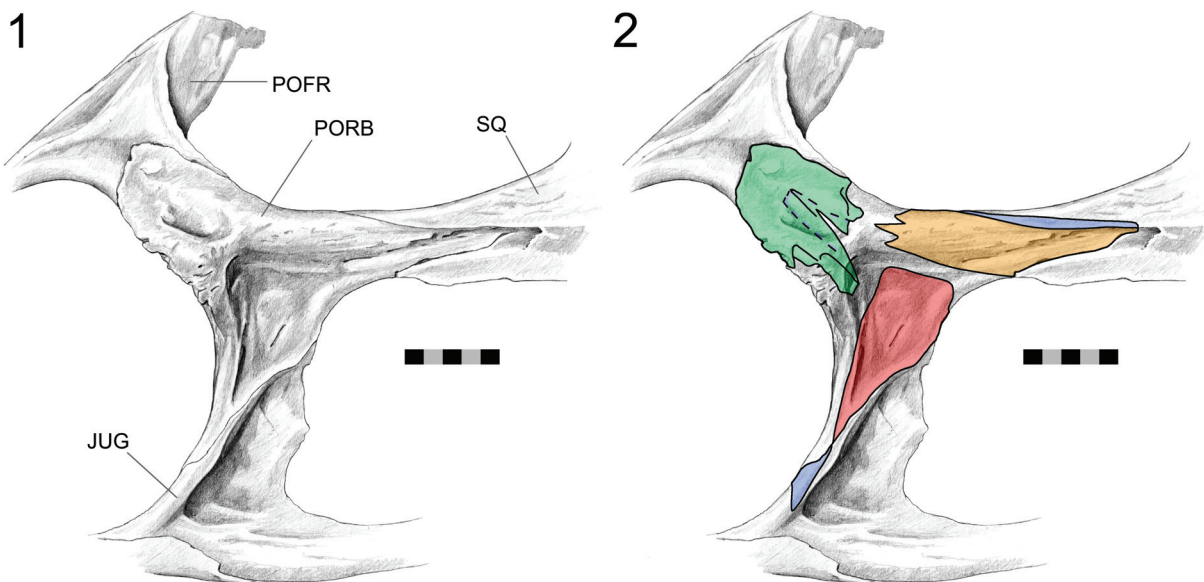


FIGURE 62. Postorbital joints (DGPC1 prior to disarticulation) in articulation in 1. dorsolateral, (2) dorsolateral views with underlaps coloured. Dark blue = postorbital, green = postfrontal, red = jugal, orange = squamosal. Scale bar equals 5 mm.

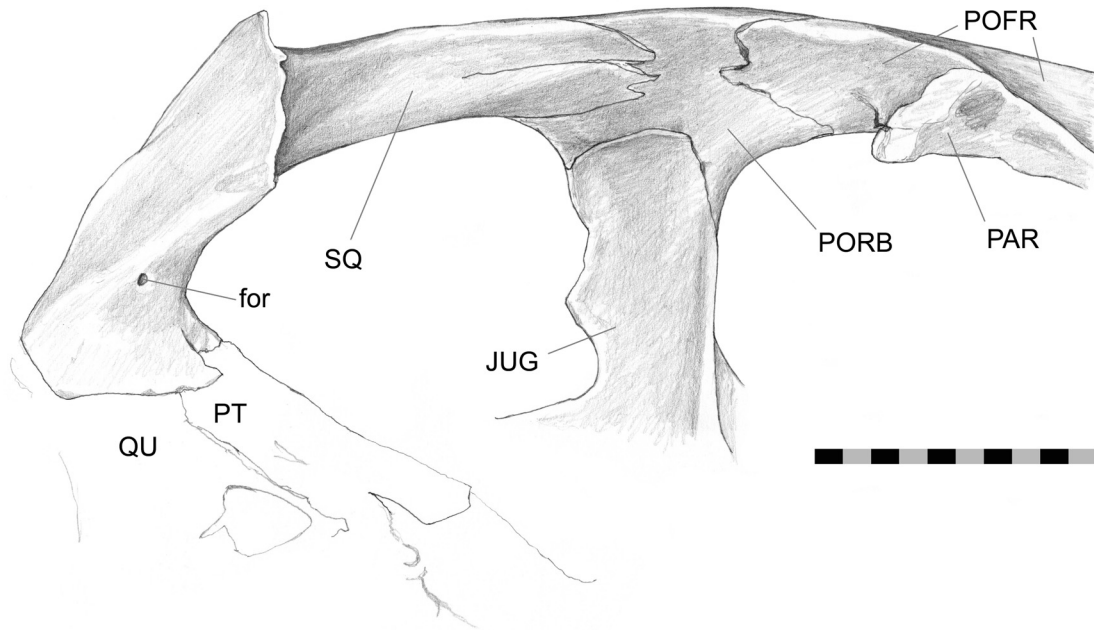


FIGURE 63. Left temporal region (DGPC1 prior to disarticulation) in medial view. Scale bar equals 10 mm.

are more slot-like. When the lower temporal bar is tall in cross-section (YPM 11419), the suture is more likely to be a simple scarfed overlap (Figure 2.5).

This joint would have resisted lateral and dorsal movement of the quadrate and medial and ventral movements of the jugal. The ventral pegs would also resist anterior movement of the quadratojugal and posterior movement of the jugal.

As known for over a hundred years, the lower temporal bar is incomplete early in ontogeny (e.g., Howes and Swinnerton 1901; Schauinsland 1903; De Beer 1937; Evans 1980; Bellairs and Kamal 1981; Whiteside 1986; Rieppel 1994; Müller 2003). In a relatively large hatchling (e.g., FMNH 65905, skull length = 12.3 mm) the jugal extends posteriorly and overlaps the quadratojugal but the contact is loose (Rieppel 1992). In smaller hatchlings (Werner 1962 skull length ~ 6 mm) and more clearly in the embryos, the jugal posterior process is only partly developed and does not reach the quadratojugal (Howes and Swinnerton 1901; Schauinsland 1903, skull lengths < 6 mm).

Jugal-squamosal

In the lower temporal bar of adult *Sphenodon*, the posterior process of the jugal overlaps the ventral process of the squamosal above the larger jugal-quadratojugal joint. In a lateral view the seam

generally runs anterodorsally from the junction with the quadratojugal; in medial view the seam runs anteroventrally from the dorsal crest of the lower temporal bar to the junction with the quadratojugal. As with the jugal-quadratojugal seam there is some individual variation. In lateral view the seam may be sigmoid (e.g., LDUCZ x146) or it may run posterodorsally before redirecting anterodorsally because the posterior tip of the jugal lies against the squamosal rather than at the junction with the quadratojugal. For example on the right side of LDUCZ x036 and left side in OMNH 908 (as shown in Jones [2008] but modified in Jones et al. [2009]). In addition, the shape of the ventral process of the squamosal and thus of the seam, can be affected by the cross-section of the lower temporal bar. The joint essentially involves the posterior process of the squamosal expanding medially around the dorsal edge of the jugal but not necessarily to the extent that it maintains contact with the quadratojugal at its anteriormost point (Figure 64.1). This arrangement resists dorsal and medial movements of the jugal. In DGPC1 the medial surface of the facet bears anteroventrally directed grooves while the dorsal surface is rugose. In small hatchling skulls (< 9 mm long), the jugal does not meet the squamosal (Howes and Swinnerton 1901; Werner 1962).

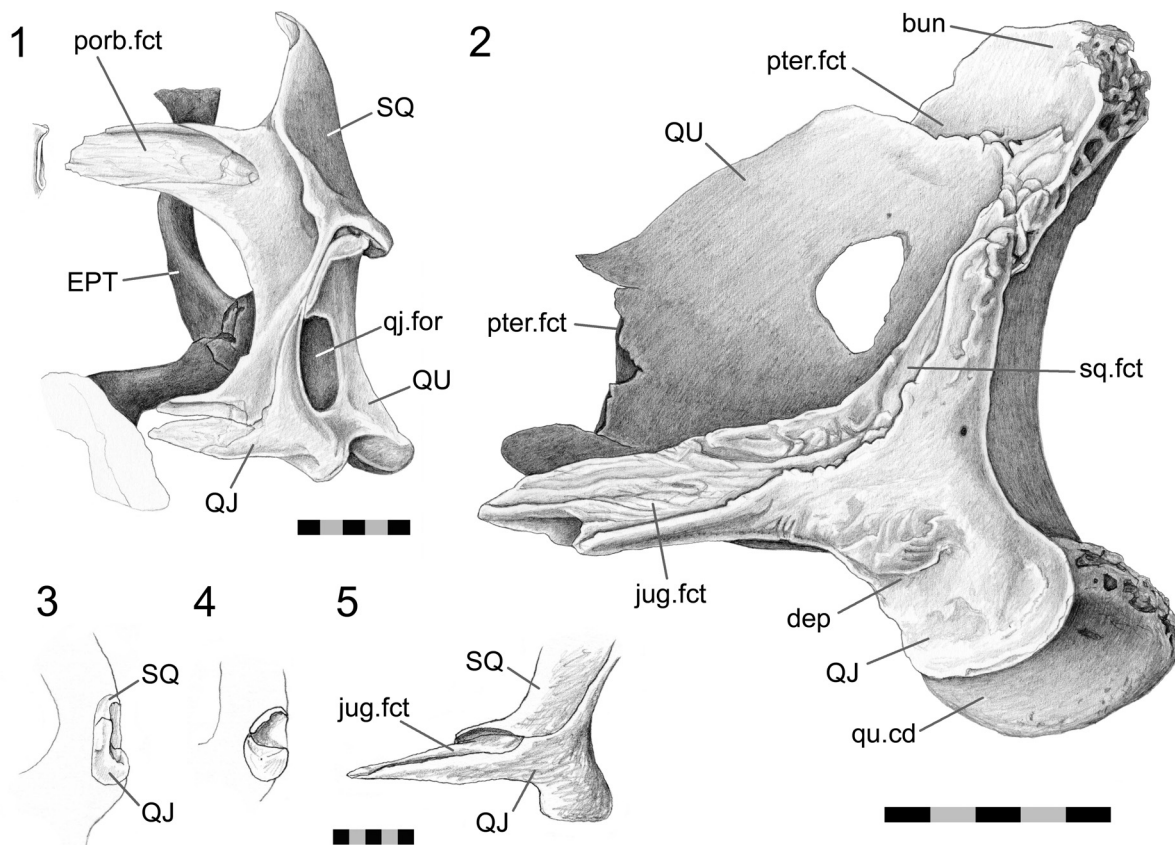


FIGURE 64. Squamosal-jugal-quadratojugal joints. 1. lateral view of the left posterior skull of a juvenile (LDUCZ x1176), with the jugal and postorbital both removed. An anterior view of the squamosal anterior process is also shown. 2. adult left quadrate and quadratojugal (DGPC1) in lateral view. 3. anterior view of the quadratojugal and squamosal facet in YPM 11419. 4. anterior view of the quadratojugal and squamosal facet in YPM 11420 (D). 5. Lateral view of the quadratojugal and squamosal facets for the posterior process of the jugal in YPM 11420. Scale bar equals 5 mm.

Postorbital-squamosal

In general, the posterior process of the postorbital overlaps the wide anterior process of the squamosal in a joint that spans almost the full length of upper temporal bar (Figures 60, 63, 64.1, 65, 66). In medial view the anterior process of the squamosal can be seen to reach the postorbital bar. The tip of the thin squamosal anterior process ends in two to four triangular points (two in LDUCZ x723, YPM 11419, LDUCZ x343; three in DGPC1, LDUCZ x036; four in LDUCZ x1176) which lie in a depression on the postorbital (Figure 63). Posteriorly, the tip of the postorbital sits against a recess in the squamosal bone (Figure 2.13). The extent of the recess varies; being very shallow in some specimens, e.g., LDUCZ x1176 (Figure 64.1); or deep with edges that envelop the posteriorly tapering postorbital, e.g., DGPC1 (Figure 65). Primarily this joint would substantially restrict lateral move-

ment of the squamosal and medial movement of the postorbital. However, when the facet of the squamosal is deeper it would also restrict anterior or dorsoventral movement of the squamosal and posterior or dorsoventral movement of the postorbital.

Squamosal-quadrate/quadratojugal

In posterolateral view, this slightly convoluted seam extends posterodorsally from the junction with the jugal, with only the posterior portion curving over the dorsal tip of the quadrate. In posterior view the seam can be seen to continue anteromedially before disappearing at the junction with the pterygoid. In medial view, the seam travels posteriorly from the junction with the jugal, curves over the quadratojugal foramen and continues dorsally before turning anteromedially to the junction with the pterygoid.

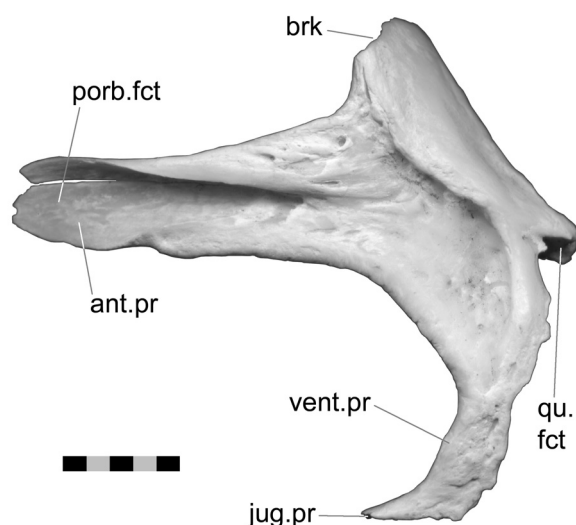


FIGURE 65. Squamosal in lateral view. Scale bar equals 10 mm.

The squamosal articulates with the head of the quadrate in a seemingly firm slotted joint (Figures 64, 67, 68, 69, and 70) that can be divided into three parts: a lateral part, a small posterior part (above the quadratojugal foramen) and large posteromedial part. In the lateral portion the ventral process of the squamosal sits on the dorsal edge of the quadratojugal but the lateral part of the interface alters along its length. Anteriorly, where this joint is associated with the jugal, the quadratojugal is 'L' shaped in cross-section with a dorsally expanded medial edge ('A' in Figure 68.3). This medial edge is enveloped by the squamosal which bears a number of anteroventrally directed ridges ('B' in Figure 68.3). The opposing facet on the quadratojugal is rough but matching grooves are not obvious (Figure 64). More posteriorly, near the posterior part of the quadratojugal-jugal joint, the lateral edge of the quadratojugal expands dorsally (Figure 64.2). At this point the dorsal surface of the quadratojugal is concave (Figure 67). Correspondingly, the squamosal surface exhibits a wide convex ridge and two grooves to accept the surface (Figure 67, 'C' in Figure 68.3). In the posterior part of the squamosal-quadratojugal joint both bones widen, and the facets are rugose but the interface between the two bones is more planar and abutting ('D' and 'E' in Figure 68.3).

The posteromedial part of the joint is associated with the pterygoid-squamosal joint, and consists of two slot joints ('F' in Figure 68.3). The posteriormost and largest of these slot joints involves the dorsal tip of the quadrate which is an expanded bun-like process with an anteromedially

directed long axis (Figures 64, 68, 69). This 'bun' is held in a large concavity in the squamosal (Figures 68) between two ventral extensions (Howes and Swinnerton 1901): a robust posteromedial process (or lappet) which extends ventrally from the dorsal process and a longer thinner process which extends anteromedially from the squamosal ventral process and is associated with the squamosa-ptyergoid joint (Figure 69.2). The second slot joint involves the thinner process and extends anteriorly into a slightly sigmoid groove on the crest of the quadrate wing (Figure 68.2). The groove itself is contiguous with the rough posterior portion of the quadrate-squamosal joint. Posteriorly, the medial border is strongest (consisting of the quadrate dorsal process) but anteriorly the lateral border is strongest. Anteriorly the base of this groove is perforated by foramina. In both the lateral and posterior parts a short curtain of bone, extending ventrally from the medial edge of the squamosal ventral process, overlaps the dorsomedial edge of the quadrate/quadratojugal. This arrangement increases the contact between the bones. The ventral extension is continuous with the anteromedial squamosal process that slots into the quadrate posteromedially. The joint would prevent significant movement between the two bones in all directions except either dorsal movement of the squamosal or ventral movement of the quadrate.

The expanded bun-like process of the quadrate is spongy and "unfinished" surface suggesting a cartilage component to the joint or small synovial cavity ('F' in Figure 68.3) (Jones 2006). Holliday and Witmer (2008) considered a synovial joint to be present here in *Sphenodon* but did not fully explain the basis for this inference.

The ventral process of the squamosal in hatchling *Sphenodon* is comparable to that of adults, bearing medial and lateral extensions to hold the quadratojugal. There also seems to be a pocket for the head of the quadrate (Rieppel 1992, figure 2). However, there is no apparent posteromedial lappet as found in juvenile specimens (LDUCZ x1176).

Pterygoid-squamosal

This joint is related to the squamosal-quadratojugal joint and the posterior part of the pterygoid-quadratojugal joint. The posterodorsal processes of the pterygoid wing (Figure 70.3) slot into a pocket formed by the anterior ends of the squamosal posteromedial and anteromedial processes (Figures 67, 68, 69). The tip of the posterodorsal process of the pterygoid wing is roughly

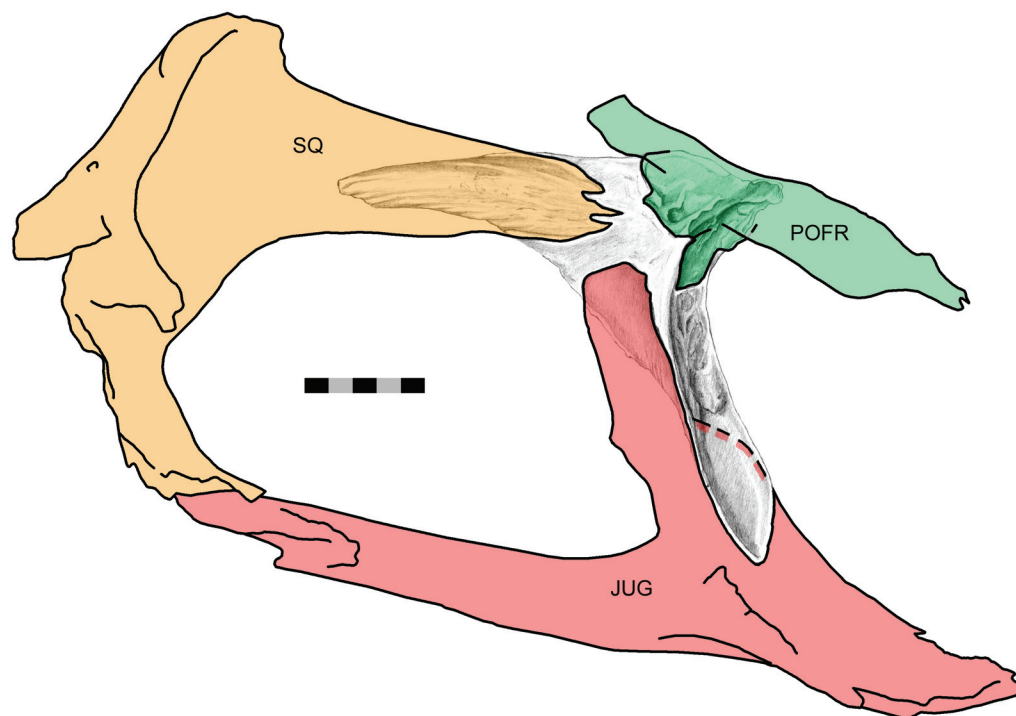


FIGURE 66. Left postorbital (DGPC1) in medial view after disarticulation, overlain by the ghosts of the surrounding bones. Blue = postorbital, orange = squamosal, red = jugal, green = postfrontal. Scale bar equals 10 mm.

rectangular in cross-section but bears longitudinal grooves and ridges along its surface. The facet on the squamosal also bears some texture. The pocket would resist mediolateral movements between the two bones.

Pterygoid-quadrate

As previously observed (e.g., Robinson 1973), the quadrate of *Sphenodon* is firmly joined to the pterygoid. Primarily, the joint involves the lateral surface of the pterygoid posterolateral process and the medial surface of the quadrate anteromedial process (Figures 69, 70, 71, 72). However, there are two features of note. Firstly, the ventral edge of the pterygoid wing slots into a gutter that runs laterally along the base of the quadrate wing (Figure 69, 72); secondly, the posterodorsal tip of the pterygoid wing abuts the main body of the quadrate and is related to the squamosal-ptyerygoid joint (Figures 67, 'G' in Figure 68.3). In posterior view the seam has a long sigmoid shape (Jones et al. 2009). From the base of the quadrate-ptyerygoid wing it passes posterodorsally, turns anterodorsally and finally turns posterodorsally again before terminating at a junction with the squamosal. In anteromedial view the short seam runs anteriorly,

dorsally and then anteriorly again, before reaching the base of the epiptyerygoid.

Quadrate-quadratejugal

In *Sphenodon* this connection is fused ventrally but a faint seam may be visible dorsolaterally above the quadratejugal foramen (e.g., DGPC1, LDUCZ x036) (Figure 72). In hatchlings the bones are not fused (Howes and Swinnerton 1901; Rieppel, 1992).

Metakinetic joints

The metakinetic joints include those located between the back of the skull and the braincase. The metakinetic unit is linked to the roofing unit by the parietal and squamosal, and to the palatal, rostral and temporal units by the pterygoid. The usage of metakinetic to describe this unit should not be taken to imply that metakinetic movements occur in this taxon.

Epiptyerygoid-quadrate

Robinson (1973) incorrectly thought the epiptyerygoid of *Sphenodon* overlapped the quadrate. In actuality, the posterior end of the epiptyerygoid base sits against the pterygoid abutting the anterior edge of the quadrate (Figures 70, 71, 72, 73;

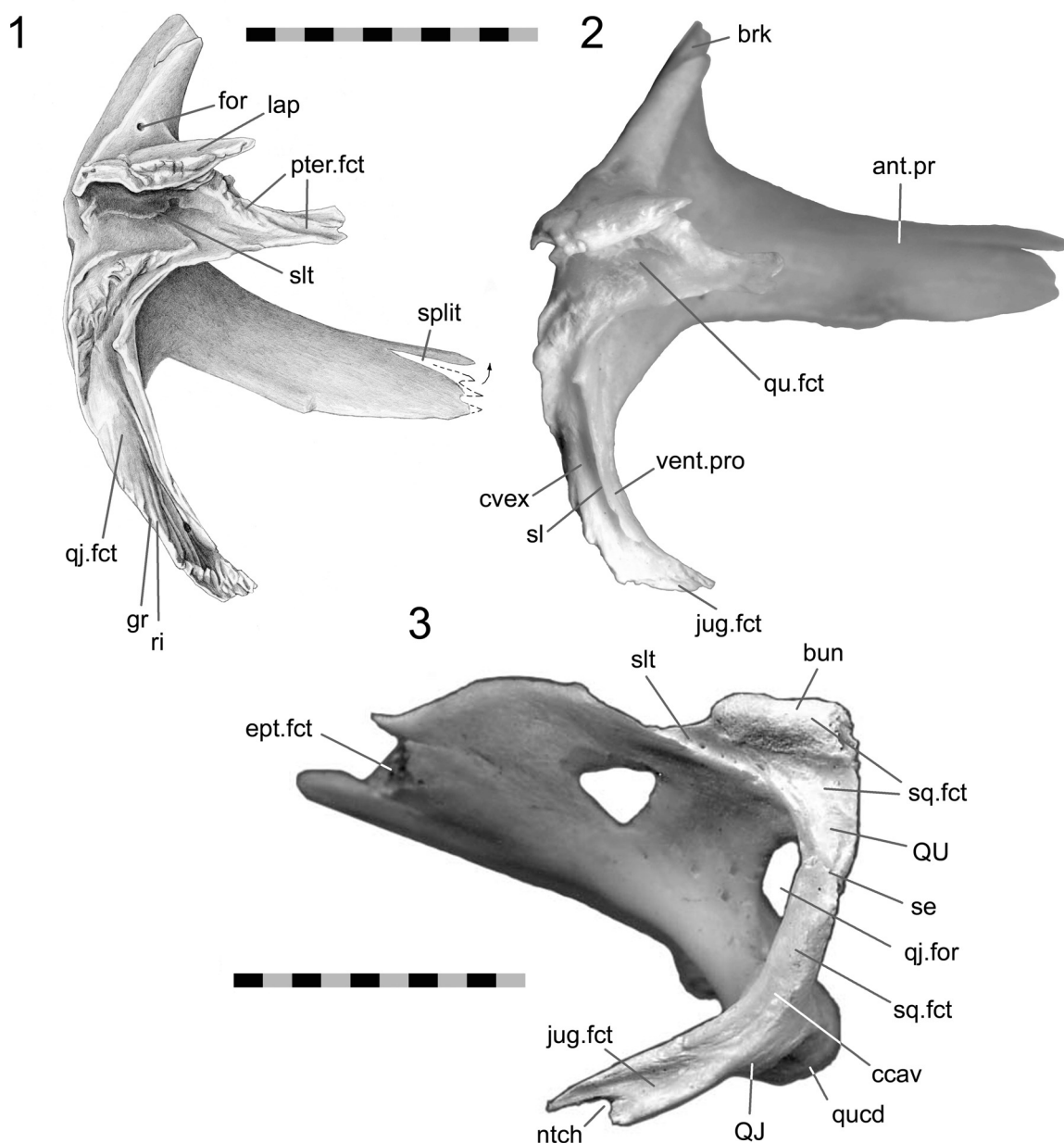


FIGURE 67. Squamosal-quadrate-quadratejugal joint (DGPC1). 1. and 2. isolated squamosal in ventromedial view. 3. quadrate-quadratejugal in dorsolateral view. Scale bar equals 10 mm.

Appendix 2). From the junction with the pterygoid base of the quadrate-ptyergoid wing, in anterolateral view, the seam travels anterodorsally, posteriorly, dorsally and finally anterodorsally again. The two anterior processes from the quadrate (dorsal and ventral) are thin but rigid, and the edge of the quadrate between them is expanded and lacks a finished anterior surface. The corresponding posterior end of the epipterygoid also lacks a surface. The dorsally orientated part of the seam (between the unfinished ends of the epipterygoid and quad-

rate) is sometimes very wide and contains substantial space for soft tissue (e.g., DGPC 2, LDUCZ x1176). In AIM LH833 and the left side of LDUCZ x036 the seam is not easily discernable which suggests that the bones may have begun to fuse. This occurrence is perhaps not unexpected as both are endochondral bones and are derived from the same palatoquadrate cartilage (Howes and Swinerton 1901; Schauinsland 1903; Werner 1962; Rieppel 1992; Evans 2008).

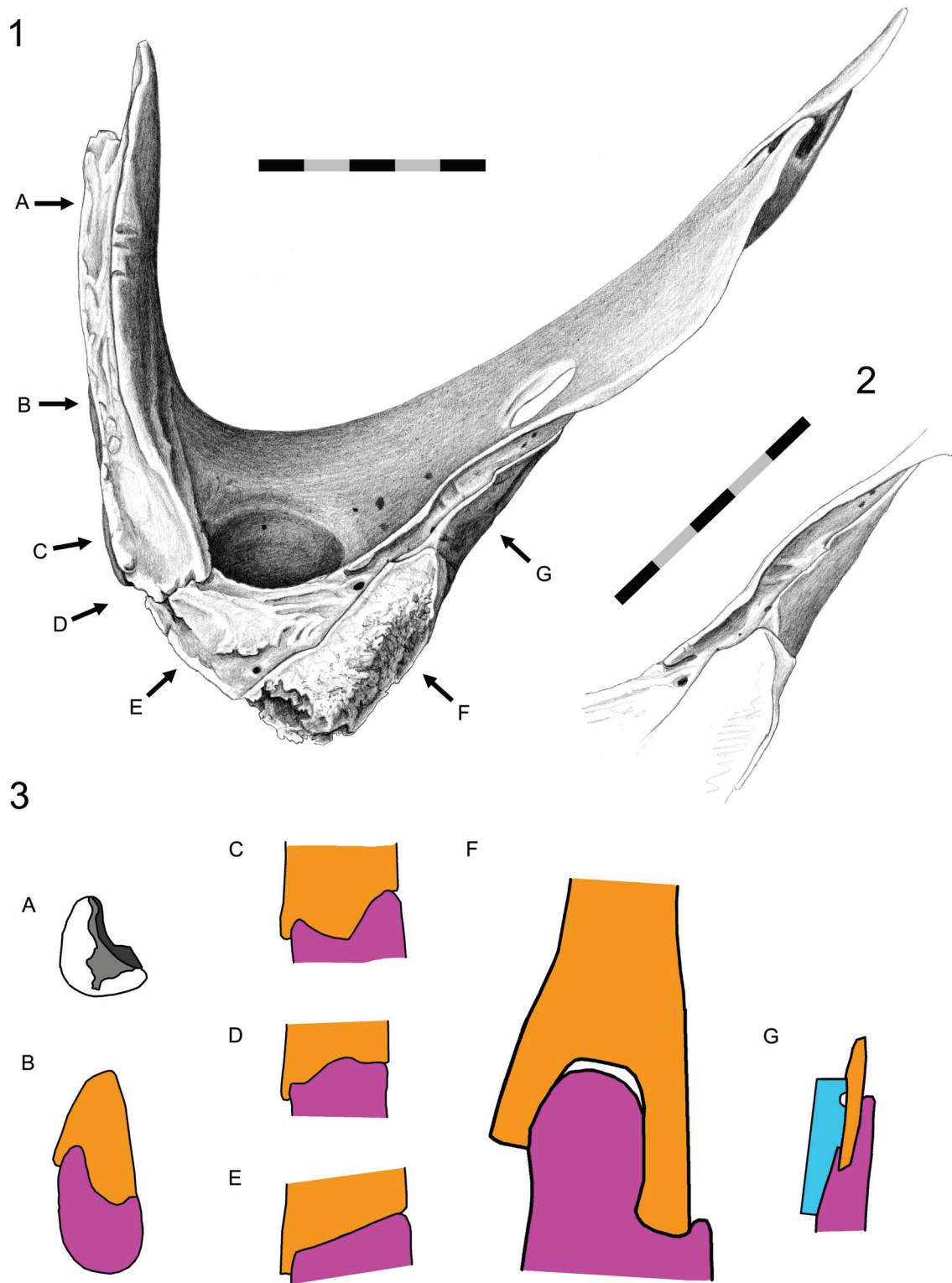


FIGURE 68. Squamosal-quadrate-quadratejugal joint (DGPC1). 1. quadrate-quadratejugal in dorsal view. 2. close up of the gutter on the crest of the quadrate wing. 3. inferred cross-sections in anterior view along the quadrate-quadratejugal-squamosal joint. Numbers indicate position of the cross-sections. Blue = pterygoid, orange = squamosal, Pink = quadrate/quadratejugal. Scale bar equals 5 mm.

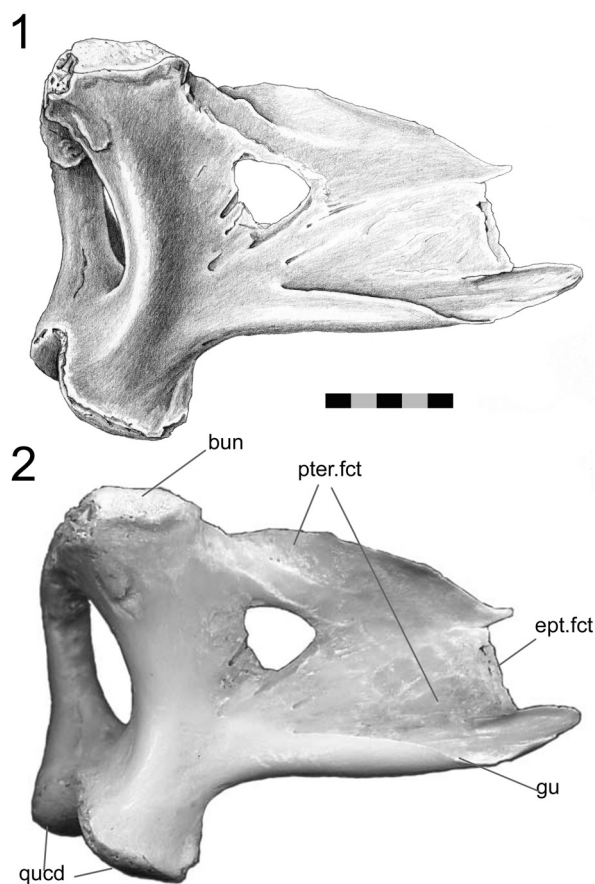


FIGURE 69. Quadrato-quadratojugal (DGPC1) in posteromedial view. Scale bar equals 5 mm.

Pterygoid-basisphenoid [sphenoid]

This joint may be referred to as the basiptyergoid articulation (e.g., Evans 2003; Johnston 2010) or basal joint (Holliday and Witmer 2008). In squamates this joint is synovial, permitting mobility associated with metakinesis (Evans 1980, 2003). Günther (1867, p. 599) referred to this joint in *Sphenodon* as “immoveable” whereas Romer (1956, p. 114) refers to it as “moveable”. Neither author illustrated the articulation or described it further. More recently, Arnold (1998, p. 325) considered this joint to be mobile in juveniles. Evidence for a synovial joint and interarticular cartilage has also been reported for *Sphenodon* based on examination of hatchling (Howes and Swinnerton 1901) and adult material (Holiday and Witmer 2008; Johnston 2010).

Several dry specimens and CT data sets of YPM 9194 and LDUCZ x036 demonstrate that the ventral tips of the basisphenoid rest in pockets on the medial surface of the pterygoids. The pockets

are enclosed ventrally, anteriorly and medially but not posteriorly or dorsally (Figures 38.3, 39.2, 70.4). In LDUCZ x1176 the pockets are comparably enclosed. However, in hatchlings the medial boundary is almost absent (CM 30660, Maisano 2001).

Pterygoid-epipterygoid

In *Sphenodon* the epiptyergoid sits against the lateral surface of the pterygoid wing (Figures 70, 71). Dorsal expansion of the pterygoid increases the surface area between the two bones and, at least in DGPC1, the dorsal edge bears three triangular processes (Figure 70.1). The facet on the epiptyergoid is inset (Figure 73) and within it there is a depression that corresponds to a mound on the pterygoid (Figure 70.1). The anterior edge of the pterygoid bears a subtle lappet which folds around the anterior edge of the epiptyergoid (Figure 70.1). Both facets possess additional texture on their surface. The joint would have physically prevented medial movements of epiptyergoid and resisted ventral, anterior and posterior movements.

Parietal-supraoccipital

In mammals, this joint is sometimes referred to as the lamboid suture (e.g., Opperman 2000). In *Sphenodon* (e.g., DGPC 2, LDUCZ x036) the lateral edges of the parietal extend ventrolaterally (Figure 59) overlapping the dorsal surface of the supraoccipital, but there is otherwise no distinct facet. The joint would have prevented the supraoccipital from moving dorsally and the parietal from moving ventrally. It would also reduce mediolateral movement between the paired bones.

Squamosal-opisthotic

At its tip, the anterolateral surface of the paroccipital process (opisthotic) rests against the posterior corner of the squamosal (e.g., DGPC2, LDUCZ x036). The joint appears to be fibrous.

Epiptyergoid-prootic

The posteromedial surface of the dorsal process of the epiptyergoid overlaps the anterior edge of the prootic. The joint appears to involve fibrous tissue (e.g., LDUCZ x036).

SUMMARY OF RESULTS

General Observations

The above description illustrates that a wide variety of joint types can be found in the skull of *Sphenodon*. For the most part, they can be

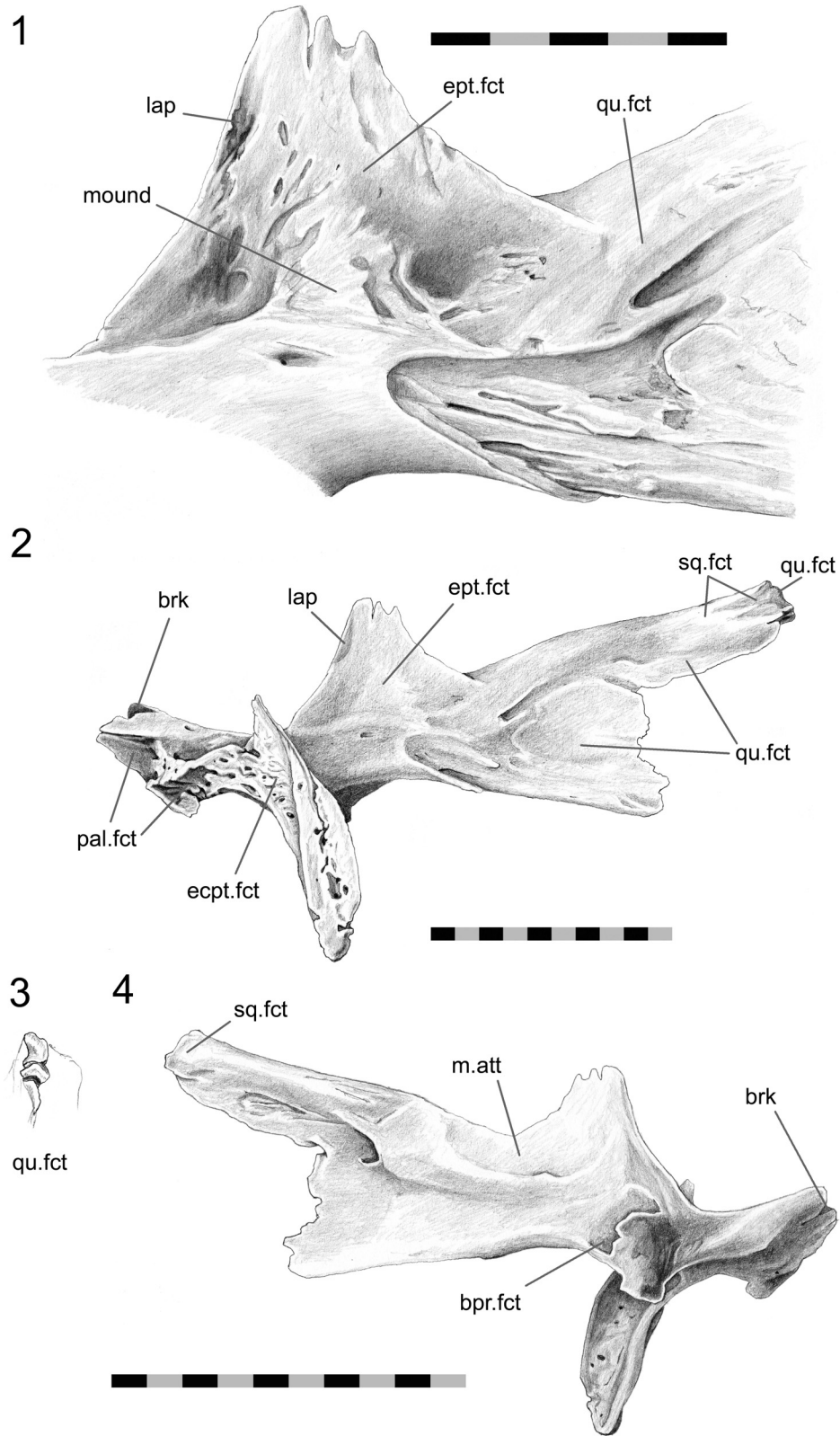


FIGURE 70. Pterygoid (DGCP1). 1. close up of the epipterygoid facet in anterolateral view. 2. anterolateral view (anterior process broken). 3. posterodorsal view of the posterodorsal process of the pterygoid. 4. posteromedial view (anterior process broken). Scale bar equals 5 mm (1), 10 mm (2-4).

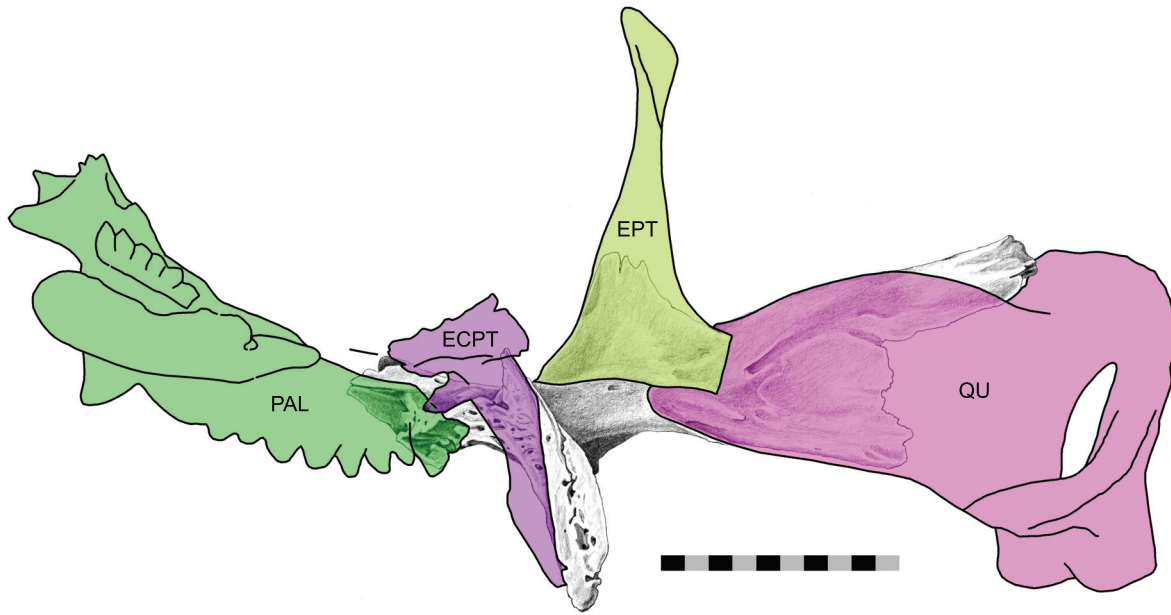


FIGURE 71. Left pterygoid (DGCP1) in anterolateral view overlain with the ghosts of surrounding bones. Purple = ectopterygoid, grass green = palatine, pea green = epipterygoid, pink = quadrate. Scale bar equals 10 mm.

grouped into the three main categories of abutments, overlaps and interdigitations, but the number and distribution of these joint types across the skull show distinct characteristics. The medial edges of midline bones tend to be dorsoventrally expanded, which increases the surface area of

contact (e.g., vomers, parietals). These midline joints are mainly abutments (e.g., interparietal), although some show limited interdigitation (e.g., vomers, pterygoids). In contrast, joints along the sides of the skull involve extensive overlaps (e.g., maxilla-jugal, postorbital-squamosal) (Appendix 2; Figures 74, 75, 76, 77). Some of these overlap joints are relatively simple contacts (e.g., internasal) whereas others have more complex interlocking arrangements (e.g., frontal-parietal, palatine-prefrontal); joints where a tongue-shaped process sits in a basin-like depression are common (e.g., jugal-maxilla, postfrontal-postorbital, nasal-frontal, postorbital-squamosal). Less frequent in *Sphenodon*, in contrast to most early tetrapods (e.g., Kathe 1995), are joints in which bones meet along the same plane. Nevertheless, some planar joints are found in the skull roof (e.g., nasal-frontal, frontal-parietal), palate (palatine-ptyergoid, palatine-vomer) or lateral surfaces (e.g., palatine-maxilla, ectopterygoid-jugal). Interdigitated joints are rare in *Sphenodon* and essentially limited to the interpterygoid and the prefrontal-palatine joints. Extensive Type-C interdigitations like those found in mammals, chelonians and crocodiles (e.g., Iordan sky 1973; Gaffney 1979; Jaslow 1990) are absent.

Two different joints may occur between the same pair of bones (e.g., palatine and maxilla, prefrontal and maxilla) and, as in other tetrapods (e.g., Clack 2002), joint morphology can change along

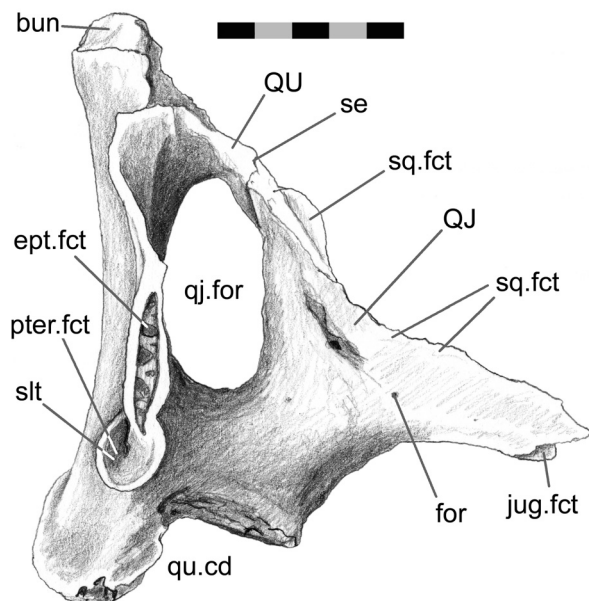


FIGURE 72. Quadrate-quadratejugal in anteromedial view (DGCP1). Scale bar equals 5 mm.

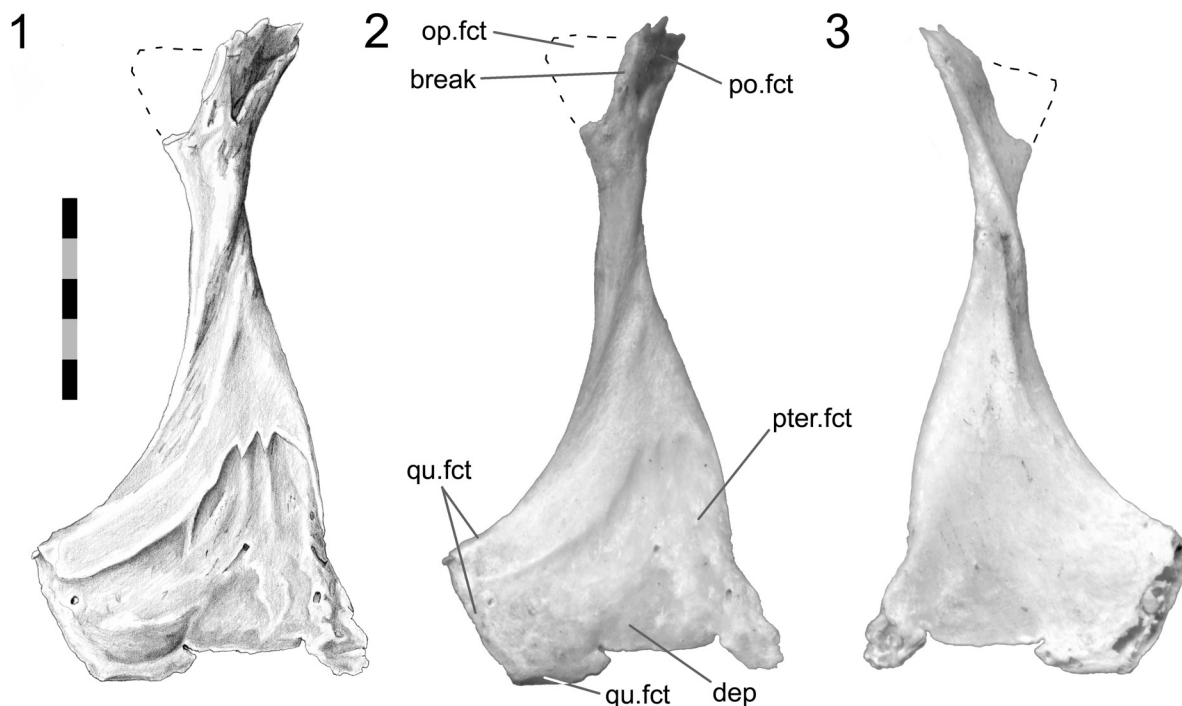


FIGURE 73. Epipterygoid. 1. lateral view. 2. lateral view labelled. 3. medial view. Scale bar equals 5 mm.

the suture (e.g., the palatine-pterygoid suture). At one point in a joint 'bone X' may overlap 'bone Y' but at another part of the suture the opposite occurs (e.g., nasal-prefrontal, prefrontal-frontal, intervomerine, postfrontal-frontal, frontal-parietal). As in other taxa (e.g., Moss 1957; Clack, 2002; Sun et al. 2004), some joints bear a complex external seam but internally the contacting surfaces are relatively smooth (e.g., ectopterygoid-jugal joint).

Many joints, particularly along the dorsal and ventral margins of the skull, involve three or, occasionally, four bones (Figure 77, e.g., jugal-maxilla-ectopterygoid, frontal-postfrontal-parietal, jugal-squamosal-quadratojugal). This arrangement can result in strong triple overlaps (e.g., the maxilla-prefrontal-nasal, vomer-palatine-pterygoid), although similar complex overlaps can occur between two bones where one possesses a pocket or tab into which the other slots (Figure 78) (e.g., premaxilla-nasal, palatine-vomer, nasal-maxilla, parietal-postfrontal, and to some extent, the palatine-prefrontal and squamosal-postorbital).

Following disarticulation of the skull, relatively few bones can be rearticulated so that they remain locked together in most orientations (e.g., the postfrontal and postorbital or the frontals and parietals). Most cranial joints require soft tissue and/or the presence of other bones to maintain the articulation (e.g., palatine-maxilla or premaxilla-palatine).

Indeed, the surfaces of a few bones bear no trace of facets and are maintained entirely by soft tissue (e.g., the premaxilla-vomerine joint). This characteristic reflects the amount of soft tissue in many of the cranial joints of this genus and explains the rarity of articulated Holocene specimens of *Sphenodon* (Gill, personal commun., 2006).

Facet surfaces, where present, are generally smooth but can be ridged (e.g., nasal-frontal), pitted (e.g., pterygoid-ectopterygoid) or striated (e.g., maxilla-jugal) to maximise the attachment area for collagen fibres. Within a single joint there may be variation in the location of texture (e.g., jugal-postorbital, maxilla-jugal). Usually the texture is reflected on opposing facet surfaces but not always (e.g., prefrontal-maxilla).

Variation within *Sphenodon*

In *Sphenodon*, sutures in larger skulls usually show a greater degree of overlap and facet texture than those in small skulls. Individual joints generally have the same gross morphology between skulls of similar size but there is variation in the edges of processes, position of seams, facet texture and other minor details. Given the limited sample of juvenile *Sphenodon* skulls, it is still difficult to disentangle ontogenetic variation from individual variation, but some differences are obvious.

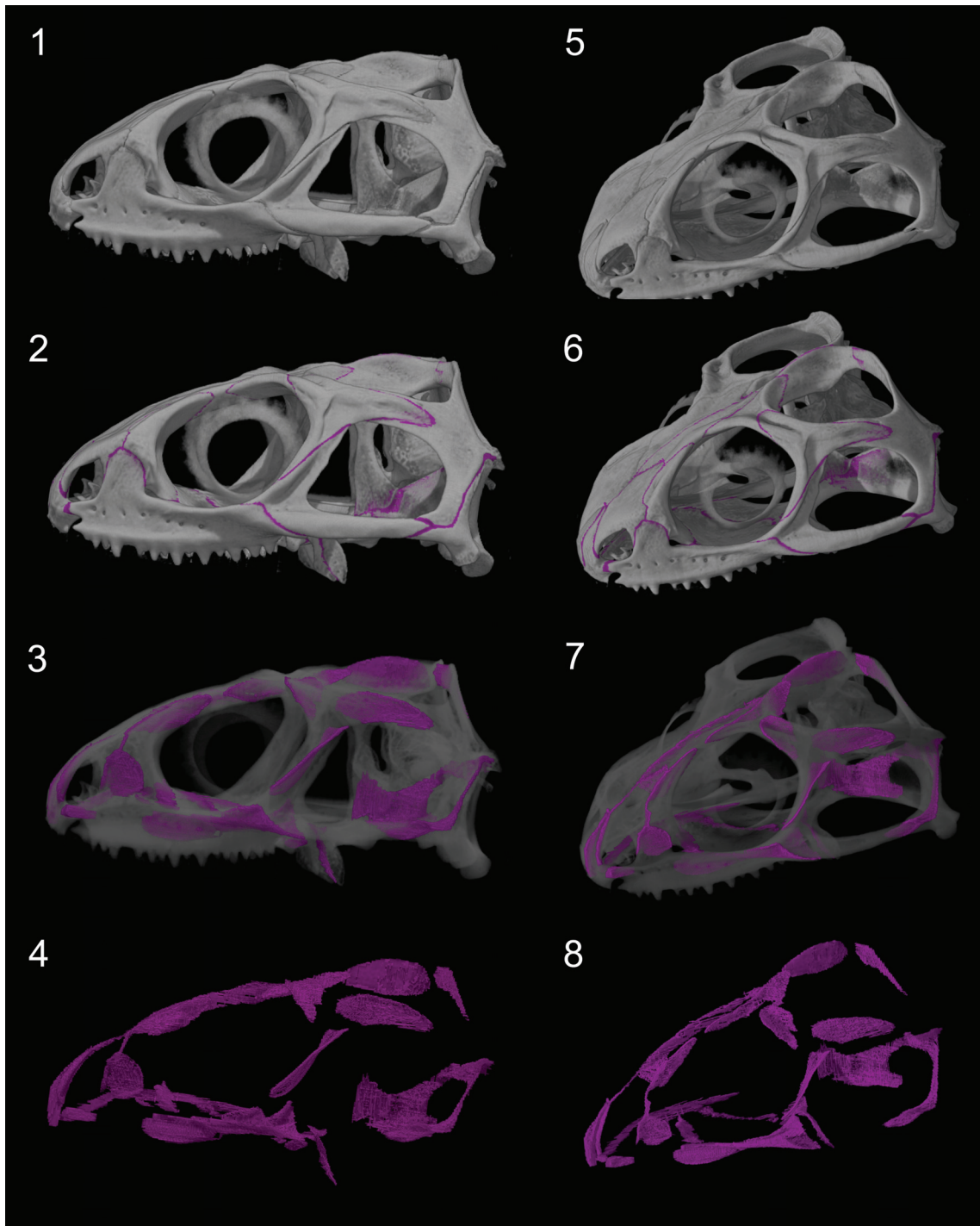


FIGURE 74. Sphenodon skull YPM9194 CT model in dorsolateral view. 1.-4. lateral view. 5.-8. dorsolateral view. 1. and 5. surface topology. 2. and 6. surface topology with sutures segmented in pink. 3. and 7. surface topology with sutures segmented in pink and bone reduced to 40% opacity. 4. and 8. sutures segmented in pink and bone invisible. All images shown in reverse for comparison. Skull length is approximately 48.75 mm.

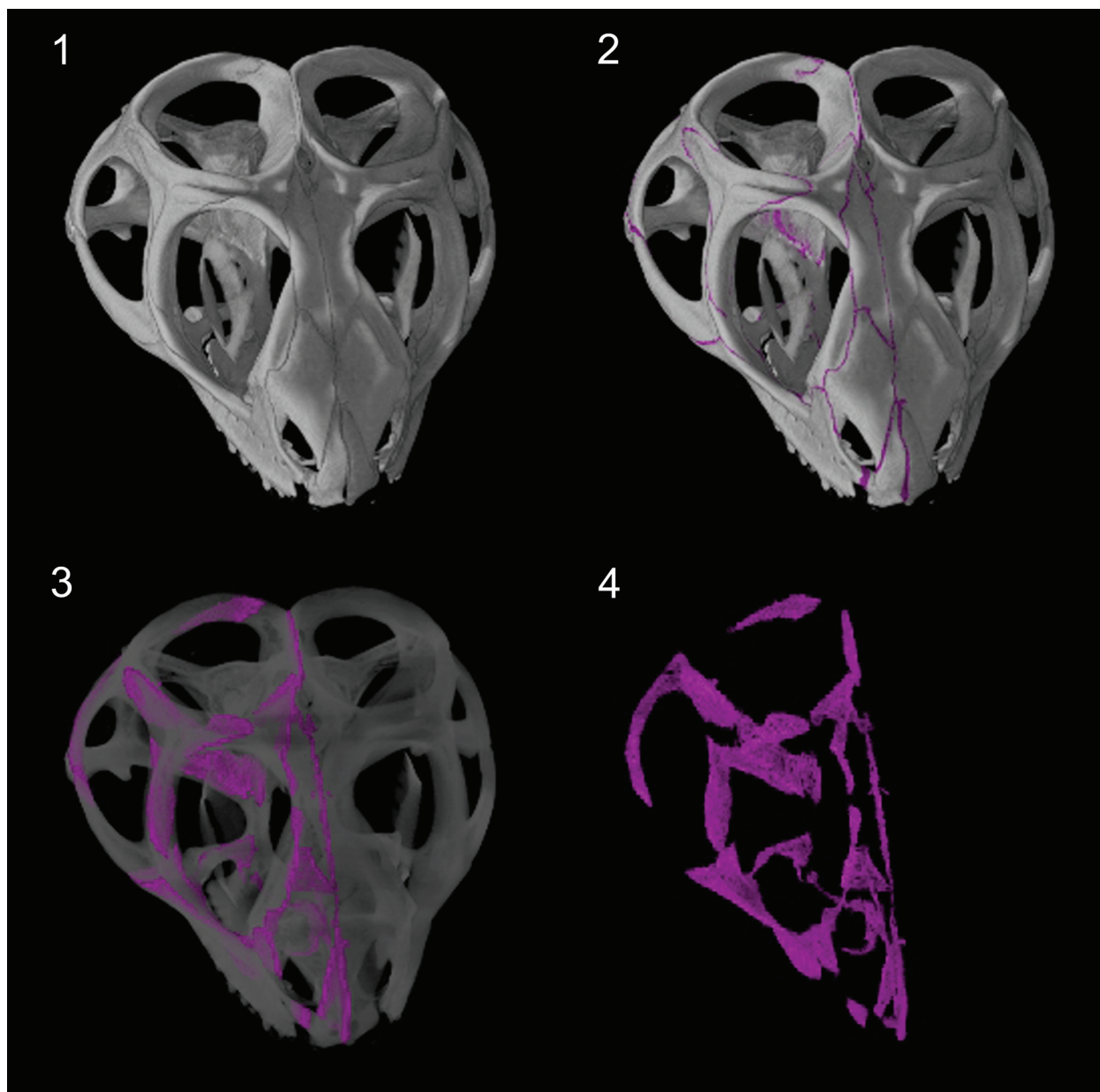


FIGURE 75. *Sphenodon* skull YPM9194 CT model in anterodorsal view. 1. surface topology. 2. surface topology with sutures segmented in pink. 3. surface topology with sutures segmented in pink and bone reduced to 40% opacity. 4. sutures segmented in pink and bone removed.

Adult (e.g., DGPC1, BMNH.K) and juvenile skulls (e.g., UCLGMX 1176) differ from large hatching skulls (e.g., Howes and Swinnerton 1901; Rieppel 1992) in the following ways: the frontoparietal and interparietal fontanelles have closed; the posterior process of the jugal is more extensively sutured to the quadrate and squamosal and the overlap between the squamosal and postorbital is more extensive. Adult skulls (e.g., BMNH.K, DGPC1) differ from juvenile skulls (e.g., UCLGMX 1176) in the following ways: the interpremaxillary

seam is less sigmoid; the ectopterygoid-jugal joint tends to be more interdigitated; the prefrontal-palatine seam tends to be more interdigitated; the jugal dorsal process has a squared off dorsal tip and the parietal crest is dorsally expanded. Between adult skulls (e.g., BMNH.K and DGPC1) the following variations occur: the presence or absence of the postfrontal cleft; the degree to which the vomer underlaps the palatine, the palatine overlaps the pterygoid centrally, the prefrontal overlaps the nasal and the frontal underlaps the nasal; the pres-

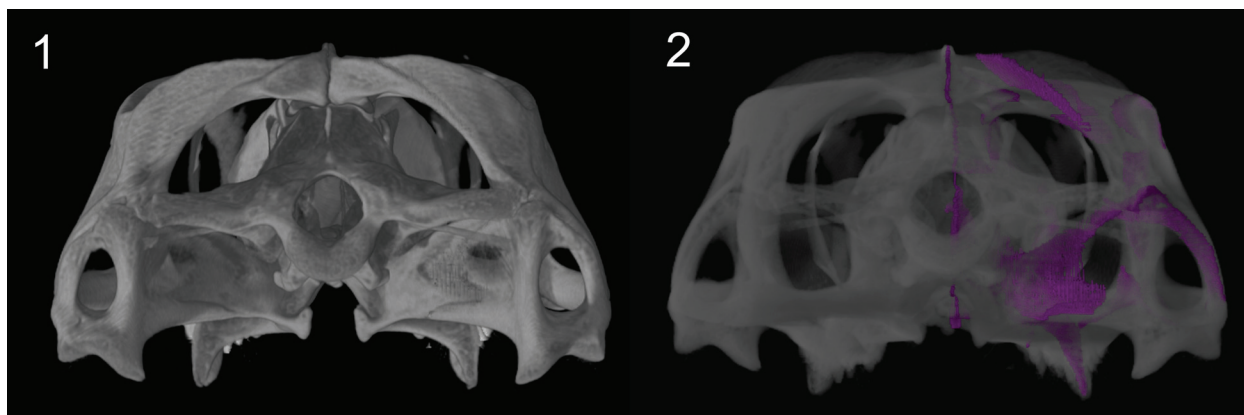


FIGURE 76. Sphenodon skull YPM9194 CT model in occipital view. 1. surface topology. 2. surface topology with sutures segmented in pink and bone reduced to 40% opacity.

ence or absence of a nasofrontal fontanelle; the shape of the nasofrontal, postfrontal-frontal and frontal-parietal seams; the level of texture present on the facets of the nasal-frontal joint; the exact arrangement of the jugal-squamosal-quadratojugal joint; and the degree to which the squamosal envelopes the postorbital.

There are several possible reasons for individual differences in joint morphology between adults of *Sphenodon*. One is variation in the pattern of mechanical forces transmitted around the skull, which is known to influence joint morphology (e.g., Moss 1954, 1961; Oudhof and Markens 1982; Nanda and Hickory 1984; Nash and Kokich 1985; Mao 2002; Mao et al. 2003). Variation in the stress regime may be the result of differences in diet (e.g., Ostrom 1962; Dalrymple 1977) so that animals with more abrasive diets experience more stress and therefore possess more complex sutures (Byron et al. 2004). It may also be related to where an individual prefers to bite along its tooth row. Variations in muscle arrangement (e.g., Haas 1973; Gorniak et al. 1981; Wu 2003; Jones et al. 2009), potentially linked to differences in genotype or behaviour, may also alter the location and orientation of stresses, as may variations in skull size and proportions linked to ontogeny (Jones 2008).

SKULL MECHANICS IN SPHENODON

Almost all of the cranial joints examined in *Sphenodon* remain patent through life, which suggests following the majority of skull growth they remain important to skull function. Using inferences similar to those employed by Herring (1972), Buckland-Wright (1978) and Taylor (1992), we combine our observations on cranial joints, with current understanding of the jaw muscles (e.g., Jones et

al. 2009) and observed skull architecture to develop a series of hypotheses about skull biomechanics in *Sphenodon*.

Forces Acting on the Skull

Forces acting on the skull in the living animal include gravity and occasional blows during fighting (Seligman et al. 2008; Jones and Lappin 2009) and prey acquisition, but most mechanical stress will be experienced during feeding: the temporal region and skull roof will be pulled downward as the jaw adductor muscles contract; the back of the cranium will be pushed up and to some extent anteriorly as the lower jaws are pulled against the quadrate condyles by the jaw adductor muscles; and the maxillae and other facial bones will be pushed dorsally as the jaws are brought against resistant food items. Therefore, in a very general way, we may expect the skull to act like a beam subject to three-point bending with compression along the dorsal surface and tension along the ventral margin (Taylor 1992; Russell and Thomaason 1993; Weishampel 1993; Preuschoft and Witzel 2002; Henderson 2002; Rafferty et al. 2003). However, this simple model is complicated by several other considerations:

- As in many other amniotes the pterygoid flanges will be pushed medially by the lower jaws as they are pulled upward and medially by the jaw muscles (Taylor 1992).
- Following jaw closure there is an anteriorly directed (prooral) shearing motion in *Sphenodon* (Farlow 1975; Gorniak et al. 1982; Curtis et al. 2010b).
- *Sphenodon* possesses a row of teeth on the lateral edge of the palatine bone parallel with the tooth row on the maxilla so that

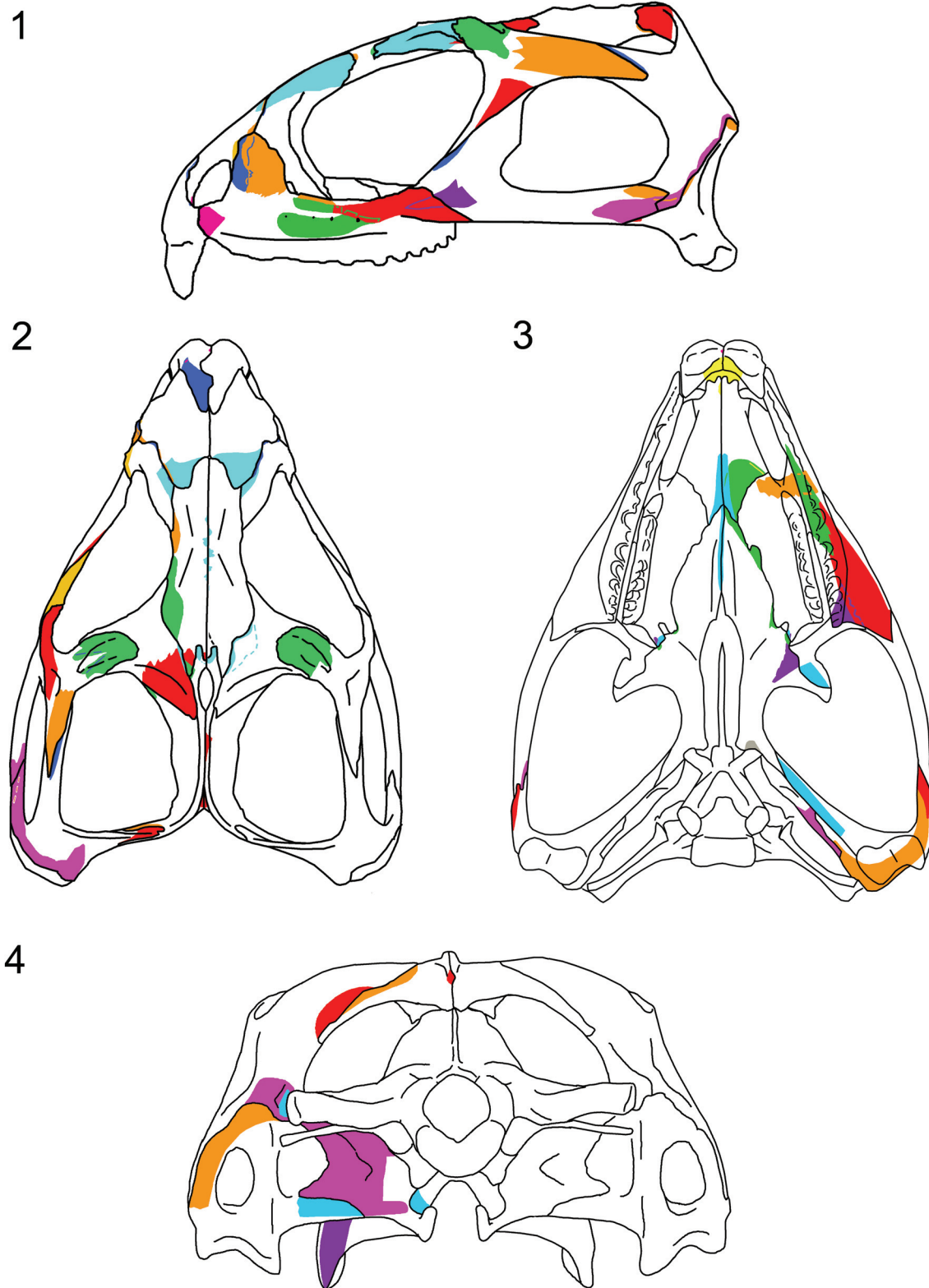


FIGURE 77. Locations and degrees of bone overlap in the skull. 1. lateral view (OMNH 908). 2. dorsal view (NMNZ RE0385). 3. ventral view (NMNZ RE0385). 4. occipital view (YPM 9194).

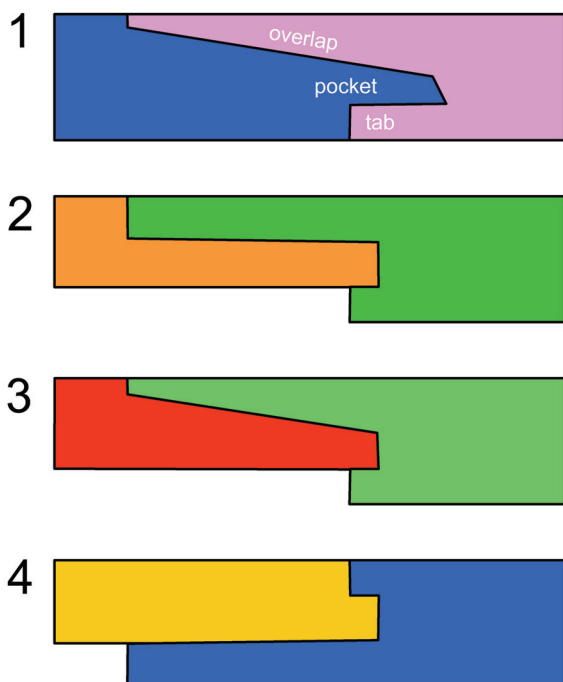


FIGURE 78. Schematic diagrams of a frequently encountered joint arrangement (an asymmetrical transverse slot and groove) shown in section and demonstrating the suture interface. Primarily the joint is an overlap but at one end there is a small pocket and tab so the joint also has the properties of a slot joint. 1. the overlap is scarfed (e.g., premaxilla-nasal). 2. the overlap is stepped (e.g., prefrontal-palatine). 3. a tab underlaps the neighbouring bone and is not hidden (e.g., parietal-postfrontal). 4. the pocket is located near the ectocranial surface rather than the endocranial surface (e.g., maxilla-nasal).

when the jaws close the lower (dentary) tooth row bites between the upper tooth rows (Gray 1831; Günther 1867; Gorniak et al. 1982; Jones et al. 2009). This type of occlusion means that during biting the palatine bones will receive a substantial component of the loading forces directly (Gorniak et al. 1982). In addition, as the jaws close, food will be forced between the upper tooth rows pushing them apart, and creating lateral forces on the posterior ends of the maxillae and medial forces on the posterior end of the palatines (Figure 79). The posteroventral surfaces of the premaxillary chisel-like teeth are also probably pushed forward at the end of the shearing action as evidenced by the wear facets found on the tips of the lower jaws (Reynoso 1996; Jones et al. 2009).

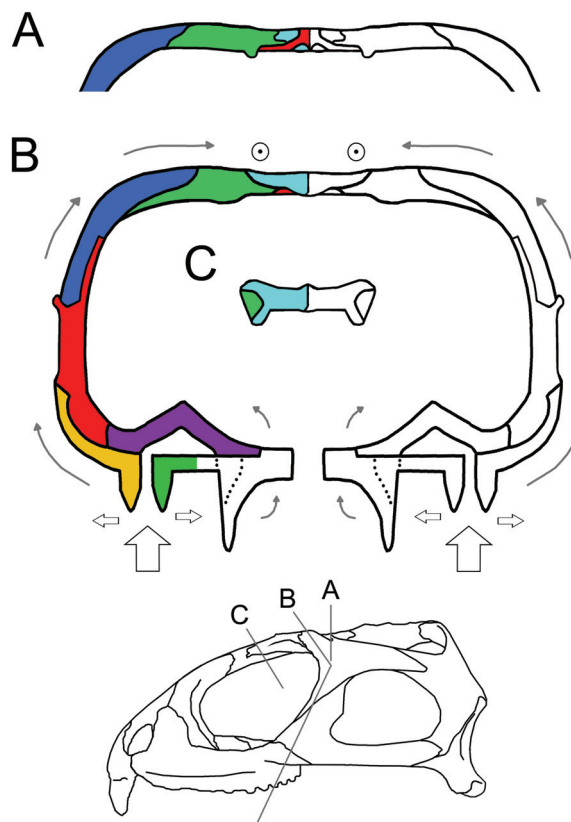


FIGURE 79. Schematic cross-sections through the skull of *Sphenodon*. A Cross-section through the posterior skull roof of *Sphenodon*; B Diagrammatic section through the central skull roof of *Sphenodon*; C Diagrammatic section through the anterior skull roof of *Sphenodon*. Light blue = frontal, purple = ectopterygoid, red = jugal or parietal, gold = maxilla, green = palatine or postfrontal, dark blue = postorbital.

- The prominent premaxillary teeth in adult *Sphenodon* are likely to contact a food item well before those on the maxilla and palatine. Hence, during a bite the premaxillae will experience loading well before the rest of the skull, causing shear or bending within the rostrum.
- *Sphenodon* is known to bite both unilaterally and bilaterally (Gorniak et al. 1982). Unilateral biting will generate complex torsional forces in the skull rather than simple long axis bending (e.g., Herring and Teng 2000; Thomason et al. 2001).
- The forces imposed on the skull by muscles are both important and complicated (Herring and Teng 2000; Herring et al. 2001; Thomason et al. 2001). When the lower jaw meets resistance (a food item) and the muscles contract, the sites of ori-

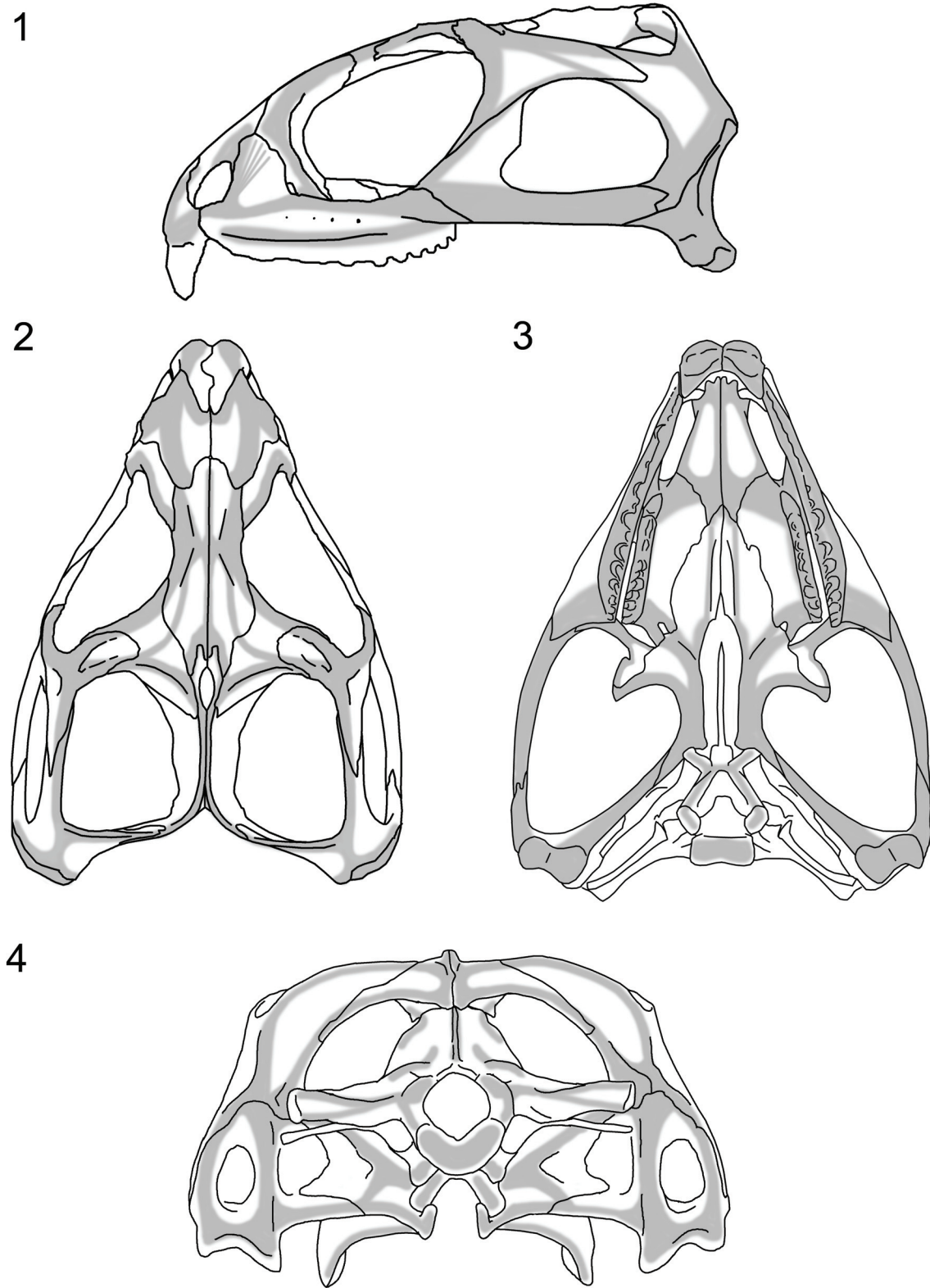


FIGURE 80. External ridges and thickenings in the skull of adult *Sphenodon*. 1. lateral view. 2. dorsal view. 3. ventral view with. 4. occipital views (YPM 9194). Based mainly on DGPC 1, DGPC 2, LDUCZ x036 and OMNH 908.

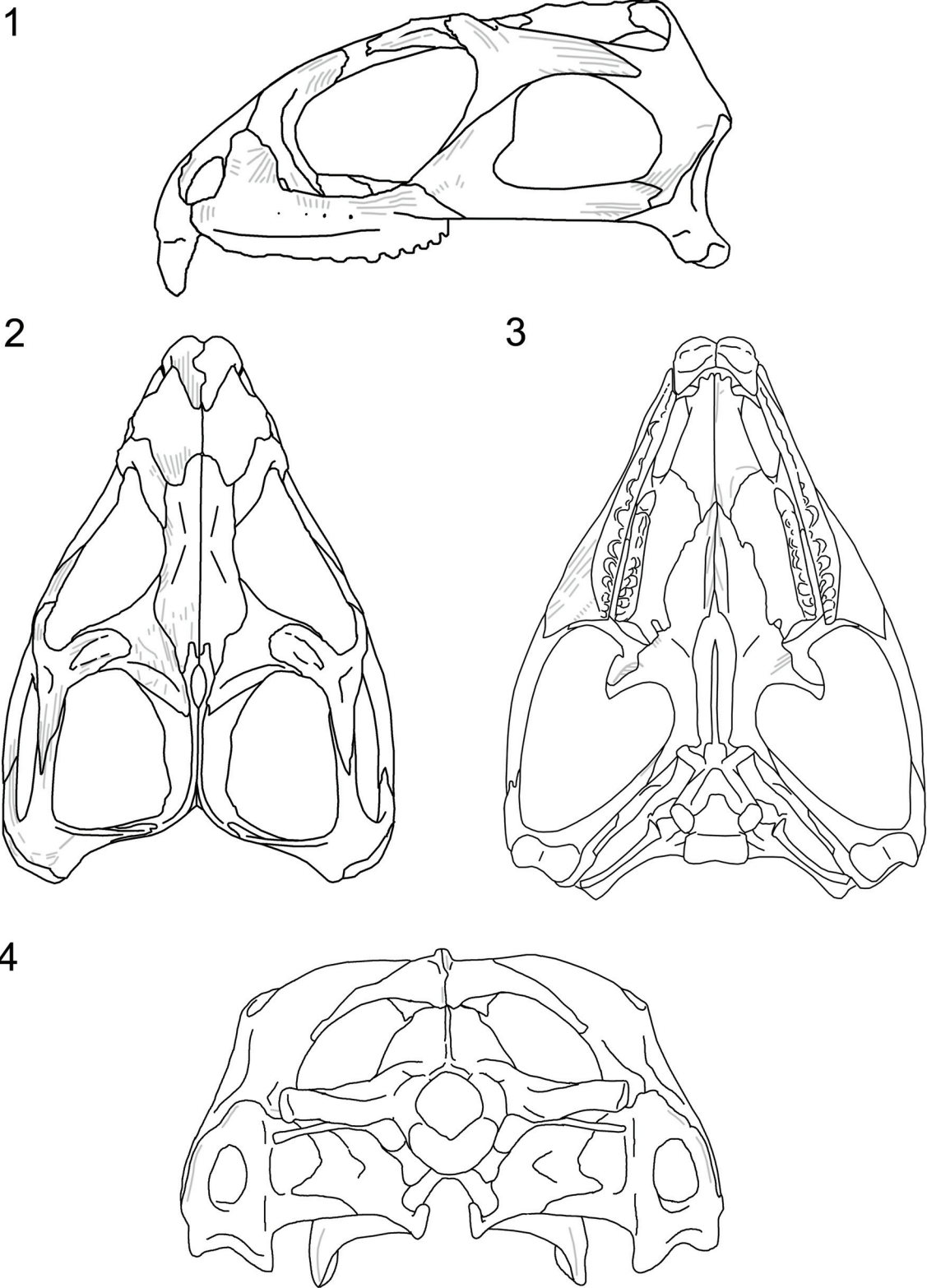


FIGURE 81. Internal ridges found on facet surfaces. 1. lateral, 2. dorsal, 3. palatal, 4. occipital views. Based mainly on specimens DGPC 1 and BMNH K.

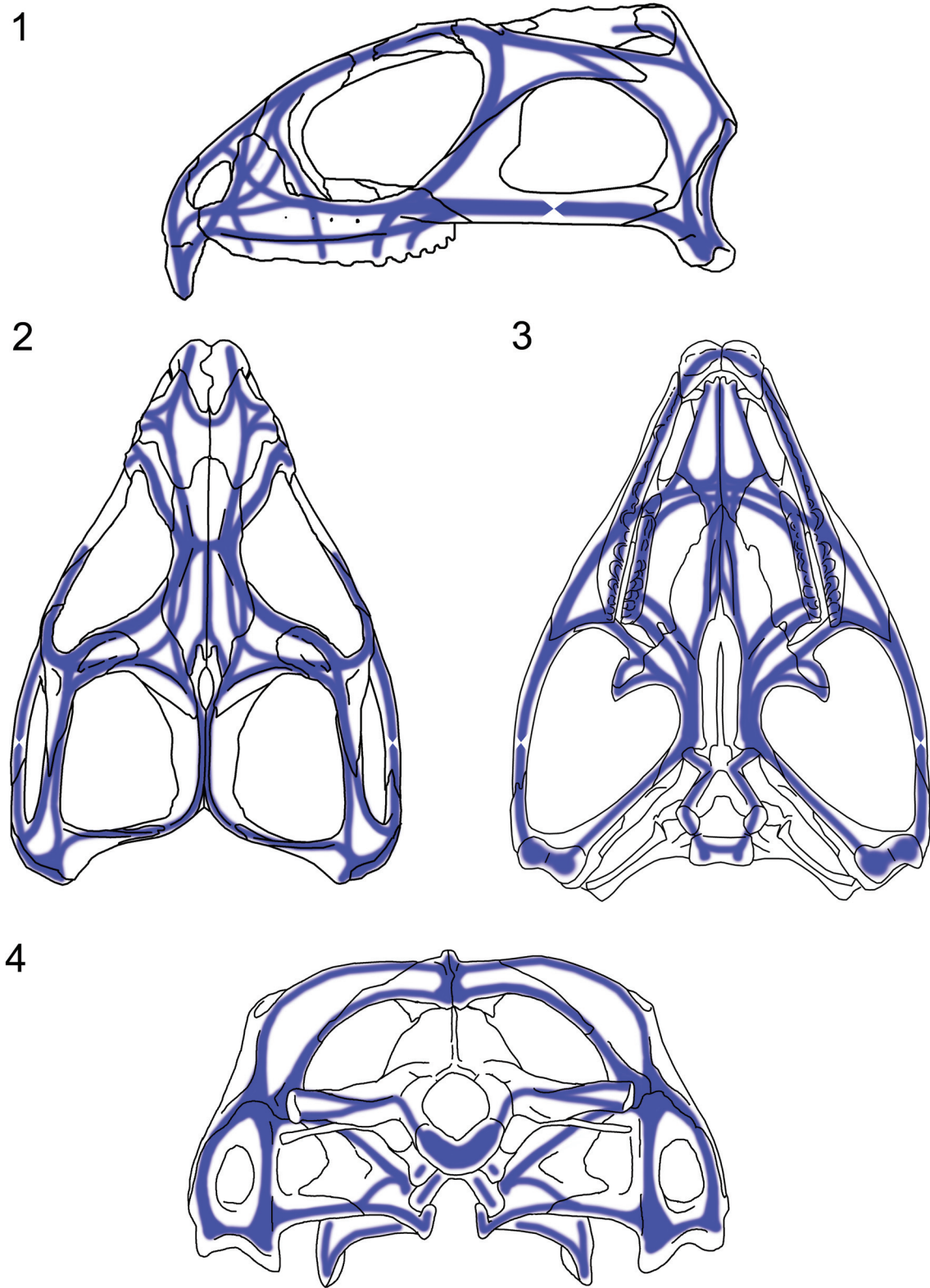


FIGURE 82. Hypothesis of compressive stress trajectories (HCST) expected in a *Sphenodon* skull during bilateral biting based on bony thickenings and facet ornament. 1. lateral, 2. dorsal, 3. palatal, 4. occipital views.

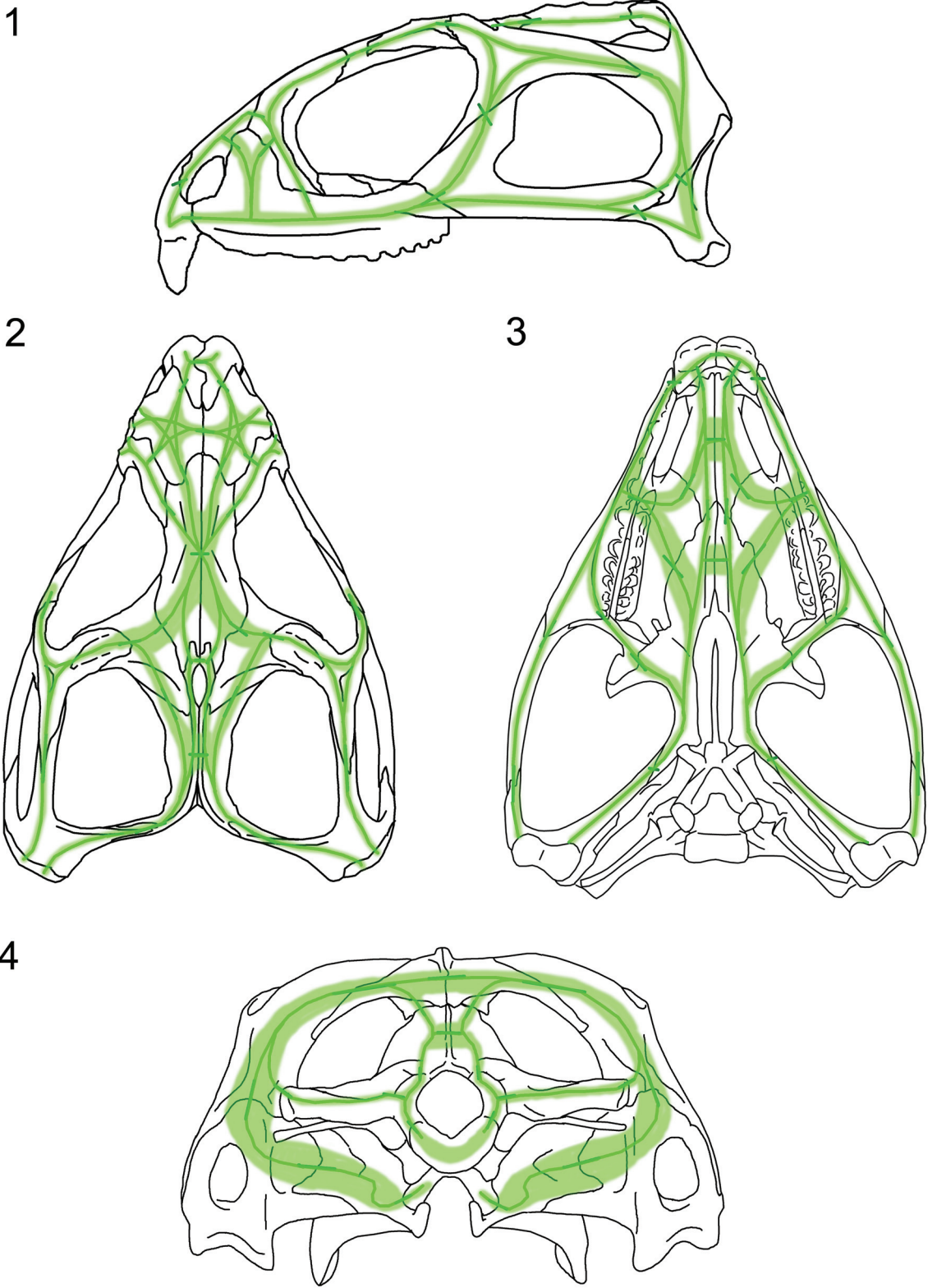


FIGURE 83. Trans-sutural web diagram for *Sphenodon* constructed using the guidelines of Thompson (1995, p. 195). 1. lateral, 2. dorsal, 3. palatal, 4. occipital views.

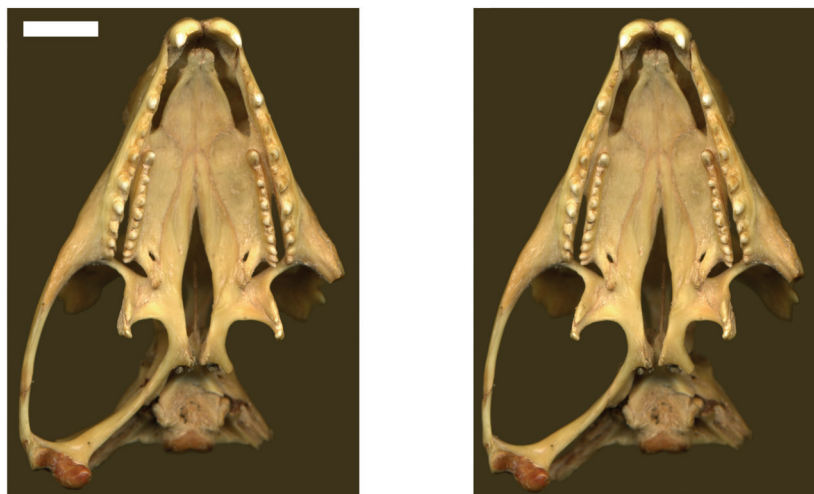


FIGURE 84. A stereopair of a *Sphenodon* skull (DGPC2) in ventral view demonstrating the vaulted nature of the palate. Scale bar equals 10 mm.

gin and attachment will experience tensile forces. The action of some muscles may cancel out the forces from others (Buckland-Wright 1978). However, the system will be dynamic because muscle vectors and forces will alter with gape and with bilateral or unilateral biting (Gorniak et al. 1982; Curtis et al. 2010b). As *in vivo* work on other taxa has demonstrated, some parts of the skull are likely to experience both tensile and compressive forces at different parts of a bite cycle during unilateral biting (e.g., Herring and Teng 2000; Herring et al. 2001; Thomason et al. 2001).

- The neck muscles may generate some posterior forces on the braincase and post-temporal arch during head movements related to feeding (e.g., Rayfield et al. 2001; Preuschoft and Witzel 2002; Jones et al. 2009).
- There may be some lateral force on the quadrates during food transport and swallowing.
- Together, the very low position of the jaw joint and the shape of the lower jaw in *Sphenodon* permit the tooth rows to meet almost evenly. As the mouth closes and the posterior teeth of the lower jaw and maxilla pass each other, so do the anterior teeth (e.g., DGPC 2). This arrangement means that when the jaws are nearly closed and the food item is relatively flat, the bite force will be evenly distributed along the tooth row. The situation will be

more complicated if the jaws encounter resistance when wide open.

- The marginal tooth rows of *Sphenodon* are relatively closer to the midline than those of many squamates (e.g., see Evans 2008) and early rhynchocephalians (e.g., Evans 1980; Whiteside 1986). The distance between the posterior ends of the tooth rows in the horizontal plane is about 60% that of the distance between the jaw joints (62%, $n = 20$, standard deviation = 0.33), which provides greater jaw stability during unilateral biting and makes bilateral biting more likely when dealing with large prey. Correspondingly, the skull is more likely to undergo bending rather than torsion in such instances.
- The skull of *Sphenodon* includes a number of bony bars and therefore, in contrast to many mammals, is an excellent example of a skull built by struts (*sensu* Preuschoft and Witzel 2002). Under torsional loading the junctions between these struts may be vulnerable to high concentrations of stress.
- Under loading, sutures will respond differently from the bones they unite.

These additional considerations highlight the unique feeding apparatus of *Sphenodon* and make it unlikely that the skull will behave exactly as a beam. Others (e.g., Thomason et al. 2001) have suggested that a tube might be a better model, at least for mammal skulls, but they also acknowledged that forces in the skull can be highly localized, as shown by Herring and Teng (2000). Thus although bite force was recently obtained for adult

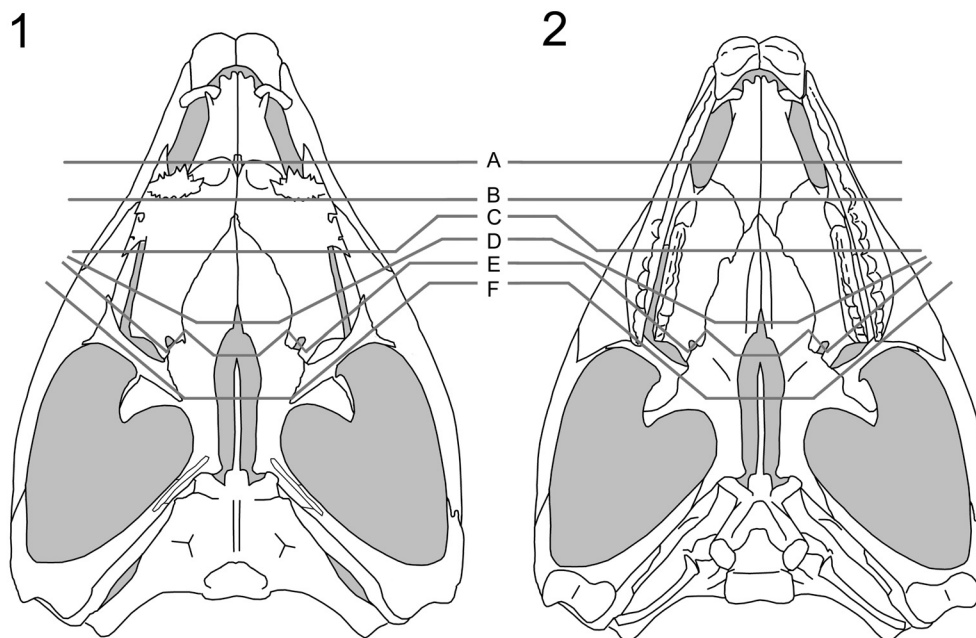


FIGURE 85. Diagrams illustrating the position of cross-sections in Figure 86. *Sphenodon* skull in (1) dorsal and (2) in ventral view.

Sphenodon (Jones and Lappin 2009; Herrel et al. 2010), the nature and magnitude of the stress generated during biting will vary depending on the exact location of the bite, gape and the amount of force used.

Ridges and Thickenings

Although the dermatocranial bones of vertebrates essentially develop as thin flat sheets, the adult elements are more complex in their morphology and typically show variation in bone thickness resulting from remodelling during ontogeny. This remodelling is thought to be a response to varying levels of mechanical loading within the skull, leading to the concept of 'Benninghoff trajectories' (Benninghoff 1934; Lehman 1973a, 1973b) whereby the areas of thickening form a network of reinforcing bony ridges (Benninghoff 1934; Fox 1964; Herring 1972; Lehman 1973a, 1973b; Buckland-Wright 1978; Lanyon 1980; Reisz 1981; Taylor 1992; Lieberman 1997; Thomason et al. 2001). In experiments that simulated biting action in dried skulls, Buckland-Wright (1978) found that these thickenings ("continua") were associated with the alignment of surface strains.

The skull of *Sphenodon* exhibits a consistent pattern of bony ridges and thickenings that is most conspicuous in larger skulls (Figures 5, 50, 80), which include ridges and thickenings in the mar-

gins of the orbits; the dorsal edges of the upper temporal bars; the anterior and posterior edges of the postfrontals; the anterior, posterior and ventral edges of the postorbitals; the dorsal and ventral margins of the pterygoid-quadrate wing; the ventral margins of the jugals; the boundaries of the jugal-postorbital and quadrate-squamosal joints and the secondary bone band along the alveolar margin of each maxilla. These ridges of bone increase the cross-sectional area and thus, by inference, the strength of the skull in particular regions liable to bending or twisting forces (e.g., the secondary bone band along the maxilla will provide a greater resistance to long-axis bending forces, Jones and Lappin 2009; Jones et al. 2009). Ridges of bone are not directed toward fontanelle locations (Figure 80), for example the nasofrontal junction, the central part of the nasal-prefrontal joint, and the central area between the pterygoid and frontal, or toward parts of the skull where the bone may be thin or absent, such as the central part of the quadrate wing (e.g., DGPS1, DGPS2, LDUCZ x036). Correspondingly bone is thought to be prone to removal where stress or (more specifically) compression is relatively low (e.g., Case 1924; Olson 1961; Frazzetta 1968; Oxnard et al. 1995; Preuschoft and Witzel 2002; Farke 2008).

Ridges and thickenings can also be found within facets (Figure 81). Herring (1972) and Buck-

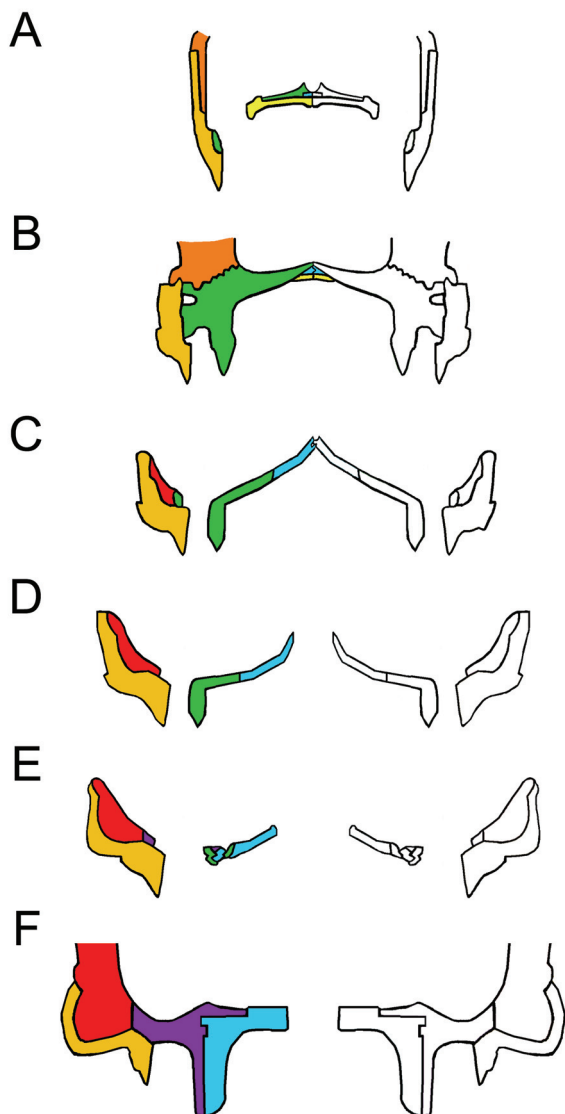


FIGURE 86. Schematic cross-sections of the palate in *Sphenodon* (A-F). Position of the sections as indicated in Figure 85.

land-Wright (personal commun., 2007) suggested that these structures were oriented parallel to the likely direction of force transmission and slippage. However, it may be more complicated than this, as work on sheep skulls (Thomason et al. 2001) found that cranial architecture corresponded to working side compression but not overall strain magnitudes. Nevertheless, the arrangement of bony ridges and internal facet ornament allows the construction of a “hypothesis of compressive stress trajectories” (HCST, Figure 82) that can be tested by comparison to cranial joint structure and Finite Element Analysis. The lines of hypothesised stress are often located along the (thickened) edges of

bones rather than running through the exact centre. As a result, the HCST is not equivalent to a “trans-suture web” (*sensu* Thompson 1995) of *Sphenodon* where lines are drawn between the midpoint of external suture seams (Figure 83). The lines also do not necessarily take the shortest route and occasionally cross each other rather than merging. This arrangement is not dissimilar to that found by Buckland-Wright (1978) in the cat skull.

Overall the HCST predicts that compressive stress in *Sphenodon* is being resisted around the orbits, postfrontals, and quadratojugal foramina, and along the lower temporal bars, the upper margin of the upper temporal fenestrae, the margins and midline of the palate, and the margins of the quadrate-pterygoid wings. This situation matches the suggestions of previous authors with respect to the orbits (e.g., Fox 1964; Frazzetta 1968; Buckland-Wright 1978; Preuschoft and Witzel 2002) and also to the lower temporal bar which is posited to act as a brace between the postorbital bar and mandibular joint (e.g., Rieppel and Gronowski 1981; Whiteside 1986). The prime locations where stress might arise during loading (the marginal dentition, the jaw joints and temporal fenestrae) are linked in a manner similar to that described Buckland-Wright (1978) as a “structural continuum.” This system potentially allows opposing stresses from different regions to be transmitted toward each other as they are reduced and absorbed by the intervening hard and soft tissues (Buckland-Wright 1978). The prefrontal in *Sphenodon* should, for example, be important in re-directing dorsally directed forces from the palate and maxilla to the skull roof (Figure 82). Similarly, the ectopterygoid is positioned to transmit forces between the marginal tooth rows and the centre of the pterygoid (Figure 82.3). Forces from the jaw joint radiate along five different pathways from a point on the quadrate-quadratojugal (Figure 82.1 and 82.4).

Preuschoft and Witzel (2002, text figures 4b, 5b, 5g, 12b) proposed a hypothesis of stress distribution during biting in *Sphenodon*, using lateral, dorsal, ventral and occipital views of the skull and depicting zones of expected tension and compression. It posits that the dorsal and occipital surfaces of the skull are held mainly in compression whereas the ventral part of the skull (including the lower temporal bar) is primarily in tension, with the postorbital bar and quadrate-pterygoid wings as “distance elements” within a neutral axis. In this scheme the skull is acting like a beam held posteriorly and loaded anteriorly. The fact that the skull

roof of *Sphenodon* is composed of thicker bone than the palate lends some support to this interpretation but, as discussed in the previous section, a simple beam model may not be appropriate. The details of the skeletal architecture described here suggest that the lower temporal bars, postorbital bars, central part of the palate and edges of the palate at some point undergo compressive forces. Tensile forces are likely to be resisted by the fibrocellular sutures, tendons, fascia, skin and other soft tissues (Preuschoft and Witzel 2002).

The Cranial Joints

Given the hypothesis of loading represented by the HCST, we would predict that key cranial joints would be those: between the premaxilla, maxilla and neighbouring bones in the rostrum; along the longitudinal axis of the skull roof; resisting the pull and torsional effects of the jaw adductor muscles; supporting the jaw joint around the suspensorium; and reinforcing the palate against bending.

Rostrum

The primary forces experienced by the rostrum will be those generated by loading on the anterior premaxillary chisel teeth and/or on the anterior maxillary teeth. The former may occur when the premaxillary teeth are used to impale relatively large prey (Gorniak et al. 1982, p. 337). This behaviour will generate dorsally directed forces within the premaxilla relative to the rest of the skull, resulting in dorsal shear in the premaxilla-nasal joints and ventral tension in the premaxilla-vomerine and premaxilla-maxilla joints (Taylor 1992; Preuschoft and Witzel 2002; Rafferty et al. 2003). The premaxilla-nasal joint will resist excessive posterodorsal slippage of the premaxilla (Figures 12, 13) whereas the extensive soft tissue between the base of the premaxilla and its neighbouring bones (vomer, maxilla) may permit some limited separation. This location of flexibility may also be important during prooral jaw movement when the premaxillary chisel tooth is contacted by the lower jaw.

The anterior maxilla will be loaded when *Sphenodon* uses its caniniform teeth (Figure 5.1), with compressive forces being directed up the anterior edge of the facial process (Figure 82.1) into the nasal and prefrontal. The rather box-like or tubular cross-section of the rostrum at this level is shaped to resist both bending and torsional stress (Preuschoft and Witzel 2002; Rafferty et al. 2003),

aided by soft tissue in the large overlaps between the prefrontal, nasal and maxilla. The maxilla-nasal slot joint (Figure 17) may serve to support the maxilla as the lower jaw pushes gripped food forward against the maxillary teeth during prooral shearing.

The Skull Roof

The skull roof may be subject to long axis bending because of upward force from the teeth and downward force from the adductor muscles (Taylor 1992; Russell and Thomason 1993; Rayfield 2004, 2005a, 2005b), aggravated by upward forces from the jaw joints and a posterior pull from the neck muscles. There will also be torsion across the orbital region, especially during unilateral biting, and mediolateral tension due to the pull of the adductor muscles.

Longitudinal bending in the antorbital skull is resisted by the long overlapping nasal-frontal joint that resists significant separation while allowing small anteroposterior adjustive movements (as postulated for *Allosaurus*, Rayfield 2005b). The longitudinal ridges on the frontal and nasal facets (Figures 41, 43) may help translate any small mediolateral movements (caused by torsion) into anteroposterior movement. Longitudinal bending of the parietal will be resisted by its dorsoventral expansion. The HCST suggests that compressive forces in the skull roof will converge between the orbits and in front of the upper temporal fenestrae (Figure 82). Significantly, this is where some of the most heavily interlocked joints are located (Figure 77, e.g., frontal-prefrontal, frontal-postfrontal, postorbital-postfrontal). The frontal-parietal joint is relatively narrow in *Sphenodon* but the interlocking structure maintains a rigid connection, resisting both dorsoventral bending forces and mediolateral torsional forces. It is reinforced laterally by the large spanning postfrontals (Figure 77.2). The interfrontal joint may act as a 'keystone' (Figure 79) to the arches of the orbits with forces travelling posteriorly up the postorbital bars (Figure 82) and being directed transversely against each other in another arch meeting around the postfrontal-parietal-frontal suture (Figure 82).

As previously suggested (e.g., Arnold 1998), the complex joints between the parietal, frontal and postfrontals would prevent fronto-parietal hingeing ('mesokinesis'). Even in the hatchling *Sphenodon* where there is a large midline fontanelle, overlaps lateral to this make bending at this joint unlikely (Rieppel 1992).

The Temporal Region and Adductor Muscles

The jaw adductor muscles originate from the sides of the parietal, from the proximal parts of the postorbital and post-temporal bars, and from fascia over the lower temporal fenestra (Gorniak et al. 1982; Jones et al. 2009). Contraction of these muscles during biting imposes powerful anteroventral, anterolateral and ventrolateral forces on the posterior skull roof and temporal region (e.g., Beherents et al. 1978; Herring and Teng 2000; Sun et al. 2004; Byron et al. 2004). At the same time, the region will be subject to a posterodorsal force from the maxilla anteriorly, and a strong upward force from the jaw joint posteriorly. Hence, there may be shear between the component parts, as well as torsion in the upper and lower temporal bars during unilateral biting.

Tension across the interparietal joint is resisted by soft tissue spanning the deep contact surface. Anteriorly, as in other amniotes, the convex “arch” formed by the postorbital bars would resist the downward pull of the adductor muscles (Frazzetta 1968), aided by the tight fit of the postorbital-postfrontal joint and, further ventrally, by the tall medial process of the jugal which is positioned to brace the postorbital (Figure 79). The long overlapping postorbital-squamosal joints in the upper temporal bars (Figure 62) should allow the small adjustive movements necessary to reduce torsion and shearing in this part of the skull. Similarly, as the plane of the jugal-postorbital joint is almost parallel to the orbital margin, the intrasutural collagen fibres should be orientated perpendicular to resist posterodorsally directed forces from the upper jaw (Figure 82). The parietal-squamosal joint alternatively resists the anteroventral pull of the m. adductor mandibulae externus and posterior pull of the m. depressor mandibulae and neck muscles (Gorniak et al. 1982; Al-Hassawi, 2007; Curtis et al. 2009; Jones et al. 2009). The slotted joint allows fibres to be arranged to resist both these movements.

The Jaw Joint and Suspensorium

The forces generated at the jaw joint may be greater than those from the upper tooth row as the jaw joint is closer to most of the muscles (Crompton and Parker 1978; Jones et al. 2009). The exact direction of these forces will also vary as gape and muscle activity changes over the course of a bite and swallowing cycle. Fusion of the quadrate and quadratojugal may reflect the need to further strengthen this part of the skull (Herring 2000). The jugal-squamosal and jugal-quadratojugal joints

appear well-structured to prevent the posterior process of the jugal from rotating medially and/or the posteroventral corner of the skull from twisting laterally. The near vertical facet surfaces permit intersutural soft tissue to be orientated so as to prevent excessive shear or torsion between the lower temporal bar and squamosal-quadratojugal. The joint between the squamosal and quadrate-quadratojugal is roughly parallel to the jaw joint (Figure 77) and is probably important for transmitting forces from the jaw joint to neighbouring parts of the skull (Figure 82). The lateral part of the interlocking quadrate-squamosal joint appears already well established in hatchlings (Rieppel 1992) but the medial lappet that supports the quadrate in adults does not. The presence of a synovial cavity within the quadrate-squamosal joint (Rayfield 2005a; Jones 2006; Holliday and Witmer 2008) needs to be confirmed by direct observation or histological sections, but it could be important for dissipating compressive forces from both the jaw joint and jaw muscles.

Medially, the quadrate-pterygoid joint may be strained as the pterygoid muscles pull the two bones down but the quadrate is pushed upward by the lower jaw. However, excessive movements of the quadrate on the pterygoid would be resisted by the strong overlap (Figure 77), present even in hatchlings, whereas the deep pterygoid-quadrate wings will resist dorsoventral bending while probably allowing for some lateral deflection during swallowing.

The Palate

During biting the palatal bones and joints in *Sphenodon* are subject to forces from the marginal and palatal tooth rows; from the lower jaws pushing against the pterygoid flanges (Taylor 1992); from the dentary teeth wedging between the maxillary and palatine tooth rows during prooral shear; and from the actions of the deeper adductor muscles pulling the braincase (e.g., m. adductor mandibular profundus) and jaws (e.g., m. pterygoideus) against the pterygoids (Haas 1973; Gorniak et al. 1982; Wu 2003; Curtis et al. 2009; Jones et al. 2009).

Overall, the palate is relatively thin but vaulted (Figures 84, 85, 86), the peak of the vault occurring where the vomer, palatine, and pterygoid meet just anterior to the palatal tooth rows. Palatal vaulting has also been described in an extinct crocodylomorph (*Pristichampsus vorax*, Busbey 1995) and non-mammalian synapsids (Jenkins et al. 2002). A disadvantage is that the palate is moved closer to

the neutral axis reducing the skull's overall resistance to torsion and dorsoventral bending (Busbey 1995, p. 190). However, vaulting may help to dissipate dorsally directed forces from the teeth in a manner analogous to the effects of a 'flying buttress' (Busbey 1995). Perhaps correspondingly the palatal bone thickenings in *Sphenodon* (and by inference compressive stresses) converge toward the midline of the palate (Figure 82.3). The vomer, for example, although apparently thin, is reinforced by medial and lateral thickenings. The large overlapping palatal joints in *Sphenodon* (Figure 77.3) potentially allow slight adjustive movements (to dissipate or redistribute torsional stress) while resisting excessive displacement. Similarly, torsional stress during unilateral biting might be reduced by long axis slippage along the midline joints, but posteriorly the interdigitated interpterygoid joint would resist medial forces from the pterygoid flanges and palatal tooth rows (via the palatine) (Rafferty and Herring 1999; Herring and Teng 2000; Markey and Marshall 2007a).

During biting and prooral shear, the complex interlocking prefrontal-palatine joint is positioned to buffer dorsally directed forces from the palatine tooth rows (Jaslow 1990; Jaslow and Biewener 1995), posterior forces generated by pterygoideus atypicus and, potentially, anterodorsal and dorso-lateral (lower jaw wedging) forces during prooral shearing. Prooral shearing also imposes lateral forces on the maxilla, particularly at the posterior end where the jaws first occlude. These will strain both the maxilla-palatine joint and the extensive maxilla-jugal joint.

Together, the maxilla and jugal form much of the lateral wall of the skull as well as the margins of the palate. The maxilla-jugal joint is thus crucial to the overall stability of the skull, linking its anterior and posterior halves. The posterior end of the maxilla is dorsally and medially expanded, giving it an 'L' shape in cross-section (Figure 86). This shape strengthens the long axis of the bone against both dorsoventral bending and torsion, and braces the jugal medially. Medial movement of the jugal (caused by *m. adductor mandibulae externus superficialis sensu stricto* pulling on the lower temporal fascia and postorbital, Jones et al. [2009]) would also be resisted by the palatine and ectopterygoid.

The ectopterygoid is a relatively small bone positioned to transfer compressive loading between the jugal and pterygoid that might occur during biting. Within the ectopterygoid-jugal joint, the dorsally located interdigitation suggests this is

an area of compression, whereas the smoother ventral part may be indicative of tension (Herring and Mucci 1991; Rafferty and Herring 1999). This pattern of stress may occur during biting as the maxillary tooth row is pushed laterally (Figure 79), and the upper temporal bars are pulled down by the muscles. The large pterygoid-ectopterygoid joint will resist compression from the overlying pterygoid muscle, medial forces from the lower jaw, maxilla and jugal (Taylor 1992) and lateral forces from contraction of the *m. pterygoideus*.

The Metakinetic Axis

Metakinesis is a movement of the whole braincase against the rest of the skull. It occurs in at least some lizards (e.g., Herrel et al. 1999, Evans 2008) but distribution within other amniotes remains uncertain. In *Sphenodon*, the joints between the braincase and the dermal skull do not appear to allow metakinetic movements comparable to those found in some lizards (*contra* Gardiner 1983, p. 50). Thus, the constrictor dorsalis muscles (Johnston 2010), important in lizard metakinesis (e.g., Evans 2008), are more likely to be important for proprioception and support in *Sphenodon* (Evans 2008; Johnston 2010). Nevertheless, the small movements that doubtless exist between the skull and braincase, particularly at the synovial basiptyergoid joint, would help to transmit or dissipate stress between the braincase and the rest of the skull (Evans 2008; Johnston 2010).

CONCLUSIONS

The cranial joints of *Sphenodon* demonstrate a variety of forms, many of which are complex. These joints include abutments (mostly midline), overlaps (laterally) and interdigitation. However, as in other lepidosaurs (e.g., Daza et al. 2008) extensive interdigitations are rare. This observation is surprising, given that recent *in vivo* research suggests such joints are suited to reducing compressive stress (Rafferty and Herring 1999; Herring and Teng, 2000; Rafferty et al. 2003; Markey and Marshall 2007a), something that must occur within the lepidosaur skull during feeding. Overlaps are the most common joint type in the skull of *Sphenodon*. Koskinen (1975) suggested that large overlapping joints might reflect more rapid growth because a larger growth surface is provided relative to the external seam width. However, *Sphenodon* is not a rapidly growing animal (e.g., Castanet et al. 1988): females, for example, take at least 13 years to reach sexual maturity (Gaze 2001). Moreover, as in other lepidosaurs (Bell et al. 2002), the degree of

overlap between bones is larger in mature animals than in juveniles.

The greater degree of joint overlap in adult animals may instead relate to differences in stress. Adult animals possess larger adductor muscles and are capable of applying larger bite forces (Jones 2008; Jones and Lappin 2009; Herrel et al. 2010). Studies of diet suggest that post-hatchling *Sphenodon* eat smaller prey than adults (Ussher 1999) and, compared to females and juveniles, the larger adult males have a greater tendency to feed on vertebrates such as sea birds (Cartland-Shaw et al. 1998; Cree et al. 1999; Cree personal commun., 2004). Consumption of the latter provides fatty acids that may be seasonally important for reproduction (Cartland-Shaw et al. 1998). Therefore, the large overlapping joints are better interpreted as a way of maximising the surface area available for soft tissues that can dissipate and/or redistribute stress while maintaining the rigidity of the skull. Such joints associated with the temporal bars maybe be particularly important during long-axis bending and torsion of the skull.

The potential for assessing the capacity for “skull kinesis” (active or passive) using skeletal material alone is admittedly limited (Schwenk 2000; Metzger 2002). Nevertheless, there is nothing in the morphology of the cranial joints of *Sphenodon* to suggest they could accommodate or promote any of the forms of “active” cranial kinesis frequently discussed in the literature (e.g., mesokinesis, amphikinesis). A small degree of metakinesis remains possible in hatchlings. As others have said (e.g., Ostrom 1962; Iordansky 1990; Rieppel 1992; Holliday and Witmer 2008), observations of live juveniles are necessary to understand kinesis in *Sphenodon*. However, because hatchling bones are less mineralised than those of adults (e.g., Erickson et al. 2003), imaging resolution needs to be sufficiently fine to distinguish between bending within bone and between individual bones. The most likely location of potential flexibility is that between the base of the premaxillae and rest of the skull. Slight expansion at these joints may be necessary to accommodate anterior loading of the premaxillae or the impact on the premaxilla by the lower jaw during prooral shearing.

ACKNOWLEDGMENTS

The work presented here was carried out by M.E.H.J. during a BBSRC funded Ph.D. at University College London under the supervision of S.E.E. and by M.E.H.J. and N.C. during research funded by BBSRC grants (BB/E007465/1, BB/

E009204/1 and BB/E007813/1) awarded to S.E.E. (UCL), M.J.F. (University of Hull) and P.O'H. (Hull York Medical School and University of Hull), respectively. For contributions toward research trips, M.E.H.J. thanks the Bogue Fellowship (UCL) and the Palaeontological Association (Sylvester-Bradley Award). For hospitality, cooperation and access to specimens we are grateful to C. McCarthy and A.C. Milner (The Natural History Museum, UK); H. Chatterjee, J. Ashby, M. Carnall, J. Hatton, S. Levey and C. Washbrook (Grant Museum of Zoology, UCL, UK); R.J. Symonds (Cambridge University Museum of Zoology, UK); R. Coory and A.J.D. Tennyson (both Museum of New Zealand Te Papa Tongarewa, NZ); B.J. Gill and R. Prasad (both Auckland Museum); N. Hudson (University of Auckland, NZ); P. Scofield (Canterbury Museum, NZ); J. Adams (Booth Museum of Natural History, Brighton and Hove, UK); A.R. Milner (Birkbeck College, University of London, UK); M. Nowak-Kemp and L. Conyers (Oxford University Museum of Natural History, UK); T. Koppe and A. Deutsch (Ernst Moritz Arndt University Greifswald); G. Sales (King's College London, UK); A. Rester, K. Kelly and A. Wolf (The Field Museum, Chicago, USA); J. Müller (Museum für Naturkunde Berlin, Germany); H. McGhie and R. Smith (The Manchester Museum, University of Manchester, UK); M. Reilly (Hunterian Museum, University of Glasgow, UK); J.M. Hay (Massey University, NZ); and the Digi-morph website (Austin, Texas, USA). In particular, we thank L.K. Murray and C.J. Bell for access to CT data for *Sphenodon* specimen YPM 9194 and other specimens on loan to them from Yale. We also thank S. Taft for CT scanning specimen LDUCZ x036. For access to literature we thank P.M. Barrett (Natural History Museum), C.J. Bell, J. Clack, W. Kathe (previously University of Zürich, Switzerland), J. Klembara (Comenius University in Bratislava) and C.A. Hipsley (Museum für Naturkunde Berlin, Germany). For help checking abbreviations we thank K. Włodarek (UCL). A preliminary version of this work was presented at ICVM 7 in Paris (Jones 2007). For suggestions and helpful discussion M.E.H.J. thanks W. Kathe (previously University of Zürich, Switzerland), K. Bird (UCLan, UK), P. Johnston (University of Auckland, NZ), C. Holliday (Marshall University, USA), I. Werneberg (Paläontologisches Institut und Museum der Universität Zürich, Switzerland), one anonymous reviewer and Ph.D. examiners E.J. Rayfield (University of Bristol, UK) and J.C. Buckland-Wright (Guy's, King's College London, UK).

REFERENCES

- Adamo, M.A. and Pollack, I.F. 2009. Current management of craniostylosis. *Neurosurgery Quarterly*, 19:82-87.
- Alaqeel, S.M., Hinton, R.J., and Opperman, L.A. 2006. Cellular response to force application at craniofacial sutures. *Orthodontics and Craniofacial Research*, 9:111-122.
- Al-Hassawi, A.M. 2007. *Comparative Anatomy of the Neck Region in Lizards*. Trafford Publishing, Victoria, Canada.
- Alibardi, L. and Gill, B.J. 2007. Epidermal differentiation in embryos of the tuatara *Sphenodon punctatus* (Reptilia, Sphenodontidae) in comparison with the epidermis of other reptiles. *Journal of Anatomy*, 211:92-103.
- Alibardi, L. and Maderson, P.F.A. 2003. Observations on the histochemistry and ultrastructure of the epidermis of the tuatara, *Sphenodon punctatus* (Sphenodontida, Lepidosauria, Reptilia): a contribution to an understanding of the lepidosaurian epidermal generation and the evolutionary origin of the squamate shedding complex. *Journal of Morphology*, 256:111-133.
- Anderson, H.T. 1936. The jaw musculature of the phytosaur, *Machaerops*. *Journal of Morphology*, 59(3):549-587. doi: 10.1002/jmor.1050590307
- Anton, S.C., Jaslow, C.R., and Swartz, S.M. 1992. Sutural complexity in artificially deformed human. *Journal of Morphology*, 214:321-332.
- Arnold, E.N. 1998. Cranial kinesis in lizards: variation, uses and origins, p. 323-357. In Hecht, M., Macintyre, R., and Clegg, M. (eds.), *Evolutionary Biology* 30. Academic Press, London, UK.
- Baur, G. 1892. On the morphology of the skull in the Mosasauridae. *Journal of Morphology*, 7:1-22.
- Behrents, R.G., Carlson, D.S., and Abdelnour, T. 1978. In vivo analysis of bone strain about the sagittal suture in *Macaca mulatta* during masticatory movements. *Journal of Dental Research*, 57:904-908.
- Bell, C.J., Evans, S.E., and Maisano, J.A. 2003. The skull of the gymnophthalmid lizard *Neusticurus ecleopus* (Reptilia: Squamata). *Zoological Journal of the Linnean Society*, 103:283-304.
- Bellairs, A.d'A. and Kamal, A.M. 1981. The chondrocranium and the development of the skull in recent reptiles, p. 1-263. In Gans, C. and Parsons, T.S. (eds.), *Biology of the Reptilia, Vol. 11: Development* A. Academic Press, London, UK.
- Benninghoff, A. 1934. Die Architektur der Kiefer and ihrer Weichteilabdeckung. *Paradentium*, 6:2-20.
- Biewener, A.A. and Bertram, J.E.A. 1994. Structural response of growing bone to exercise and disuse. *Journal of Applied Physiology*, 76:946-955.
- Bock, W.J. 1964. Kinetics of the avian skull. *Journal of Morphology*, 114:1-42.
- Böhme, W. and Ziegler, T. 2009. A review of iguanian and anguimorph lizard genitalia (Squamata: Chamaeleonidae; Varanoidea, Shinisauridae, Xenosauridae, Anguinae) and their phylogenetic significance: comparisons with molecular data sets. *Journal of Zoological Systematics and Evolutionary Research* 47:189-202.
- Bolt, J.R. 1974. Evolution and functional interpretation of some suture patterns in Palaeozoic labyrinthodont amphibians and other lower tetrapods. *Journal of Palaeontology*, 48:434-459.
- Bolt, J.R. and Wassersug, R.J. 1975. Functional morphology of the skull in *Lysorophus*: a snake-like Paleozoic amphibian. *Palaeobiology*, 1:320-332.
- Boyd, A. 2003. The real response of bone to exercise. *Journal of Anatomy*, 203:173-189.
- Bramble, D.M. 1989. Cranial specialization and locomotor habit in the Lagomorpha. *American Zoologist*, 29:303-317.
- Brash, J.C. 1934. Some problems in the growth and developmental mechanics of bone. *Edinburgh Medical Journal*, 41:305-387.
- Buckland-Wright, J.C. 1972. The shock absorbing effect of cranial sutures in certain mammals. *Journal of Dental Research*, 51:1241.
- Buckland-Wright, J.C. 1978. Bone structure and the patterns of force transmission in the cat skull (*Felis catus*). *Journal of Morphology*, 155:35-62.
- Buller, W.L. 1877. Notes on the tuatara lizard (*Sphenodon punctatum*), with a description of a supposed new species. *Transactions and Proceedings of the New Zealand Institute*, 9:317-325.
- Burr, D.B., Robling A.G., and Turner, C.H. 2002. Effects of biomechanical stress on bones in animals. *Bone*, 30:781-786.
- Burrows, A.M., Caruso, K.A., Mooney, M.P., Smith, T.D., Losken W., and Stiegel, M.I. 1997. Sutural bone frequency in synostotic rabbit crania. *American Journal of Physical Anthropology*, 102:555-563.
- Busbey, A.B. 1995. The structural consequences of skull flattening in crocodiles, Chapter 10, p. 173-192. In Thomason, J.J. (ed.), *Functional Morphology in Vertebrate Palaeontology*. Cambridge University Press, Cambridge, UK.
- Byerly, T.C. 1925. The myology of *Sphenodon punctatum*. University of Iowa Studies in Natural History, 9(6):1-51.
- Byron, C.D., Maness, H., Yu, J.C., and Hamrick, M.W. 2008. Enlargement of the temporalis muscle and alterations in the lateral cranial vault. *Integrative and Comparative Biology*, 48:338-344
- Byron, C.D., Borke, J., Yu, J., Pashley, D., Wingard, C.J., and Hamrick, M. 2004. Effects of increased muscle mass on mouse sagittal suture morphology and mechanics. *The Anatomical Record Part A: Discoveries in Molecular, Cellular, and Evolutionary Biology*, A279:676-684.

- Callison, G. 1967. Intracranial mobility in mosasaurs. *University of Kansas Paleontology Contributions*, 26:1-15.
- Cartland-Shaw, L.K., Cree, A., Skeaff, C.M., and Grimmond, N.M. 1998. Differences in dietary and plasma fatty acids between wild and captive populations of a rare reptile (the tuatara, *Sphenodon punctatus*). *Journal of Comparative Physiology*, B168:569-580.
- Case, E.C. 1924. A possible explanation of fenestration in the primitive reptilian skull, with notes on the temporal region of the genus *Dimetrodon*. *Contribution from the Museum of Geology, University of Michigan*, 2:1-12.
- Castanet, J., Newman, D.G., and Saint Girons, H. 1988. Skeletochronological data on the growth, age, and population structure of the tuatara, *Sphenodon punctatus*, on Stephens and Lady Alice islands, New Zealand. *Herpetologica*, 44:25-37.
- Clack, J.A. 2002. The dermal skull roof of *Acanthostega gunnari*, an early tetrapod from the Late Devonian. *Transactions of the Royal Society of Edinburgh: Earth Sciences*, 93:17-33.
- Cohen, M. 2000. Sutural biology, chapter 2, p. 11-23. In Cohen, M.M. and Mclean, R.E. (eds.), *Craniosynostosis*. University Press, Oxford, UK.
- Cohen, M.M. Jr. and Kreiborg, S. 1998. Suture formation, premature sutural fusion, and suture default zones in Apert syndrome. *American Journal of Medical Genetics*, 62:339-344.
- Cong, L., Hou L.-H., and Wu, X.-C. 1998. *The Gross Anatomy of Alligator sinensis Fauvel*. CIP China, Beijing. (In Chinese with English summary)
- Cope, E.D. 1896. *Primary Factors of Organic Evolution*. Open Court, Chicago.
- Corruccini, R.S. and Beecher, R.M. 1982. Occlusal variation related to soft diet in a nonhuman primate. *Science*, 218:74-76.
- Cracraft, J. 1968. The lacrimal-ectethmoid bone complex in birds: a single character analysis. *American Midland Naturalist*, 80:316-359.
- Cree, A., Daugherty, C.H., and Hay, J.M. 1995. Reproduction of a rare New Zealand reptile, the tuatara *Sphenodon punctatus*, on rat-free and rat-inhabited islands. *Conservation Biology*, 9:373-383.
- Cree, A., Lyon, G., Cartland Shaw, L., and Tyrrel, C. 1999. Stable isotope ratios as indicators of marine versus terrestrial inputs to the diets of wild and captive tuatara (*Sphenodon punctatus*). *New Zealand Journal of Zoology*, 26:243-253.
- Crompton, A.W. and Parker, P. 1978. Evolution of the mammalian masticatory apparatus. *American Scientist*, 66:192-201.
- Currie, P.J., Hurum, J.H., and Sabath, K. 2003. Skull structure and evolution in tyrannosaurid dinosaurs. *Acta Palaeontologica Polonica*, 48:227-234.
- Curtis, N., Jones, M.E.H., Evans, S.E., O'Higgins, P., and Fagan, M.J. 2009. Visualising muscle anatomy using three-dimensional computer models - An example using the head and neck muscles of *Sphenodon*. *Palaeontologia Electronica* 12. 3.7T:18p, 6.4MB; http://palaeo-electronica.org/2009_3/194/index.html
- Curtis, N., Jones, M.E.H., Evans, S.E., O'Higgins, P., and Fagan, M.J. 2010a. Feedback control from the jaw joints during biting: an investigation of the reptile *Sphenodon* using multibody modelling. *Journal of Biomechanics*, 43:3132-3137.
- Curtis, N., Jones, M.E.H., Evans, S.E., Shi, J., O'Higgins, P., and Fagan, M.J. 2010b. Predicting muscle activation patterns from motion and anatomy: modelling the skull of *Sphenodon* (Diapsida: Rhynchocephalia). *Royal Society Interface*, 7:153-160.
- Curtis, N., Jones, M.E.H., Lappin A.K., Evans, S.E., O'Higgins, P., and Fagan, M.J. 2010c. Comparison between in vivo and theoretical bite performance: using multi-body modelling to predict muscle and bite forces in a reptile skull. *Journal of Biomechanics*, 43:2804-2809.
- Dalrymple, G.H. 1977. Intraspecific variation in the cranial feeding mechanism of turtles of the genus *Trionyx* (Reptilia, Testudines, Trionychidae). *Journal of Herpetology*, 11:255-285.
- Dawbin, W.H. 1982. The tuatara *Sphenodon punctatus* (Reptilia: Rhynchocephalia): a review. In Newman, D.G. (ed.), *New Zealand herpetology. New Zealand: Wildlife Service occasional publication*, 2:149-181.
- Daugherty, C.H., Cree, A., Hay, J.M., and Thompson, M.B. 1990. Neglected taxonomy and continuing extinctions of tuatara (*Sphenodon*). *Nature*, 347:177-179.
- David, L., Glazier, S., Pyle, J., Thompson, J., and Argenta, L. 2009. Classification system for sagittal craniosynostosis. *The Journal of Craniofacial Surgery*, 20:279-282.
- Daza, J.D., Abdala, V., Thomas, R., and Bauer, A.M. 2008. Skull anatomy of the miniaturized gecko *Sphaerodactylus roosevelti* (Squamata: Gekkota). *Journal of Morphology*, 269: 1340-1364. doi:10.1002/jmor.10664
- De Beer, G.R. 1937. *The Development of the Vertebrate Skull*. Clarendon Press, Oxford, UK.
- Depew, M.J., Compagnucci, C., and Griffin, J. 2008. Suture neontology and paleontology: the bases for where, when and how boundaries between bones have been established and have evolved, p. 57-78. In Rice, D.P. (ed.), *Craniofacial Sutures: Development, Disease and Treatment. Frontiers of Oral Biology* 12. Karger Press, Basel.
- Edgeworth, F.H. 1935. *The Cranial Muscles of Vertebrates*, Cambridge University Press, Cambridge.
- Enlow, D.H. 1990. *Facial Growth*. 3rd edition. WB Saunders Co., Philadelphia, USA.

- Erickson, G.M., Lappin, A.K., and Vliet, K.A. 2003. The ontogeny of biteforce performance in American alligator (*Alligator mississippiensis*). *Journal of Zoology London*, 260:317-327.
- Evans, S.E. 1980. The skull of a new eosuchian reptile from the Lower Jurassic of South Wales. *Zoological Journal of the Linnean Society*, 70:203-264.
- Evans, S.E. 2003. At the feet of the dinosaurs: the early history and radiation of lizards. *Biological Reviews*, 78:513-551. doi:10.1017/S1464793103006134
- Evans, S.E. 2008. The skull of lizards and tuataras, p. 1-344. In Gans, C., Gaunt, A.S., and Adler, K. (eds.). *Biology of the Reptilia, Vol. 20, Morphology H: The skull of Lepidosauria*. Society for the Study of Amphibians and Reptiles, Ithaca, New York.
- Evans, S.E. and Jones, M.E.H. 2010. The origins, early history and diversification of lepidosauromorph reptiles, p. 22-44. In Bandyopadhyay, S. (ed.), *New Aspects of Mesozoic Biodiversity. Lecture Notes in Earth Sciences*. Springer, Berlin, Heidelberg.
- Evans, S.E. and Klembara, J. 2005. A choristoderan reptile (Reptilia: Diapsida) from the Lower Miocene of Northwest Bohemia (Czech Republic). *Journal of Vertebrate Palaeontology*, 25:171-184.
- Evans, S.E., Prasad, G.V.R., and Manhas, B.K. 2001. Rhynchocephalians (Diapsida: Lepidosauria) from the Jurassic Kota Formation of India. *Zoological Journal of the Linnean Society*, 133(3):309-334. doi:10.1111/j.1096-3642.2001.tb00629.x
- Evans, S.E., Prasad, G.V.R., and Manhas, B.K. 2002. An acrodont iguanian from the Mesozoic Kota Formation of India. *Journal of Vertebrate Paleontology*, 22:299-312. doi:10.1671/0272-4634(2002)022[0299:FLFTJK]2.0.CO;2
- Farke, A.A. 2008. Frontal sinuses and head-butting in goats: a finite element analysis. *The Journal of Experimental Biology*, 211:3085-3094 doi:10.1242/jeb.019042
- Farlow, J.O. 1975. Observation on a captive tuatara (*Sphenodon punctatum*). *Journal of Herpetology*, 9:353-355.
- Fox, R.C. 1964. The adductor muscles of the jaw in some primitive reptiles. *University of Kansas Publications Museum of Natural History*, 12:657-680.
- Fraser, N.C. 1982. A new rhynchocephalian from the British Upper Trias. *Palaeontology*, 25:709-725.
- Frazzetta, T.H. 1962. A functional consideration of cranial kinesis in lizards. *Journal of Morphology*, 111:287-320.
- Frazzetta, T.H. 1968. Adaptive problems and possibilities in the temporal fenestration of tetrapod skulls. *Journal of Morphology*, 125:145-158.
- Frost, H.M. 2003. Bone's mechanostat: a 2003 update. *The Anatomical Record*, A275:1081-1101.
- Gaffney, E.S. 1979. Comparative cranial morphology of recent and fossil turtles. *Bulletin of the American Museum of Natural History*, 164:67-376.
- Gans, C. 1960. Studies on amphisbaenians (Amphisbaenia, Reptilia), I. A taxonomic revision of the Trogonophidae, and a functional interpretation of the amphisbaenid adaptive pattern. *Bulletin of the American Museum of Natural History*, 119:131-204.
- Gans, C. 1974. *Biomechanics: An Approach to Vertebrate Biology*. Lippincott Co., Philadelphia, USA.
- Gans, C. 1983. Is *Sphenodon punctatus* a maladapted relic? p. 613-620. In Rhodin, A.G.J. and Miyata, K. (eds.), *Advances in Herpetology and Evolutionary Biology, Essays in Honor of Ernest E. Williams*. Harvard University Press, Cambridge, MA, USA.
- Gardner, S.L. and Anderson, S. 2001. Persistent fontanelles in rodent skulls. *American Museum Novarties*. 3327:1-15.
- Gardiner, B.G. 1983. Gnathostome vertebrae and the classification of the Amphibia. *Zoological Journal of the Linnean Society*, 79:1-59.
- Gaze, P. 2001. *Tuatara Recovery Plan No. 47, 2001-2011*. Department of Conservation, Te Papa Atawhai.
- Gillingham, J.C., Carmichael, C., and Miller, T. 1995. Social behavior of the tuatara, *Sphenodon punctatus*. *Herpetological Monographs*, 9:5-16.
- Gorniak, G.C., Rosenberg, H.I., and Gans, C. 1982. Mastication in the Tuatara, *Sphenodon punctatus* (Reptilia: Rhynchocephalia): structure and activity of the motor system. *Journal of Morphology*, 171:321-353.
- Gower, D.J. and Weber, E. 1998. The braincase of *Euparkeria*, and the evolutionary relationships of birds and crocodylians. *Biological Reviews*, 73:367-411.
- Graubner, W. 1992. *Encyclopedia of Wood Joints*. Taunton Press, USA.
- Gray, J.E. 1831. Note on a particular structure in the head of an *Agama*. *Zoological Miscellany*, 1:13-14.
- Günther, A. 1867. Contribution to the anatomy of *Hatteria* (*Rhynchocephalus*, Owen). *Philosophical Transactions of the Royal Society*, 157:1-34.
- Haas, G. 1973. Muscles and the jaws and associated structures in the Rhynchocephalia and Squamata, chapter 4, p. 285-490. In Gans, C. and Parsons, T.S. (eds.), *Biology of the Reptilia 4 Morphology D*. Academic Press, London and New York, UK and USA.
- Hay, J.M., Sarre, S.D., Lambert, D.M., Allendorf, F.W., and Daugherty, C.H. 2010. Genetic diversity and taxonomy: a reassessment of species designation in tuatara (*Sphenodon*: Reptilia). *Conservation Genetics*, 11:1063-1081.
- Heller, J.B., Gabbay, J.S., Wasson, K., Mitchell, S., Heller, M.M., Zuk, P., and Bradley, J.P. 2007. Cranial suture response to stress: expression patterns of noggin and runx2. *Plastic and Reconstructive Surgery*, 119:2037-2045.

- Henderson, D.M. 1998. Skull and tooth morphology as indicators of niche partitioning in sympatric Morrison Formation theropods. In Perez-Moreno, B.P., Holtz, T., Sanz, J.L., and Moratalla, J. (eds.), *Aspects of Theropod palaeobiology*, *Gaia*, 15:219-226.
- Henderson, D.M. 2002. The eyes have it: the sizes, shapes, and orientations of theropod orbits as indicators of skull strength and bite force. *Journal of Vertebrate Palaeontology*, 22:766-778.
- Herrel, A., Aerts, P., and De Vree, F. 1998. Static biting in lizards: functional morphology of the temporal ligaments. *Journal of Zoology*, 244:135-143.
- Herrel, A., De Vree, F., Delheusy, V., and Gans, C. 1999. Cranial kinesis in gekkonid lizards. *The Journal of Experimental Biology*, 202:368-3698.
- Herrel, A., Moore, J.A., Bredeweg, E.M., and Nelson, N.J. 2010. Sexual dimorphism, body size, bite force and male mating success in tuatara. *Biological Journal of the Linnean Society*, 100:287-292.
- Herrel, A., Schaerlaeken, V., Meyers, J.J., Metzger, K.A., and Ross, C.F. 2007. The evolution of cranial design and performance in squamates: consequences of skull-bone reduction on feeding behaviour. *Integrative and Comparative Biology*, 47:107-117. doi:10.1093/icb/icm014
- Herring, S.W. 1972. Sutures - a tool in functional cranial analysis. *Acta anatomica*, 83:222-247.
- Herring, S.W. 1974. A biometric study of suture fusion and skull growth in peccaries. *Anatomy and Embryology*, 146:167-180.
- Herring, S.W. 2000. Sutures and craniosynostosis: a comparative functional, and evolutionary perspective, chapter 1, p. 3-10. In Cohen, M.M. and Mclean, R.E. (eds.), *Craniosynostosis*. University Press, Oxford, UK.
- Herring, S.W. 2008. Mechanical influences on suture development and patency, p. 41-56. In Rice, D.P. (ed.), *Craniofacial sutures Development Disease and Treatment*. *Frontiers in Oral Biology* 12. Karger Press, Basel.
- Herring, S.W. and Mucci, R.J. 1991. In vivo strain in cranial sutures: the zygomatic arch. *Journal of Morphology*, 207:225-239.
- Herring, S.W. and Teng, S. 2000. Strain on the braincase and its sutures during function. *American Journal of Physical Anthropology*, 112:575-593.
- Herring, S.W., Rafferty, K.L., Liu, Z.J., and Marshall, C.D. 2001. Jaw muscles and the skull in mammals: the biomechanics of mastication. *Comparative Biochemistry and Physiology Part, A* 131:207-219. doi:10.1016/S1095-6433(01)00472-X
- Hinrichsen, G.J. and Storey, E. 1968. The effect of force on bone and bones. *The Angel Orthodontist*, 38:155-165.
- Hinton, R.J. 1988. Response of the intermaxillary suture cartilage to alterations in masticatory function. *The Anatomical Record*, 220:376-387. doi:10.1002/ar.1092200406
- Holliday, C.M. and Witmer, L.M. 2007. Archosaur adductor chamber evolution: integration of musculoskeletal and topological criteria in jaw muscle homology. *Journal of Morphology*, 268:457-484. doi:10.1002/jmor.10524
- Holliday, C.M. and Witmer, L. M. 2008. Cranial kinesis in dinosaurs: intracranial joints, protractor muscles, and their significance for cranial evolution and function in diapsids. *Journal of Vertebrate Paleontology*, 28(4):1073-1088. doi:10.1671/0272-4634-28.4.1073
- Howes, G.B. and Swinnerton, H.H. 1901. On the development of the skeleton of the Tuatara, *Sphenodon punctatus*; with remarks on the egg, on the hatchling, and on the hatched young. *Transactions of the Zoological Society London*, 16:1-86.
- Hunt, N. 1998. Muscle function and the control of facial form, p. 120-133. In Harris, M., Edgar, M., and Meghji, S. (eds.), *Clinical Oral Science*. Wright, Oxford.
- Hurum, J.H. and Sabath, K. 2003. Giant theropod dinosaurs from Asia and North America: Skulls of *Tarbo-saurus bataar* and *Tyrannosaurus rex* compared. *Acta Palaeontologica Polonica*, 48(2):161-190.
- Impey, O. 1967. *Functional aspects of cranial kinesis in the Lacertilia*. Unpublished PhD thesis. University of Oxford, Oxford, UK.
- Iordansky, N.N. 1973. The skull of the Crocodylia, chapter 3, p. 201-262. In Gans, C. and Parsons, T.S. (eds.), *Biology of the Reptilia 4 Morphology D*. Academic Press, London and New York, UK and USA.
- Iordansky, N.N. 1990. The evolution of cranial kinesis in lower tetrapods. *Netherlands Journal of Zoology*, 40:32-54.
- Jasinowski, S.C., Rayfield, E.J., and Chinsamy, A. 2010a. Functional implications of dicynodont cranial suture morphology. *Journal of Morphology*, 271:705-728. doi:10.1002/jmor.10828
- Jasinowski, S.C., Rayfield, E.J., and Chinsamy, A. 2010b. Mechanics of the scarf premaxilla-nasal suture in the snout of *Lystrosaurus*. *Journal of Vertebrate Paleontology*, 30:1283-1288. doi:10.1080/02724634.2010.483556
- Jaslow, C.R. 1989. Sexual dimorphism of cranial suture complexity in wild sheep (*Ovis orientalis*). *Zoological Journal of the Linnean Society*, 95:273-284.
- Jaslow, C.R. 1990. Mechanical properties of cranial sutures. *Journal of Biomechanics*, 23:313-321.
- Jaslow, C.R. and Biewener, A.A. 1995. Strain patterns in the horncones, cranial bones and sutures of goats (*Capra hircus*) during impact loading. *Journal of Zoology*, 235:193-210.
- Jenkins, I., Thomason, J.J., and Norman, D.B. 2002. Primates and engineering principles: applications to craniodental mechanisms in ancient terrestrial predators. *Senckenbergiana Lethaea*, 82:223-240.
- Johnston, P. 2010. The constrictor dorsalis musculature and basipterygoid articulation in *Sphenodon*. *Journal of Morphology*, 271:280-292. doi:10.1002/jmor.10797

- Jones, H.H., Priest, J.D., Hayes, W.C., Tichenor, C.C., and Nagel, D.A. 1977. Humeral hypertrophy in response to exercise. *Journal of Bone and Joint Surgery*, A59:204-208.
- Jones, M.E.H. 2006. *Skull evolution and functional morphology in Sphenodon and other Rhynchocephalia (Diapsida: Lepidosauria)*. Unpublished Ph.D. thesis. University of London, London, UK.
- Jones, M.E.H. 2007. Cranial suture morphology of the lepidosaur *Sphenodon* (Diapsida: Rhynchocephalia) and implications for functional morphology. *Journal of Morphology*, 268:1090-1091A.
- Jones, M.E.H. 2008. Skull shape and feeding strategy in *Sphenodon* and other Rhynchocephalia (Diapsida: Lepidosauria). *Journal of Morphology*, 269:945-966. doi: 10.1002/jmor.10634
- Jones, M.E.H. 2009. Dentary tooth shape in *Sphenodon* and its fossil relatives (Diapsida: Lepidosauria: Rhynchocephalia), p. 9-15. In Koppe, T., Meyer, G., and Alt, K.W. (eds.), *Interdisciplinary Dental Morphology. Frontiers in Oral Biology* 13. Karger, Greifswald.
- Jones, M.E.H. and Lappin, A.K. 2009. Bite-force performance of the last rhynchocephalian (Lepidosauria: *Sphenodon*). *Journal of the Royal Society of New Zealand*, 39(3):71-83. doi:10.1080/03014220909510565
- Jones, M.E.H., Curtis, N., O'Higgins, P., Fagan, M., and Evans, S.E. 2009. Head and neck muscles associated with feeding in *Sphenodon* (Reptilia: Lepidosauria: Rhynchocephalia). *Palaeontologia Electronica*, 12.2.7A: 56p, 15.7MB; http://palaeo-electronica.org/2009_2/179/index.html
- Judex, S., Gross, T.S., Bray, R.C., and Zernicke, R.F. 1997. Adaptation of bone to physiological stimuli. *Journal of Biomechanics*, 30:421-429.
- Kathe, W. 1995. Morphology and function of the sutures in the dermal skull roof of *Discosauriscus austriacus* Makowsky, 1876 (Seymouriamorpha; Lower Permian of Moravia) and *Onichiodon labrinthicus* Geinitz, 1861 (Temnospondyli, Lower Permian of Germany). *Geobios*, 19:255-261.
- Kathe, W. 1999. Comparative morphology and functional interpretation of the sutures in the dermal skull roof of temnospondyl amphibians. *Zoological Journal of the Linnean Society*, 126:1-39.
- Kearney, M., Maisano, J.A., and Rowe, T. 2005. Cranial anatomy of the extinct amphisbaenian *Rhineura hatcherii* (Squamata, Amphisbaenia) based on high-resolution X-ray computed tomography. *Journal of Morphology*, 264:1-33.
- Kemp, T.S. 1972. Whaitioid Therocephalia and the origin of cynodonts. *Philosophical Transactions of the Royal Society of London*, B 264:1-54.
- Kesteven, H.L. 1910. The anatomy of the head of the green turtle *Chelone midas*, Latr. Part I. The skull. *Journal of the Proceedings of the Royal Society of New South Wales*, 44:368-400.
- Kieser, J.A., Tkatchenko, T., Dean, M.C., Jones, M.E.H., Duncan, W., and Nelson, N.J. 2009. Microstructure of dental hard tissue and bone in the tuatara dentary, *Sphenodon punctatus* (Diapsida: Lepidosauria: Rhynchocephalia), p. 80-85. In Koppe, T., Meyer, G., and Alt, K.W. (eds), *Interdisciplinary Dental Morphology, Frontiers of Oral Biology* 13. Karger, Greifswald.
- Klembara, J. 1994. The sutural pattern of skull-roof bones in Lower Permian *Discosauriscus austriacus* from Moravia. *Lethaia*, 27:85-95.
- Klembara, J., Tomasik, A., and Kathe, W. 2002. Subdivisions, fusions and extended sutural areas of dermal skull bones in *Discosauriscus* Kuhn (Seymouriamorpha). *Neues Jahrbuch für Geologie und Paläontologie, Abhandlungen*, 223:317-349.
- Kokich, V.G. 1976. Age changes in the human frontozygomatic suture from 20 to 95 years. *American Journal of Orthodontics*, 69:411-430.
- Koskinen, L., Isotupa, K., and Kosko, K. 1975. A note on craniofacial suture growth. *American Journal of Physical Anthropology*, 45:511-516.
- Kupczik, K., Dobson, C.A., Fagan, M.J., Crompton, R.H., Oxnard, C.E., and O'Higgins, P. 2007. Assessing mechanical function of the zygomatic region in macaques: validation and sensitivity testing of finite element models. *Journal of Anatomy* 210:41-53. doi:10.1111/j.1469-7580.2006.00662.x
- Lakjer, T. 1926. Studien über die Trigeminus-versorgte Kaumuskulatur der Sauropsiden. Bianco Lunos Buchdruckerei, Kopenhagen, Denmark.
- Lanyon, L.E. 1980. The influence of function on the development of bone curvature. An experimental study on the rat tibia. *Journal of Zoology*, 192:457-466.
- Lehman, M.L. 1973a. Stress distribution in bone, a study of Benninghoff trajectories of the facial skeleton, p. 187-192. In Schumacher, G.-H. (ed.), *Morphology of the maxillo-mandibular apparatus*. VEB G. Thieme, Leipzig, Germany.
- Lehman, M.L. 1973b. Stress distribution in bone: a study of Benninghoff trajectories of the facial skeleton. *Proceedings of the Royal Society of Medicine*, 66:390-391.
- Lieberman, D.E. 1997. Making behavioral and phylogenetic inferences from hominid fossils: considering the developmental influence of mechanical forces. *Annual Review of Anthropology*, 26:185-210. doi:10.1146/annurev.anthro.26.1.185
- MacAvoy, E.S., McGibbon, L.M., Sainsbury, J.P., Lawrence, H., Wilson, C.A., Daugherty, C.H., and Chambers, G.K. 2007. Genetic variation in island populations of tuatara (*Sphenodon spp*) inferred from microsatellite markers. *Conservation Genetics*, 8:305-318. doi:10.1007/s10592-006-9170-5
- Maisano, J. 2001. "*Sphenodon punctatus*" (On-line), Digital Morphology. In http://digimorph.org/specimens/Sphenodon_punctatus/juvenile/

- Mann, R.W., Manabe, J., and Byrd, J.E. 2009. Relationship of the parietal foramen and complexity of the human sagittal suture. *International Journal of Morphology*, 27:553-564.
- Mao, J.J. 2002. Mechanobiology of craniofacial sutures. *Journal of Dental Research*, 81:810-816.
- Mao, J.J., Wang, X., and Kopher, R.A. 2003. Biomechanics of craniofacial sutures: orthopedic implications. *The Angle Orthodontist* 73:128-135.
- Margulies, S.S. and Thibault, K.L. 2000. Infant skull and suture properties: measurements and implications for mechanisms of pediatric brain injury. *Journal of Biomechanical Engineering*, 122:364-371.
- Markens, I.S. and Oudhof, H.A.J. 1980. Morphological changes in the coronal suture after replantation. *Acta Anatomica*, 107:289-296.
- Markey, M.J. and Marshall, R. 2007a. Linking form and function of the fibrous joints in the skull: a new quantification scheme for cranial sutures using the extant fish *Polypterus endlicherii*. *Journal of Morphology*, 268:89-102.
- Markey, M.J. and Marshall, R. 2007b. Terrestrial-style feeding in a very early aquatic tetrapod is supported by evidence from experimental analysis of suture morphology. *PNAS*, 104:7134-7138. doi:10.1073/pnas.0701706104
- Markey, M., Main, R., and Marshall, R. 2005. *In vivo* cranial suture function and suture morphology in extant fish: implication for inferring skull function in fossil taxa. *Journal of Vertebrate Palaeontology*, 25(Supplement to No. 3):88A-89A.
- Markey, M., Main, R., and Marshall, R. 2006. *In vivo* cranial suture function and suture morphology in extant fish *Polypterus*: implication for inferring skull function in living and fossil fish. *Journal of Experimental Biology*, 209:2085-2102.
- Massler, M. and Schour, I. 1951. The growth pattern of the cranial vault in the albino rat as measured by vital staining with alizarine red 'S'. *The Anatomical Record*, 110:83-101.
- McCormack, T. 2006. Joints for concrete. Paving expert.com. Accessed March 9, 2006 at www.pavingexpert.com/concjoint1.htm.
- McLaughlin, E., Zhang, Y., Pashley, D., Borke J., and Yu, J. 2000. The load-displacement characteristics of neonatal rat cranial sutures. *The Cleftpalate-Craniofacial Journal*, 37:590-595.
- Meikle, M.C., Reynolds, J.J., Sellers, A., and Dingle, J.T. 1979. Rabbit cranial sutures in vitro: a new experimental model for studying the response of fibrous joints to mechanical stress. *Calcified Tissue International*, 28:137-144.
- Meikle, M.C., Heath, J.K., and Reynolds, J.J. 1984. The use of in vitro models for investigating the response of fibrous joints to tensile mechanical stress. *American Journal of Orthodontics*, 85:141-153. doi:10.1016/0002-9416(84)90006-X
- Metzger, K. 2002. Cranial kinesis in lepidosaurs: skulls in motion, 15-46. In Aerts, P., D'Avouët, K., Herrel, A., and van Damme, R., (eds.), *Topics in functional and ecological vertebrate morphology*. Shaker publishing, Antwerp, Netherlands.
- Meyer-Rochow, V.B., Wohlfahrt, S., and Ahnelt P.K. 2005. Photoreceptor cell types in the retina of the tuatara (*Sphenodon punctatus*) have cone characteristics. *Micron*, 423-428.
- Miyawaki, S. and Forbes, D.P. 1987. The morphologic and biochemical effects of tensile force application to the interparietal suture of the Sprague-Dawley rat. *American Journal of Orthodontics and Dentofacial Orthopedics*, 92:123-133. doi:10.1016/0889-5406(87)90367-2
- Moazen, M., Curtis, N., O'Higgins, P., Jones, M.E.H., Evans, S.E., and Fagan, M.J., 2009. Assessment of the role of sutures in a lizard skull: a computer modelling study. *Proceedings of the Royal Society B*, 276:39-46. doi:10.1098/rspb.2008.0863
- Montero, R. and Gans, C. 1999. The head skeleton of *Amphisbaena alba* Linnaeus. *Annals of the Carnegie Museum*, 68:15-80.
- Monteiro, L.R. and Lessa, L.G. 2000. Comparative analysis of cranial suture complexity in the genus *Caiman* (Crocodylia, Alligatoridae). *Review of Brazilian Biology*, 60:689-694.
- Moore, W.J. 1965. Masticatory function and skull growth. *Journal of Zoology*, 146:123-131.
- Morriss-Kay, G.M. 2001. Derivation of the mammalian skull vault. *Journal of Anatomy*, 199:143-151.
- Morriss-Kay, G.M. and Wilkie, A.O.M. 2005. Growth of the normal skull vault and its alteration in craniosynostosis: insights from human genetics and experimental studies. *Journal of Anatomy*, 207:637-653.
- Moss, M.L. 1954. Growth of the calvaria in the rat, the determination of osseous morphology. *American Journal of Morphology*, 94:333-361.
- Moss, M.L. 1957. Experimental alteration of sutural area morphology. *The Anatomical Record*, 127:569-590.
- Moss, M.L. 1961. Extrinsic determination of sutural area morphology in the rat calvaria. *Acta Anatomica*, 44:263-272.
- Moss, M.L. and Young, R.W. 1960. A functional approach to craniology. *American Journal of Physical Anthropology*, 74:305-307.
- Müller, J. 2003. Early loss and multiple return of the lower temporal arcade in diapsid reptiles. *Naturwissenschaften*, 90:473-476.
- Nanda R. and Hickory W. 1984. Zygomaticomaxillary suture adaptations incident to anteriorly-directed forces in Rhesus Monkeys. *The Angle Orthodontist*, 54:199-210.
- Nash, S.B. and Kokich, V.G. 1985. Evaluation of cranial bone suture autotransplants in the growing rabbit. *Acta anatomica*, 123:39-44.

- Nicolay, C.W. and Vaders, M.J. 2006. Cranial suture complexity in white-tailed deer (*Odocoileus virginianus*). *Journal of Morphology*, 267:841-849. DOI: 10.1002/jmor.10445
- Norman, D.B. and Weishampel, D. B. 1985. Ornithopod feeding mechanisms: their bearing on the evolution of herbivory. *The American Naturalist*, 126:151-164.
- Olson, E.C. 1961. Jaw mechanisms in rhipidistians, amphibians, reptiles. *American Zoologist*, 1:205-215. doi:10.1093/icb/1.2.205
- Opperman, L.A. 2000. Cranial sutures as intramembranous bone growth sites. *Developmental Dynamics*, 219:472-485.
- Ostrom, J. 1962. On the constrictor dorsalis muscles of *Sphenodon Copeia*, 1962:732-735.
- Oudhof, H.A.J. 1982. Sutural growth. *Acta anatomica*, 112:58-68.
- Oudhof, H.A.J. and Markens, I.S. 1982. Transplantation of the interfrontal suture in the Wistar Rat. *Acta anatomica*, 113:39-46.
- Oxnard, C.E., Lannigan, F., and O'Higgins, P. 1995. The mechanism of bone adaptation: tension and resorption in the human incus, p. 105-125. In Odegaard, A. and Weinans, H. (eds.), *Bone Structure and Remodelling, Recent Advances in Human Biology 2: Series Editor Oxnard, C.E.* World Scientific, Singapore.
- Paphangkorakit, J., and Osborn, J.W. 1989. Effects on human maximum bite force of biting on a softer or harder object. *Archives of Oral Biology*, 43:833-839
- Parkinson, B. 2002. *The tuatara, New Zealand wild series (2nd edition)*. Reed Publishing, New Zealand.
- Payne, S.L., Holliday, C.M., and Vickaryous, M.K. 2011. An osteological and histological investigation of cranial joints in geckos. *Anatomical Record*, 294:399-405.
- Persson, M. 1995. The role of sutures in normal and abnormal craniofacial growth. *Acta Odontologica Scandinavica*, 53:152-161.
- Persson, K.M., Roy, W.A., Persing, J.A., Rodeheaver, G.T., and Winn, H.R. 1979. Craniofacial growth following experimental craniosynostosis and craniectomy in rabbits. *Journal of Neurosurgery*, 50:187-197.
- Persson, M. and Thilander, B. 1977. Palatal suture closure in man from 15 to 35 years of age. *American Journal of Orthodontics*, 72:42-52. doi:10.1016/0002-9416(77)90123-3
- Persson, M., Magnusson, B.C., and Thilander, B. 1978. Sutural closure in rabbit and man: a morphological and histochemical study. *Journal of Anatomy*, 125:313-321.
- Preuschoft, H. and Witzel, U. 2002. Biomechanical investigations on the skulls of reptiles and mammals. *Senckenbergiana Lethaia*, 82:207-222.
- Pritchard, J.J., Scott, J.H., and Girgis, F.G. 1956. The structure and development of cranial and facial sutures. *Journal of Anatomy*, 90:73-86.
- Radhakrishnan, P. and Mao, J.J. 2004. Nanomechanical properties of facial sutures and sutural mineralization front. *Journal of Dental Research*, 83:470-475.
- Rafferty, K.L. and Herring, S.W. 1999. Craniofacial sutures: morphology, growth, and in vivo masticatory strains. *Journal of Morphology*, 242:167-179. doi:10.1002/(SICI)1097-4687(199911)242:2<167::AID-JMOR8>3.0.CO;2-1
- Rafferty, K.L., Herring, S.W., and Marshall, C.D. 2003. Biomechanics of the rostrum and the facial sutures. *Journal of Morphology*, 257:33-44.
- Rayfield, E.J. 2004. Cranial mechanics and feeding in *Tyrannosaurus rex*. *Proceedings of the Royal Society London*, B271:1451-1459. doi:10.1098/rspb.2004.2755
- Rayfield, E.J. 2005a. Using finite-element analysis to investigate suture morphology: a case study using large carnivorous dinosaurs. *The Anatomical Record*, A283:349-365.
- Rayfield, E.J. 2005b. Aspects of comparative cranial mechanics in the theropod dinosaurs *Coelophysis*, *Allosaurus* and *Tyrannosaurus*. *Zoological Journal of the Linnean Society*, 144:309-316.
- Rayfield, E.J., Norman, D.B., Horner, C.C., Horner, J.R., Smith, P.M., Thomason, J.J., and Upchurch, P. 2001. Cranial design and function in a large theropod dinosaur. *Nature*, 409:1033-1037.
- Reiner, A. and Northcutt, R.G. 2000. Succinic dehydrogenase histochemistry reveals the location of the putative primary visual and auditory areas within the dorsal ventricular ridge of *Sphenodon punctatus*. *Brain, Behaviour and Evolution*, 55:26-36.
- Reisz, R.R. 1981. A diapsid reptile from the Upper Pennsylvanian of Kansas, *University of Kansas Publications of the Museum of Natural History*, 7:1-74.
- Rest, J.S., Ast, J.C., Austin, C.C., Waddell, P.J., Tibbetts, E.A., Hay, J.M., and Mindell, D.P. 2003. Molecular systematics of primary reptilian lineages and the tuatara mitochondrial genome. *Molecular Phylogenetics and Evolution*, 29:289-297. doi:10.1016/S1055-7903(03)00108-8
- Reynoso, V.H. 1996. A Middle Jurassic *Sphenodon*-like sphenodontian (Diapsida: Lepidosauria) from Huizachal Canyon, Tamaulipas, Mexico. *Journal of Vertebrate Paleontology*, 16:210-221.
- Reynoso, V.H. 2003. Growth patterns and ontogenetic variation of the teeth and jaws of the Middle Jurassic sphenodontian *Cynosphenodon huizachalensis* (Reptilia: Rhynchocephalia). *Canadian Journal of Earth Sciences*, 40:609-619.
- Reynoso, V.H. and Clark, J.M. 1998. A dwarf sphenodontian from the Jurassic of La Boca Formation of Tamaulipas, Mexico. *Journal of Vertebrate Palaeontology* 18:333-339.
- Rieppel, O. 1978. The evolution of the naso-frontal joint in snakes and its bearing on snake origins. *Zeitschrift für zoologische Systematik und Evolutionsforschung*, 1978:12-27.
- Rieppel, O. 1992. The skull in a hatchling of *Sphenodon punctatus*. *Journal of Herpetology*, 26:80-84.

- Rieppel, O. 1994. Lepidosauromorpha: an overview with special emphasis on the Squamata, p. 23–37. In Fraser, N.C., and Sues, H.-D. (eds.), *In the Shadow of the Dinosaurs: Early Mesozoic tetrapods*. Cambridge University Press, Cambridge, UK.
- Rieppel, O. and Gronowski, R.W. 1981. The loss of the lower temporal arcade in diapsid reptiles. *Zoological Journal of the Linnean Society*, 72:203-217.
- Robb, J. 1977. *The Tuatara*. Meadowfield Press, Limited, Durham, England.
- Robinson, P.L. 1973. A problematic reptile from the British Upper Trias. *Journal of the Geological Society*, 129:457-479.
- Romer, A.S. 1956. *Osteology of the reptiles*. University of Chicago Press, Chicago.
- Russell, A.P. and Thomason, J.J. 1993. Mechanical analysis of the mammalian head skeleton, chapter 8, p. 345-383. In Hanken, J. and Hall, B.K. (eds.), *The skull, volume 3, Functional and evolutionary mechanisms*. The University of Chicago, Chicago, USA.
- Rybczynski, N., Tirabasso, A., Bloskie, P., Cuthbertson, R., and Holliday, C. 2008. A three-dimensional animation model of *Edmontosaurus* (Hadrosauridae) for testing chewing hypotheses. *Palaeontologia Electronica* Vol. 11, Issue 2; 9A:14p; http://palaeo-electronica.org/2008_2/132/index.html
- Sánchez-Villagra, M. 2010. Suture closure as a paradigm to study late growth in recent and fossil mammals: a case study with giant deer and dwarf deer skulls. *Journal of Vertebrate Paleontology*, 30:1895-1898.
- Säilä, L.K. 2005. A new species of the sphenodontian reptile *Clevosaurus* from the Lower Jurassic of South Wales. *Palaeontology*, 48:817-831.
- Sarnat, B.G. 2008. Some factors related to experimental snout growth. *Journal of Craniofacial Surgery*, 19(5):1308-1314. doi:10.1097/SCS.0b013e3181843532
- Schaunisland, H. 1903. Beiträge zur Entwicklungsgeschichte und Anatomie der Wirbeltiere. I. *Sphenodon*, *Callorhynchus*, *Chameleo*. *Zoologica, Original-Abhandlungen aus dem Gesamtgebiete der Zoologie (Stuttgart)*, 39:1-93.
- Schmid, K.L., Howland, H.C., and Howland, M. 1992. Focusing and accommodation in tuatara (*Sphenodon punctatus*). *Journal of Comparative Physiology A*, 170:263-266.
- Schumacher, G-H. 1973. The maxilla-mandibular apparatus in the light of experimental investigations, p. 13–25. In Schumacher, G-H. (ed.), *Morphology of the maxillo-mandibular apparatus*. VEB G. Thieme, Leipzig, Germany.
- Schwenk, K. 1986. Morphology of the tongue in the tuatara, *Sphenodon punctatus* (Reptilia: Lepidosauria), with comments on function and phylogeny, *Journal of Morphology*, 188:129-156. doi:10.1002/jmor.1051880202.
- Schwenk, K. 2000. Feeding in lepidosaurs Chapter 8, p. 175–291. In Schwenk, K. (ed.), *Feeding. Form, Function, and Evolution in Tetrapod Vertebrates*. Academic Press, San Diego.
- Segura, V. and Flores, D. 2009. Qualitative approach and function in the cranial ontogeny of *Puma concolor* (Felidae). *Mastozoología neotropical*, 16:169-182.
- Seligmann, H., Beiles, A., and Werner, Y.L. 2003. More injuries in left-footed individual lizards and *Sphenodon*. *Journal of Zoology*, 260:129-144.
- Seligmann, H., Moravec, J.Í., and Werner, Y.L. 2008. Morphological, functional and evolutionary aspects of tail autotomy and regeneration in the 'living fossil' *Sphenodon* (Reptilia: Rhynchocephalia). *Biological Journal of the Linnean Society*, 93:721-743.
- Sharell, R. 1966. *The Tuatara, Lizards and Frogs of New Zealand*. Collins, London.
- Sherick, D.G., Buchman, S.R., Goulet, R.W., and Goldstein, S.A. 2000. A new technique for the quantitative analysis of cranial suture biology. *The Cleft Palate-Craniofacial Journal*, 37:5-11.
- Shibazaki, R., Dechow, P.C., Maki, K.D.D.S., and Opperman, L.A. 2007. Biomechanical strain and morphologic changes with age in rat calvarial bone and sutures. *Plastic and Reconstructive Surgery*, 119:2167-2178.
- Siebenrock, F. 1893. Zur Osteologie des Hatteria-Kopfes. *Sitzungsberichte der kaiserlichen Akademie der Wissenschaften in Wien, Mathematisch-naturwissenschaftliche Klasse*, 102:250-268.
- Siebenrock, F. 1894. A contribution to the osteology of the head of *Hatteria*. *Annals and Magazine of Natural History*, 13:297-311.
- Slater, B.J., Lenton, K.A., James, A., and Longaker, M.T. 2009. Ex vivo model of cranial suture morphogenesis and fate. *Cell Tissues and Organs*, 190:336-346.
- Sun, Z., Lee, E., and Herring, S.W. 2004. Cranial sutures and bones: growth and fusion in relation to masticatory strain. *The Anatomical Record*, A276:150-161. doi:10.1002/ar.a.20002
- Taylor, M.A. 1992. Functional anatomy of the head of the large aquatic predator *Rhomaleosaurus zetlandicus* (Plesiosauria, Reptilia). *Philosophical Transactions of the Royal Society of London*, B335:247-280.
- Taylor, M.A. and Cruickshank, A.R.I. 1993. Cranial anatomy and functional morphology of *Pliosaurus brachyspondylus* (Reptilia: Plesiosauria) from the Upper Jurassic of Westbury, Wiltshire. *Philosophical Transactions: Biological Sciences*, 341:399-418.
- Thomason, J.J., Grovum, L.E., Deswysen, A.G., and Bignell, W.W. 2001. *In vivo* surface strain and sterology of the frontal and maxillary bones of sheep: Implications for the structural design of the mammalian skull. *The Anatomical Record*, 264:325-338.
- Thompson, M.B. and Daugherty, C.H. 1992. Living a lie: New Zealand's tuatara. *Australian Natural History*, 23(12):928-935.

- Thomson, K.S. 1995. Graphical analysis of dermal skull roof patterns Chapter 11, p. 193-204. In Thomason, J.J. (ed.), *Functional Morphology in Vertebrate Palaeontology*. Cambridge University Press, Cambridge, UK.
- Tyler, M.J. 1976. Comparative osteology of the pelvic girdle of Australian frogs and description of a new fossil genus. *Transactions of the Royal Society Australia*, 100:3-14.
- Ussher, G.T. 1999. Tuatara (*Sphenodon punctatus*) feeding ecology in the presence of kiore (*Rattus exulans*). *New Zealand Journal of Zoology*, 26:117-125.
- Verstuyf, J. 1912. Das Streptostylie-Problem und die Bewegungen im Schädel bei Sauropsiden. *Zoologisches Jahrbuch, Supplement-Band 5(2)*:545-716.
- Wagemans, P.A.H.M., van de Velde, J-P., and Kuljpers-Jagtman, A.M. 1988. Sutures and forces: A review. *American Journal of Orthodontics and Dentofacial Orthopedics*, 94:129-141.
- Wang, Q., Strait, D.S., and Dechow, P.C. 2006. Fusion patterns of craniofacial sutures in rhesus monkey skulls of known age and sex from Cayo Santiago. *American Journal of Physical Anthropology*, 131:469-485.
- Watanabe, M., Laskin, D.M., and Brodie, A.G. 1957. The effect of autotransplantation on growth of the zygomaticomaxillary suture. *American Journal of Anatomy*, 100:319-329.
- Wegner, R.N. 1959. Der Schädelbau der Lederschildkröte *Dermochelys coriacea* Linné (1766). *Abhandlungen Deutschen Akademie der Wissenschaften zu Berlin, Klasse für Chemie, Geologie und Biologie*, 4:3-80.
- Weishampel, D. 1984. Evolution of jaw mechanisms in ornithomimid dinosaurs. *Advances in Anatomy, Embryology and Cellular Biology*, 87:1-116.
- Werner, G. 1962. Das Cranium der Brückenechse, *Sphenodon punctatus* Gray, von 58 mm Gesamtlänge. *Journal of Anatomy and Embryology*, 123(4):323-368.
- Wettstein, O.v. 1931. Ordnung der Klasse Reptilia: Rhynchocephalia, *Kükenthal und Krumbach's Handbuch der Zoologie*, 7:1-128.
- Wettstein, O.v. 1932. Ordnung der Klasse Reptilia: Rhynchocephalia, In *Kükenthal and Krumbach's Handbuch der Zoologie*, 7:129-224.
- Wettstein, O.v. 1937. Ordnung der Klasse Reptilia: Rhynchocephalia, *Kükenthal and Krumbach's Handbuch der Zoologie*, 7:225-235.
- White, C.D. 1996. Sutural effects of fronto-occipital cranial modification. *American Journal of Physical Anthropology*, 100:397-410.
- Whiteside, D.I. 1986. The head skeleton of the Rhaetian sphenodontid *Diphydontosaurus avonis* gen. et sp. nov., and the modernising of a living fossil. *Philosophical Transactions of the Royal Society of London*, B312:379-430.
- Wilson, L.A.B. and Sánchez-Villagra, M.R. 2009. Heterochrony and patterns of cranial suture closure in hystricognath rodents. *Journal of Anatomy*, 214:339-354. doi:10.1111/j.1469-7580.2008.01031.x
- Witmer, L.M. 1995. Homology of facial structure in extant archosaurs (birds and crocodylians), with special reference to paranasal pneumaticity and nasal conchae. *Journal of Morphology*, 225:269-327.
- Wu, X.-C. 2003. Functional morphology of the temporal region in the Rhynchocephalia. *Canadian Journal of Earth Sciences*, 40:589-607.

APPENDIX 1 TABLE OF ABBREVIATIONS

Abbreviations in alphabetical order according to the abbreviation. Combinations of abbreviations are separated by a full stop (e.g., low.pr), in such

combinations abbreviations for bones are not capitalized (e.g., mx.fct).

AN	ANGULAR
ant	anterior
ant.par.fct	anterior facet for the parietal
ant.pr	anterior process
ant.sl	anterior slot
apmx	anterior process of the maxilla
ART	ARTICULAR
bifur	bifurcation
bone	bone
bpr	basipterygoid process
bpr.fct	facet for the ventrolateral process of the basisphenoid
bra	braincase
brk	breakage
BS	BASISPHEOID
bun	bun-like process
cam.lay	cambrial layer
can	caniniform
cap.layer	capsular layer
ccav	concavity
cd	condyle
chi	chisel-like tooth
cle	cleft
CO	CORONOID BONE
colfib	collagen fibre
cvex	convexity
DEN	DENTARY
dep	depression
dors	dorsal
dors.pr	dorsal process
dura	dura mater
ECPT	ECTOPTYERYGOID
ecpt.fct	facet for the ectopterygoid
ecpt.vent.pr	ventral process of the ectopterygoid
ectomenix	ectomenix
EPT	EPIPTYERYGOID
ept.fct	facet for the epiptyrygoid
fct	facet
fl	flange
foot	foot-like process
for	foramen
fpmx	facial process of the maxilla
FR	FRONTAL
fr.fct	facet for the frontal
gl	glue
gr	groove
gu	gutter

JUG	JUGAL
jug.fct	facet for the jugal
keel	keel
lap	lappet
lat	lateral
lat.pr	lateral process
lc	lacrima canal
ledge	ledge
lft	left
low.mx.fct	lower facet for the maxilla
ltb	lower temporal bar
ltf	lower temporal fenestra
m.att	muscle attachment site
med.fct	medial facet
med.pr	medial process
mf	maxillary foramen
mid.space	middle space
mound	mound
musatt	muscle attachment surface
MX	MAXILLA
mx.fct	facet for the maxilla
n	external nares
NA	NASAL
na.fct	facet for the nasal
neck	neck-like feature
ntch	notch
OP	OPISTHOTIC
orb	orbit
PAL	PALATINE
pal.can.t	palatine caniniform tooth
pal.fct	facet for the palatine
PAR	PARIETAL
par.fct	facet for the parietal
par.for	parietal foramen
pericran	pericranium
pit	pit
pkt	pocket
plat	posterolateral
plat.pr.pal	posterolateral process of the palatine
pmed	posteromedial
pmed.pr.pal	posteromedial process of the palatine
PMX	PREMAXILLA
pmx.fct	facet for the premaxilla
pmx.t	premaxillary tooth
pmxlp	premaxillary lateral process
PO	PROTIC
po.fct	facet for the postorbital
POFR	POSTFRONTAL
pofr.fct	facet for the postfrontal
PORB	POSTORBITAL
porb.fct	facet for the postorbital

post	Posterior
post.par.fct	posterior facet for the parietal
post.pr	posterior process
post.sl	posterior slot
pr	process
PRE	PREARTICULAR
PRFR	PREFRONTAL
prfr.fct	facet for the prefrontal
PT	PTERYGOID
pter.fct	pterygoid facet
ptfl	pterygoid flange
ptne	pterygoid neck
QJ	QUADRATOJUGAL
qj.fct	quadratojugal facet
qj.for	quadratojugal foramen
QU	QUADRATE
qu.cd	quadrate condyle
qu.fct	facet for the quadrate
rgt	right
ri	ridge
rim	rim
sbb	secondary bone band
se	seam
sf	Sharpey's fibres
sft	soft tissue
sh	shelf
skin	skin
slt	slot
SMX	SEPTOMAXILLA
smx.fct	location of contact with the septomaxilla
SO	SUPRAOCCIPITAL
sorb	suborbital fenestra
sosm	suborbital section of the maxilla
sot	spheno-occipital tubercle
split	Split
SQ	SQUAMOSAL
sq.fct	facet for the squamosal
ST	STAPES
stp	Step
str	striations (check through figures)
succ	successional teeth
SUR	SURANGULAR
sym	symphysis
t	tooth
tab	tab
tng	tongue of bone
tro	trough
tub	tubercle
upp.mx.fct	upper facet for the maxilla
utb	upper temporal bar
vent	ventral

vent.pr	ventral process
vent.pr	ventral process
VO	VOMER
vo.fct	facet for the vomer
wal	wall
wf	wear facet
wi	wing
zz	zig zag processes

APPENDIX 2 VIDEO OF SKULL CT-MODEL WITH SUTURES

A three dimensional computer model of a *Sphenodon* skull which shows that the soft tissue component of cranial joints (pink) occupies a complex ribbon-like volume. MicroCT slices of specimen YPM9194 (skull length = 48.75 mm) were viewed in the software programme VG studio max (Volume Graphics GmbH, Heidelberg, Germany).

Bone was selected using the thresholding tool whereas sutures were manually segmented slice by slice in the x, y, and z planes. This work was carried out under the supervision of Dr. Jessie Maisano, at the High-Resolution X-ray Computed Tomography Facility, University of Texas, Austin, USA.